2009

AN EVALUATION OF THE TRAVELING WAVE ULTRASONIC MOTOR FOR FORCE FEEDBACK APPLICATIONS

Nishant Venkatesan
University of Kentucky

ABSTRACT OF THESIS

AN EVALUATION OF THE TRAVELING WAVE ULTRASONIC MOTOR FOR FORCE FEEDBACK APPLICATIONS

The traveling wave ultrasonic motor is considered for use in haptic devices where a certain input-output relation is desired between the applied force and the resulting motion. Historically, DC motors have been the standard choice for this purpose. Owing to its unique characteristics, the ultrasonic motors have been considered an attractive alternative. However, there are some limitations when using the ultrasonic motor for force-feedback applications. In particular, direct torque control is difficult, and the motor can only supply torque in the direction of motion. To accommodate these limitations we developed an indirect control approach. The experimental results demonstrate that the model reference control method was able to approximate a second order spring-damper system.

KEYWORDS: Traveling wave ultrasonic motor, haptic device, force-feedback, model reference control method, spring-damper system

Nishant Venkatesan

February 13, 2009

AN EVALUATION OF THE TRAVELING WAVE ULTRASONIC MOTOR FOR FORCE FEEDBACK APPLICATIONS

By

Nishant Venkatesan

Dr. Thomas M. Seigler
Director of Thesis

Dr. L.S.Stephens
Director of Graduate Studies

February 13, 2009

RULES FOR THE USE OF THESIS

Unpublished theses submitted for the Masters degree and deposited in the University of Kentucky Library are as a rule open for inspection, but are to be used only with due regard to the rights of the authors. Bibliographical references may be noted, but quotations or summaries of parts may be published only with the permission of the author, and with the usual scholarly acknowledgments.

Extensive copying or publication of the thesis in whole or in part also requires the consent of the Dean of the graduate School of the University of Kentucky.

A library that borrows this dissertation for use by its patrons is expected to secure the signature of each user.

Name Date

_____

_____

_____

_____

_____

_____

_____

_____

THESIS

Nishant Venkatesan

The Graduate School
University of Kentucky
2009

AN EVALUATION OF THE TRAVELING WAVE ULTRASONIC MOTOR FOR FORCE FEEDBACK APPLICATIONS

THESIS

A thesis submitted in partial fulfillment of the
requirements for the degree of Master of Science
in Mechanical Engineering in the College of Engineering at the University of Kentucky

By

Nishant Venkatesan

Lexington, Kentucky

Director: Dr. Thomas M. Seigler, Professor of

Mechanical Engineering

Lexington, Kentucky

2009

DEDICATION

To my parents, relatives, and friends

ACKNOWLEDGEMENTS

"A champion is someone who goes so far they can't go another inch—and then they go that inch." I wondered why that was important. Now I know,winning in business or in personal life is all about inches: going small distances successfully, then going farther still."

I believe we are all born with a purpose and the potential to achieve it. It may take us years to decide to go for it. When we do, that is the moment we begin our personal road of trials. We know we are moving closer to our goal when the trials get bigger, and we see many people around us giving up – we keep going, over the last massive trial and achieve our pot of gold.

A BIG thanks to you, Dr. Seigler for giving me an opportunity to be part of your team, share your ideas, pick up threads from your wisdom, constantly upgrade my knowledge and above all bearing with me and relentlessly encouraging me whenever I erred. For every life there must be a path breaker and you have proved to be one for my success. By your presence, by your example, by your action and inaction, by your words and deeds, by your blessings and support, by your understanding and love, today I stand in front of you as a 'MAN' with a sense of accomplishment and achievement. Yes, I do remember your words that education is a progressive discovery of our own ignorance and in this world there is no real achievement till we retire and leave a legacy that the humanity would recognize and remember for years to come by.

My thanks to my mother and father, Revathi and Venkatesan, Jayshri, Ramakrishnan, my brother Thejaswin and to a very special person, Varsha Kumar who contributed to this effort, and kept me going with their belief, support and inspiration when it was most needed. I extend my heart full greetings to my friends from India, specially Dr. Anantharaman Muthuswamy and Dr. Padhma Ranganathan who have been with me all through my turmoil, downs, ill health, slips, and sleepless nights. Never did they exhibit their anguish or anxiety that made my journey smoother and pleasanter.

TABLE OF CONTENTS

LIST OF TABLES

LIST OF FIGURES

1 Introduction

The purpose of this research is to evaluate the traveling wave type ultrasonic motor for use in devices that require force feedback. A general overview of the thesis work, including motivation, objectives and outlines are laid out in this chapter.

1.1 Motivation

The traveling wave ultrasonic motor (USM), hereafter referred to as simply USM, is considered for use in haptic devices where feedback forces are required, in particular force-feel systems where a certain input-output relation is desired between the applied torque and the response. Owing to some of its unique characteristics, there are circumstances where the ultrasonic motor may be considered an attractive alternative to the more standard electromagnetic motor. In particular:

1. The USM is a low speed high torque device. To achieve this with the electromagnetic motor requires gearing which can add dynamic complexity.

2. The ultrasonic motor has a torque density in the range three to ten times higher than a DC motor.

3. USM neither generates nor is affected by an electromagnetic field.

4. The motor has a high holding torque in the absence of input energy, where as the electromagnetic motor requires both electrical energy and feedback control to hold a desired position under load.

However, the USM and electromagnetic motor are significantly different in their operating principles and are not necessarily interchangeable in all applications. The USM can only output torque in the direction of the rotation. The electromagnetic motor is not so constrained. Additionally, the output torque of the USM is difficult to directly control. In contrast, for the DC motor the output torque is simply controlled by current. Hence, to be considered a viable alternative in force-feedback applications, we seek an approach to torque control for the USM.

1.2 Objectives

The primary objective of this research is to develop a control method for the USM that can be used in force feedback applications; and to experimentally evaluate its performance. This objective was achieved by the following tasks.

1. Experiment development, which includes arranging a closed loop experimental setup and evaluating the steady state performance.

2. Control development, which includes formulating the control algorithms, based on the steady state characteristics of the USM.

3. Experimental validation of the control method, which includes the evaluation of the USM in force feedback operation.

Evaluation was based on the ability to generate a desired input-output response between the user input and the output motion.

1.3 Outline

This thesis is divided into six chapters, the contents of which are as follows.

Chapter 2 contains a literature review, which discusses in detail the construction and working principle of USM. A survey of various mathematical models is presented, the purpose of which is to analyze the relationship between the input parameters and the output torque, which is normally required for force-feedback control.

Chapter 3 contains a detailed description of the experimental setup. Specifications of the major components and data acquisition methods are discussed.

Chapter 4 introduces the force-feedback control approach that is considered in this work. Experimental results are provided to demonstrate the basic functionality of the motor.

Chapter 5 presents an experimental validation of the USM force-feedback control methodology.

Chapter 6 contains the conclusion of the research and suggestions for future work.

The Appendix contains supplementary experimental results, not crucial to the main contents of the work.

1.4 Contributions

As mentioned, controlling the torque of the USM is a difficult task. Previous researches have developed complex approaches that have mostly relied on steady state operating characteristics. However, none of these works has considered an arbitrary time varying load that occurs in force-feedback applications. Nor, in their control formulations have they considered the basic limitation that the USM can supply torque only in the direction of motion. To accommodate these limitations we have developed a model reference force-feedback control method. Experimental results demonstrate that the closed-loop system is able to approximate a simple second-order response, thus producing the feel of a spring and damper.

2 Background

This chapter presents a brief summary of the working principle, historical background, and the various mathematical models of the traveling wave ultrasonic motor. The basic operating principles of the USM are examined to explain the basic limitations. Keeping in mind that the focus of investigation is force-feedback application, various mathematical models are surveyed for their usefulness in predicting the torque produced by the USM.

2.1 Operating Principles

The ultrasonic motor is a type of piezoelectric actuator that consists of three basic parts: a piezoelectric actuator, an elastic vibrator, and a sliding piece, as shown in Figure 2-1[1]. The piezoelectric actuator is attached to the elastic vibrator. The friction coat along with the elastic moving part constitutes the sliding piece. A high frequency input signal, in the ultrasonic range (> 20kHz), is supplied to the actuator to excite the elastic vibrator at high amplitude. The vibration of surface points of the elastic vibrator is transmitted through contact friction and generates motion of the sliding piece.

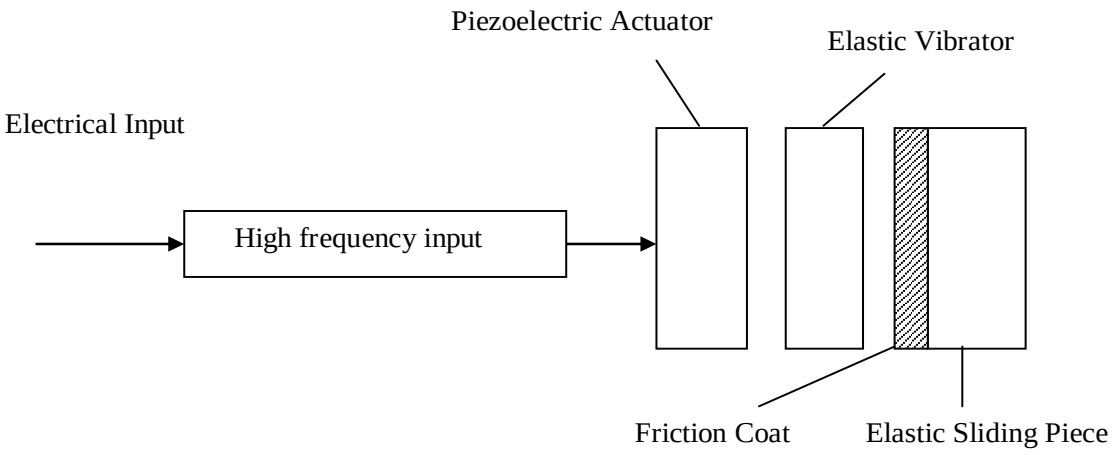

Figure 2-1. Basic Construction of Ultrasonic Motor [1]

There are various types of ultrasonic motors. As shown in Figure 2-2, they are broadly classified into *standing wave type* and *traveling wave type* [1, 2, 3]. Standing wave ultrasonic motor use the standing wave generated in the elastic vibrator to drive the sliding piece. The direction of motion of the particles on the standing wave depends on the position of the particle. The traveling wave USM uses the traveling wave generated in the elastic vibrator to drive the sliding piece.

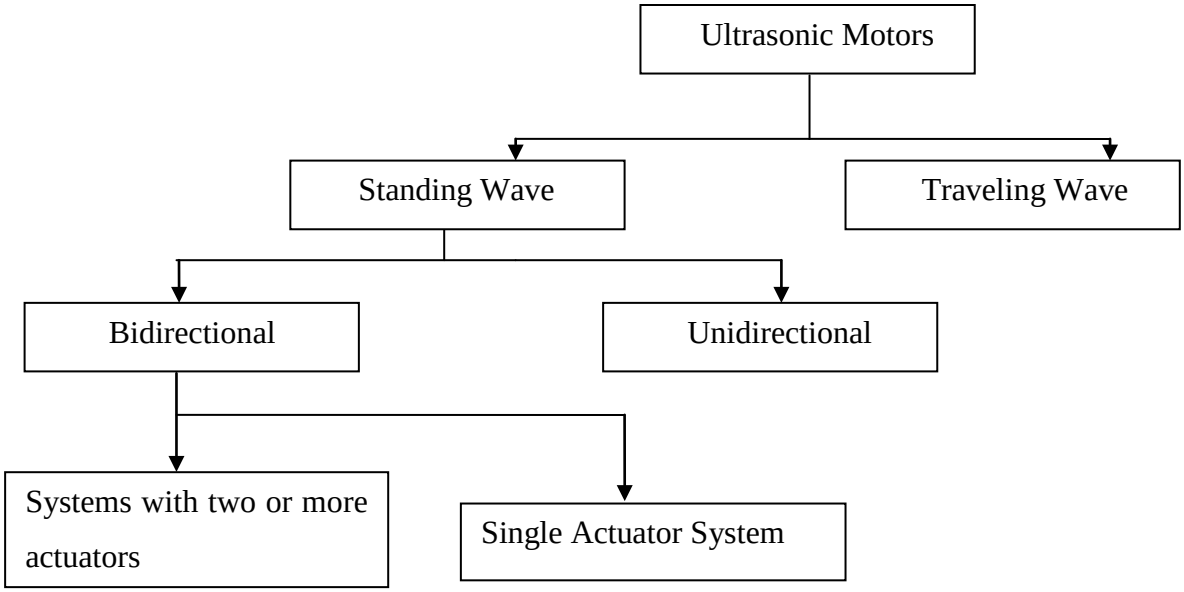

Figure 2-2. Classifications of Ultrasonic Motors

Though the first standing wave ultrasonic motor was invented in 1965 by V.V. Lavrinenko, the first practical ultrasonic motor, proposed by H.V Barth of IBM came into existence in 1973. Various mechanisms based on the same principle were proposed by Lavrinenko and Vasilev in the former USSR [1, 4]. The traveling wave ultrasonic motor was invented by T.Sashida in 1982. The following section details the traveling wave ultrasonic motor, since this is the focus of the current work.

2.1.1 The Traveling Wave Ultrasonic Motor

The traveling wave ultrasonic motor (USM) is designed on the basic principle that by actuating transverse traveling wave motion of an elastic medium, the surface points of that medium produce an elliptical trajectory that can be used to transfer energy to a contacting surface. Referring to Figure 2-1, for the USM, the elastic vibrator in conjunction with the piezoelectric actuator constitutes the *stator*. For an elastic medium of arbitrary geometry, the generation of a traveling wave is not trivial; however thin circular disks and shells are amenable to this type of motion. The transverse free vibration solution, (i.e. mean plane solution) of a thin disk (Figure 2-3), is $w(r,\varphi,t) = B(r)\cos m\varphi \cos \omega t$ **,** where $B(r)$ is a dimensionless Bessel's function, r and φ are the spherical coordinates, and ω is the angular frequency.

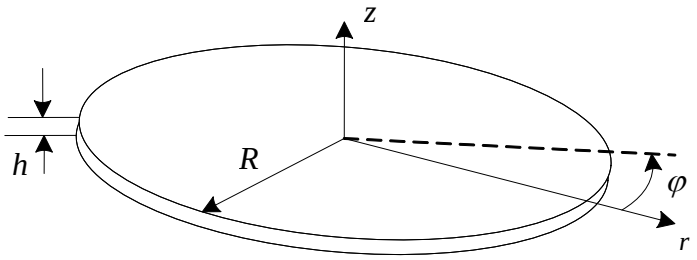

Figure 2-3. Disc Type Stator

For a disk, the defined origin for measurement of angular displacement is arbitrary, hence $B(r)sinm\varphi\ sin\omega t$ is also another vibration solution for the disk. Both the solutions represent standing waves. A traveling wave is obtained by the superposition of these standing waves, that is

$$B(r)\cos m\phi \cos \omega t + B(r)\sin m\phi \sin \omega t = B(r)\cos(m\phi - \omega t) \qquad (2.1)$$

For $r=R$, the outer radius of the disk, the surface motion of the disk is written as $A\cos(\omega t-\phi)$. The surface motion is calculated by Euler's hypothesis, which assumes that the mean plane sections remain plane during deformation. It can be shown that the motion of the surface points on the stator is an elliptical trajectory [5], of the form

$$[w_z(r,\phi,z,t)]^2+[\frac{r}{hm}w_\phi(r,\phi,z,t)]^2=A^2R^2(r) \tag{2.2}$$

where, w_z and w_φ are vibration amplitudes in z and φ directions. The velocity of the points on the peak of the ellipse is found by differentiating Equation 2.2 with respect to time [3, 5, 6, 7, 8]:

$$v_s=\frac{\pi\omega hA}{\lambda} \tag{2.3}$$

where h is the mean plane thickness, and λ is the wave length. Note from Equation 2.3 that the velocity of the particles on the surface increases with increase in frequency, thickness and vibration amplitude. However, increasing the vibration amplitude or the stator thickness requires larger actuation energy. Also, Equation 2.3 seems to imply that the velocity of surface points is proportional to frequency. However, the amplitude A is a function of frequency. In particular, the amplitude decreases with an increase in frequency; hence the velocity is not proportional to frequency.

The construction principle for the USM is shown in the Figure 2-4 (a). Ceramics with opposite polarization are placed consecutively so that one will expand while the other will contract when a voltage is supplied. The expansion and contraction of the ceramics causes a transverse traveling wave on the mean plane of the elastic body, which produces elliptical motion of the surface points. Two input signals $A\cos(2\pi ft)$ and $A\sin(2\pi ft+\varphi)$ are supplied to the actuator. Thus, the control parameters are the input frequency, amplitude and phase. A physical arrangement of piezoelectric ceramics is shown in the Figure 2-4 (b) for a mode-4 actuation scheme.

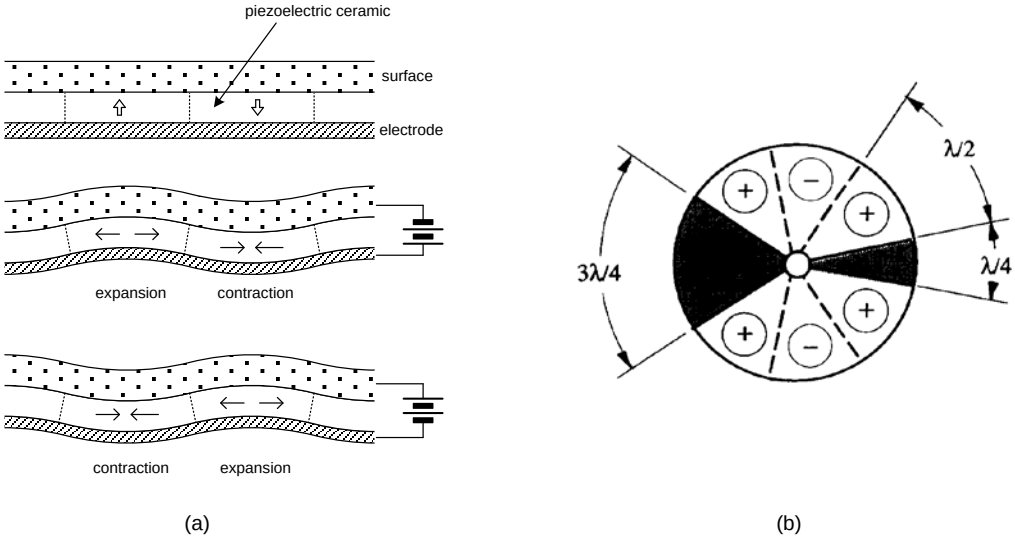

Figure 2-4 (a) and (b). Piezoelectric actuation of the traveling wave ultrasonic motor: actuation concept and 2-4 (b) actuator arrangement for a 4-λ stator.

A cut-away section indicating the parts of the motor is shown in the Figure 2-5, which includes the piezoelectric ceramic, the stator, the rotor, the bearings, and the case. Another part which requires special mention is the comb teeth. They are the grooves that appear between the stator and the rotor. To explain these comb teeth, note from Equation 2.3 that the velocity of the surface points is proportional to mid plane thickness of the stator; hence the velocity can be effectively increased by increasing the thickness of the stator, which is achieved by adding comb teeth. The teeth helps to increase the thickness of the stator without substantially changing the natural frequency. The gaps between the teeth also help in removing the dust produced due to friction.

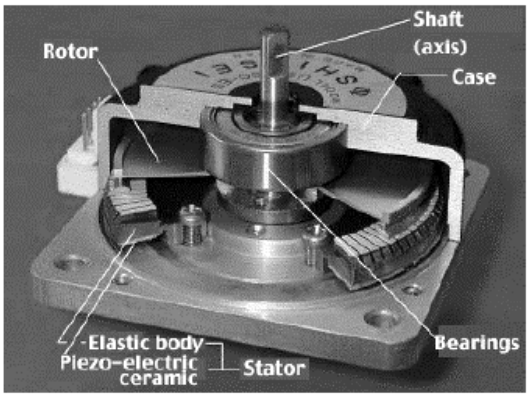

Figure 2-5. Traveling Wave Ultrasonic Motor USR 60 [42]

2.2 Mathematical Models of the USM

Due to the complexity in the working principle, the motor's physical behavior is difficult to model. Determination of the output torque of the USM is highly complex because it is dependent not only on the surface motion of the stator but also on the interaction between the stator and the rotor. In contrast, a model of the DC motor, which is the actuator most often used for force-feedback applications, is relatively simple. There exists an approximate linear relationship between the input current and the output torque.

Over the past several years, researchers have been working toward the development of mathematical models for the USM that can be used to predict the relationship between the input excitation parameters and output parameters such as speed and torque. The following discussion provides an overview of the various mathematical models that have been suggested in the literature.

2.2.1 Equivalent Electrical Model

The theory of electrical circuits is often useful in resolving the complex dynamic or static behavior of mechanical systems. Electrical equivalent components such as capacitors, inductors, and resistors have been used for modeling components of the USM. Such a model for the USM stator is shown in Figure 2-6. The first stage constitutes the voltage supply to the ceramic, which is indicated by the AC supply to the piezoelectric ceramic. Actuation of the two modes is possible by supplying the voltages with a phase difference. An equivalent capacitance, C_d, represents the piezoelectric ceramic. The stator's mass is equivalent to the inductor L_m, its capacitance is given by C_m, and an overall loss is modeled by a resistor denoted by r_o. The two loops represent the two out of phase vibration solutions of the stator. In this model, it is assumed that there is no cross coupling, in that the two vibration modes do not affect one another.

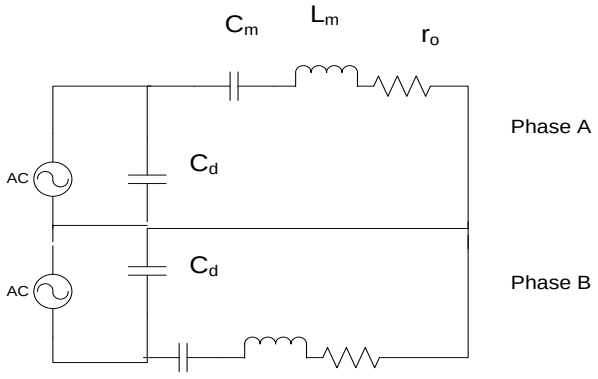

Figure 2-6. Stator model of TWUSM

Figure 2-7 represents an electrical equivalent model of the entire USM [4, 9, 10, 11, 12, 13, 14, 15, 16] for the case where the two input excitation signals are 90° out of phase. The rotor is considered to be a rigid body of mass L_m. Ideally, there are no frictional losses in converting the vibration of the stator into motion of the rotor. However, in reality some amount of heat is generated due to the sliding between the stator and the rotor. This is considered frictional loss,

which is represented by a diode and a resistor connected in parallel to a transformer. The vibration during the actuation of the motor, mechanical losses and viscous losses in the bearings and other related parts of the USM determines the total losses in the motor which is given by r_L. The transformer between the stator and the rotor provides the simplest possible description of the contact mechanics.

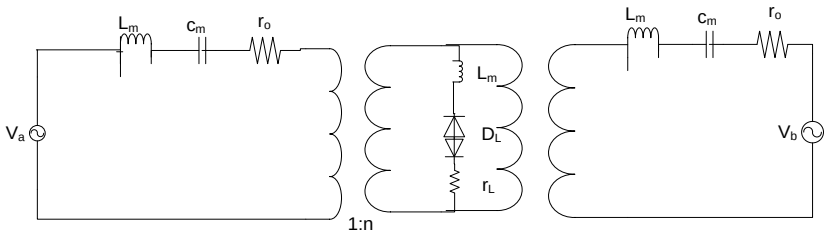

Figure 2-7. Simplified equivalent circuit of the USM [4]

From Figure 2-7, the two circuits represent the out-of-phase vibration solution of the stator, while the output obtained is the current across the diode, which is representative of the motor speed. We note that this equivalent circuit model cannot be used to predict the torque of the motor and is thus of little use for force-feedback applications.

2.2.2 Equivalent mechanical model

One modeling approach, which builds upon the equivalent electrical model of the USM to encompass more details such as the cross coupling between modes, was suggested by Kandare *et al*. [16, 17]. This approach we refer to as the *equivalent mechanical model*. Mechanical equivalents such as mass, spring and dampers are used to develop the equivalent mechanical model. Resistor R_P, represents losses in the piezo-ceramics and the capacitor C_P represents its capacitance. The transformer with a ratio A, represents the electromechanical coupling between the electrical and the mechanical system.

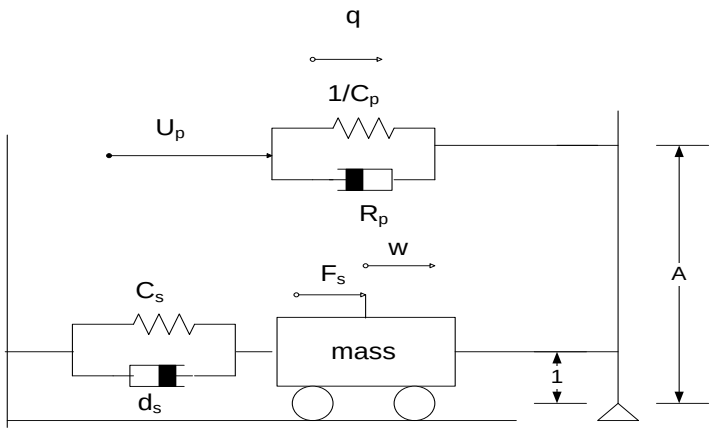

Figure 2-8. Equivalent Mechanical Circuit-Single input [17]

The model shown in Figure 2-8 is identical to the equivalent electrical model shown in Figure 2-7. Here the symmetrical disturbances are not taken into consideration, which makes the model an ideal one [18]. To account for cross coupling between the vibration modes, symmetrical disturbances, indicated by E1 and E2 in Figure 2-9, are added [16]. As with the equivalent circuit model, the purpose of this model is to output the speed of the motor as a function of excitation parameters. However, in this model, in addition to amplitude and frequency, the excitation phase can also be considered.

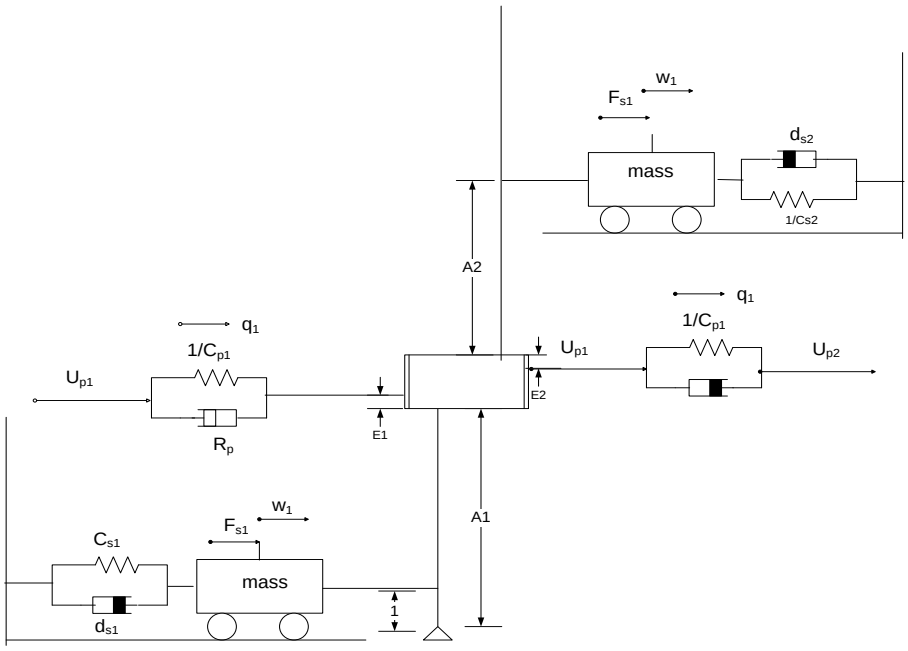

Figure 2-9. Equivalent Mechanical Model [17]

2.3 Contact Mechanics

The contact mechanics are the most difficult component in modeling the USM. For the previous two approaches discussed in Sections 2.2.1 and 2.2.2, the contact mechanics are modeled with simple electrical and mechanical components. To obtain more accuracy, the contact model must be substantially improved.

A summary of various contact models have been discussed in Refs.4, 5, 15, 17, 19, 20, and 21. According to Wallaschek, an accurate mathematical model of the contact mechanics provides several important characteristics such as no load speed, stall torque, efficiency, and speed-torque curves. The main approach to modeling the contact mechanics is shown in Figure 2-10. The stator is assumed undeformable while the rotor is deformable with some uniform stiffness. Hence, upon actuation the stator presses into the rotor. As shown in Figure 2-10, the forces applied to the rotor are the compressive load, F_{ext}, which presses the stator and rotor together,

and the stator-rotor interaction forces, F_N and F_T, the normal and tangential force, respectively. The forces applied to the stator are provided by the piezoelectric actuating elements and the stator-rotor interaction. Here we have a fundamental difficulty in modeling the dynamics of this system (as with all systems that involve contact mechanics): the interaction forces acting between the stator and rotor are dependent on the motion of the stator and rotor. That is, in order to even define the interaction forces, the motion must be known; knowing the motion amounts to solving equations of motion, for which the forces must be specified. The contact mechanics problem can be resolved to some degree by numerical simulation, where time delays can be imposed. However, this is not very useful for analytical evaluation, and in particular for control design where, ideally, the torque is expressed as a function of the piezo ceramic inputs (voltage amplitude, excitation frequency and phase). Moreover, the equations of motion that have been developed for the USM, through consideration of the contact mechanics, are highly nonlinear. The torque is related to the input parameters (voltage amplitude, frequency, and phase) through several coupled nonlinear ordinary differential equations, and transcendental algebraic equations. Even steady-state analytical solutions are, to our knowledge, not possible for these equations. This poses a severe difficulty in attempting to design a model-based compensator to control the torque. As discussed in Chapter 4, we will circumvent this difficulty with a model reference based control approach.

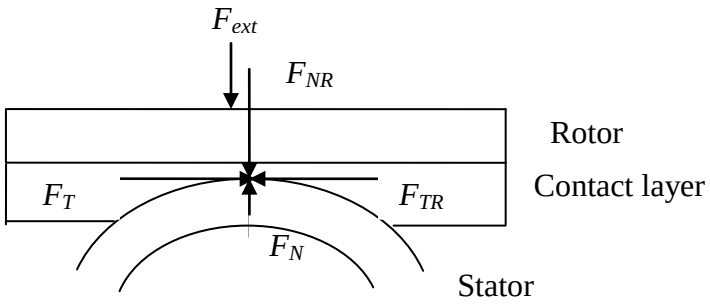

Figure 2-10. Stator-rotor Contact Model

2.4 Controls Research

Various control techniques have been developed for the USM. We divide these techniques into speed and position control, and torque control. As mentioned in Section 2.1.1, the input parameters than can be used to control the motor's output parameters are frequency, phase and amplitude of applied voltage. Most control techniques in the literature have utilized only frequency and phase. Effects of varying amplitudes on the motor's performance is not examined because it does not have the ability to control the motor at low speeds and the range of amplitude in which the motor must operate to achieve high speeds is large.

Speed control based on frequency modulation was demonstrated in Refs. 22 and 23, and a phase modulation technique was shown in Ref. 24. Arguing that frequency modulation is best suited for quick response, and phase modulation provides precise positioning, a method called *dual mode control*, which combines both frequency and phase modulation simultaneously, was demonstrated to achieve quick response and precise positioning [25, 26]. To account for time varying parameters an adaptive control technique was developed [27]. Due to continuous interaction between the stator and the rotor, there might be wear in the friction coat, which affects the performance characteristics of the USM. The heat generated during the motor's operation also affects its performance. The adaptive control techniques developed accounts for these losses. In this work, the motor model was assumed to be linear. To accommodate nonlinearities such as dead-zone effects and hysteresis (discussed later in Chapter 4), controllers based on fuzzy logic and neural networks were developed [28, 29, 30, 31, 32]. In Ref. 28, the model reference adaptive control was used to perform precise positioning, while the fuzzy-logic controller was used to compensate for dead-zone effects.

As discussed in the previous section, torque control of the USM is not straight-forward. Previous approaches to control torque typically have employed an inverse plant model based on steady state torque-speed data [33, 34]. Giraud *et. al*. developed model based control for precise positioning [35], while J.Maas *et.al.* developed a model based speed control technique [24]. These works, however, do not consider an arbitrarily time varying load, which occurs in force-

feedback applications. Also not taken into account is the inability of the motor to generate torque in the opposite direction of motion. In force-feedback applications, these limitations do not allow the motor to produce an arbitrarily specified torque. For example, as detailed in Chapter 4, the USM cannot be expected to mimic a simple spring damper system

2.5 Summary

The unique characteristics of the USM make it attractive for use in many applications. However, the operating principles are significantly different than more commonly used electromagnetic motors, and cannot provide the same functionality in all applications. For example, we cannot expect the ultrasonic motor to produce the interaction torque that would be provided by a spring-damper system. Additionally, the models necessary for accurately describing the motion and torque produced by the ultrasonic motor are complex. Thus, model based control is not straight-forward. Researchers have been forced to rely on substantial simplifications and learning algorithms to accommodate model-based control for force feedback operation. Further, the control approaches that have previously been developed are not applicable to the current study, which requires that the USM interact with an arbitrarily, and unknown, time-varying load.

3 Experimental Setup

The basic experimental setup for our investigation is shown in Figure 3-1. The USM used in these experiments (Shinsei USR60) requires two input signals at amplitudes of 130 V and at frequencies in the range of 40 KHz. The sinusoidal waveforms are provided by a DSpace control board. Two high-voltage amplifiers are used to gain outputs from the DSpace source to the USM. The torque transducer is coupled to the USM to measure the interaction torque between the USM and the DC motor. The purpose of the DC motor is to provide positive torque for torque-speed measurements, and also to act as the human input load for force-feedback experiments. Negative torques for torque-speed measurements are provided by a mechanical brake. An incremental position encoder measures the angular position of the motor, which is fed back to the DSpace control board where it is numerically differentiated to obtain the angular velocity. Feedback of the torque and the position measurements are later used for active control.

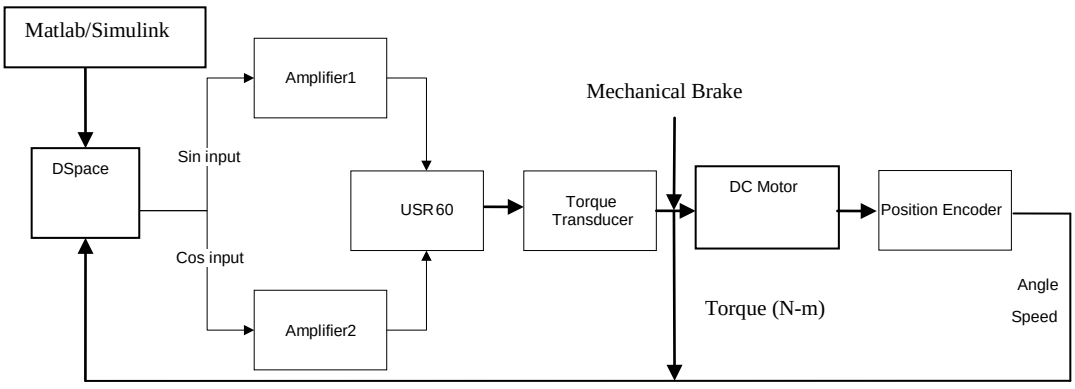

Figure 3-1. Test bench set up for determining the Speed Torque Characteristics

The actual experimental setup is shown in Figure 3-2. A more detailed description of the components of this experimental setup is provided in Section 3.1. Data acquisition methods used in this study detailed in Section 3.2.

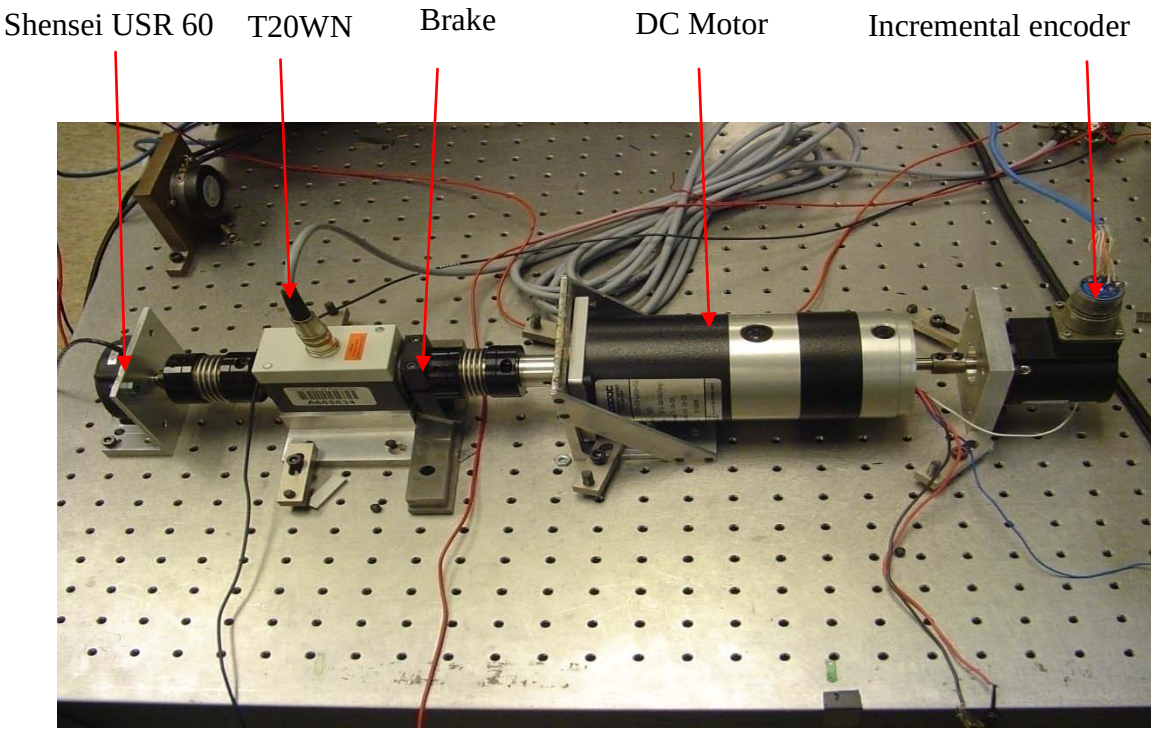

Figure 3-2. Experimental Setup

3.1 Instrumentation

The DSpace control board used for the current work contains 16 input and 8 output channels. Of the 16 input channels 2 input channels are used to supply the excitation signals to the USM. The operating voltage range for the I/O channels is ± 10V. The channels have an operating frequency range of 133 MHz at 16 bit resolution. The following subsections detail the specifications of other components that are used in the experimental setup.

3.1.1 USR 60 Shensei

All experimental testing was conducted with the Shensei USR60 ultrasonic motor. The operating characteristics of the USR 60 are given in the Table 3.1[37]. Note that the response time of the motor is 0.001 seconds. By the response time, it is meant the time taken for the rotational speed of the motor to reach steady state given a step input of the excitation parameters (amplitude, frequency, and phase). This response time is relatively fast compared to dynamics in typical human interface force-feedback applications; human's motion is typically confined to the range of 0 – 5Hz. The response time is thus an important feature, since we can ignore the transient response of the motor, and focus on steady-state response. This will be an important assumption in the control development of Chapter 4.

Table 3.1. Specifications of USR 60

Driving Frequency	50 KHz
Driving Voltage	120 V
Rated Torque	0.5 N-m(5 KgF-cm)
Rated Power	5.0W
Rotational Speed	100 rpm
Maximum Torque	1 N-m or above
Holding Torque	1-N-m or above
Response Time	1 m sec or below
Rotational Direction	CW,CCW
Lifetime	1000 Hrs
Operating Temperature Range	-10ºC to 50ºC
Operating Temperature Range	55ºC
Mass	260 g

3.1.2 AG 1006 amplifier

Two T&C Power Conversion AG 1006 high-voltage amplifiers are used to amplify the DSpace source. The amplifier is a source of RF power used for ultrasonic, industrial, laser modulation and plasma generation. It can supply up to 300 Watts of power with the frequency ranging between 20 KHz to 4 MHz. Note that it is possible to use a single amplifier to provide two signals exactly 90° out of phase. This can be done by integration. In Chapter 4 and 5 we will consider phase control, where the phase must be varied real-time. Performing this task with a single amplifier becomes more difficult in this case. Hence, two amplifiers are used in the test so that an independent sine and a cosine signal can be supplied. Specifications for the amplifier are provided in Ref. 38.

3.1.3 Torque transducer

The shaft of the motor is coupled to the torque transducer, T20WN, which measures the interaction torque between the user input provided by the DC motor and the USM. The nominal torque rating of the transducer used is 5 N-m. The nominal sensitivity is 2V/N-m. The T20WN has an accuracy class of 0.2, which means that the signal range could be 10 V±0.2% (of the nominal sensitivity). Some of the special features of the transducer are contactless transmission of measurement signal, measurement on rotating and stationary parts, integrated measuring system for speed and angle.

3.1.4 Mechanical brake

A mechanical brake is mounted on the shaft of the transducer that is coupled to the DC motor. The brake was made of Nylon in order reduce wear to the shaft of the transducer. By tightening or loosening the brake the torque is increased or decreased, respectively. Figure 3-3 shows a picture of the mechanical brake used in the experiment.

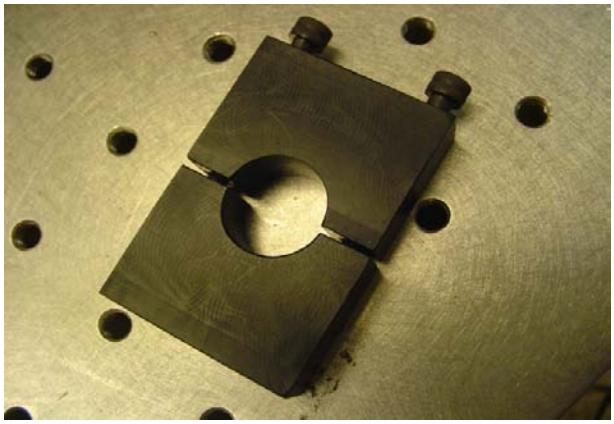

Figure 3-3. Mechanical Brake Provided for Applying Resistive Torque

3.1.5 DC motor

The other end of the torque transducer shaft is coupled to a brush-type DC servo motor (Aerotech 1000 DC) which applies an input force to the USM. The continuous torque ranges from 0.25 N-m to 1.48 N-m and the peak torque ranges from 1.84 N-m to 7.1 N-m. The specifications of the motor are provided in Table 3.2.

Table 3.2. Specifications of DC Motor

Model number	1000 DC
Motor K_T	4.1 oz-in/amp
Continuous Torque	17 oz-in
Peak Torque	130 oz-in
Tachometer Kg	3V/KRPM

3.1.6 Rotary Incremental Encoder

The shaft on the other end of the DC motor is coupled to a rotary incremental encoder which generates two data signals that are electrically 90º out of phase [39]. Three signals are given by the encoder, A, B and index, where A gives the position when the encoder shaft moves in clockwise direction, while B gives the signal when it moves in counter clockwise direction. The index signal is given by the respective pins mentioned in Ref. 39. A few of the specifications of Model 8225 are given in Table 3.3 [39].

Table 3.3. Specifications of Incremental encoder

line count on disc	6,000
cycles/rev with internal electronics	48,000
counts/rev (after quad edge detection)	192,000
cycles/rev with external electronics	120,000
Instrument error	± 20 arcsec

3.2 Data Acquisition

All control simulations were conducted in Matlab Simulink and all data were recorded by DSpace. The basic Simulink block diagram framework is shown in Figure 3-4. This Simulink code is used to experimentally evaluate the steady state characteristics of the motor (Chapter 4), and is later updated for control experiments (Chapter 5). The baseline simulation frequency is set to 160kHz, four times the vibration natural frequency of the USM. Two input signals with a phase shift are supplied to the amplifiers through two DAC channels with a gain (labeled as *gain*). Each of these signals must be amplified to 130 V before provided to the USM. This amplification is performed by adjusting the gains manually on the T&C amplifiers. By adjusting the gains on the T&C amplifier it is difficult to obtain two voltage signals exactly equal to 130V. By adjusting the gain values in Simulink, minor tuning of the signals can be performed to obtain two voltage signals exactly equal to 130 V. A change in the rotational direction of the motor is induced by the switches (labeled *Direction Change Switches* in Figure 3-4). For a positive value the motor rotates in the forward direction, and for a negative value the motor rotates in the reverse direction. The saturation block (labeled *Saturation* in Figure 3-4) maintains the frequency within specified operating limits; this feature is required for feedback control using frequency modulation. The atomic subsystem shown in Figure 3-4, is used to sample the angular position and the change in angular position, interaction torque, and load torque supplied by DC motor. The measurements made within the subsystem are later used as feedback signals to perform control. The sample frequency of the atomic subsystem is 1000 Hz.

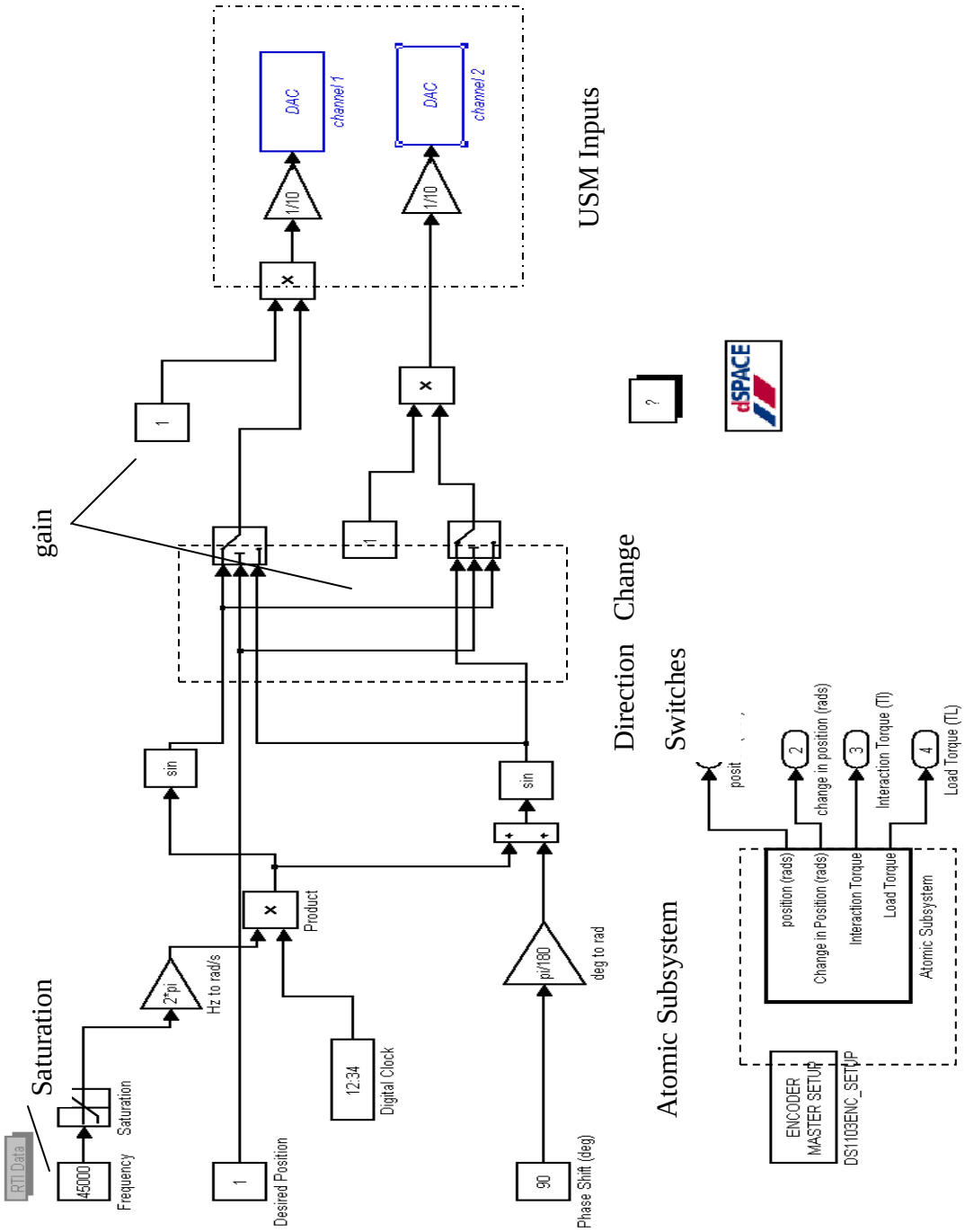

Figure 3-4. Simulink Block Diagram

4 Force Feedback Control

The application considered for the USM is a torque source for haptic systems. Generally, a haptic system is a device that simulates stiffness, weight and inertia [40]. These devices are important in virtual reality simulations, teleoperation, and various "by-wire" systems. Historically, brushless DC motors have been the standard choice for providing force feedback in haptic systems. Due to the unique features mentioned in Chapter 1, the USM may be an attractive alternative in some applications that require higher energy density, low-speed high-torque operation, or those where a magnetic field is intolerable. However, as briefly discussed in Chapter 2, the operating principle of the DC motor is significantly different from the USM. In this chapter we discuss the major differences more thoroughly, with specific regard to force-feedback operation. The major contribution of the work is also contained in this chapter, namely a method of control that can be applied to the USM in force-feedback operation. Because the response time of the motor is fast relative to the human motor action, the control formulation relies on basic steady-state behavior as observed in experiments.

4.1 Force Feedback Operation

The primary difference between the DC motor and the USM is the type of force involved. The DC motor utilizes electromagnetic force while the USM involves contact forces. Figure 4-1 shows the free body diagrams which are subsequently used to discuss the differences in the principle of operation between the two types of motor.

For the DC motor, the output torque is approximately proportional to the current, where K_t is the proportionality factor. The dynamics of a load driven by a DC motor are well approximated by the linear ordinary differential equations

$$J\ddot{\theta}_m + c\dot{\theta}_m = \tau_a + \tau_m$$

$$L\frac{di}{dt} + Ri - k_e\dot{\theta}_m = v \tag{4.1}$$

$$\tau_m = k_t i$$

where θ_m is the rotational velocity of the shaft rotation, J is the inertia of the load, c is a damping coefficient, τ_a is the input torque, τ_m is the motor torque, L is the motor inductance, R is the motor resistance, i is the current, and v is the input voltage.

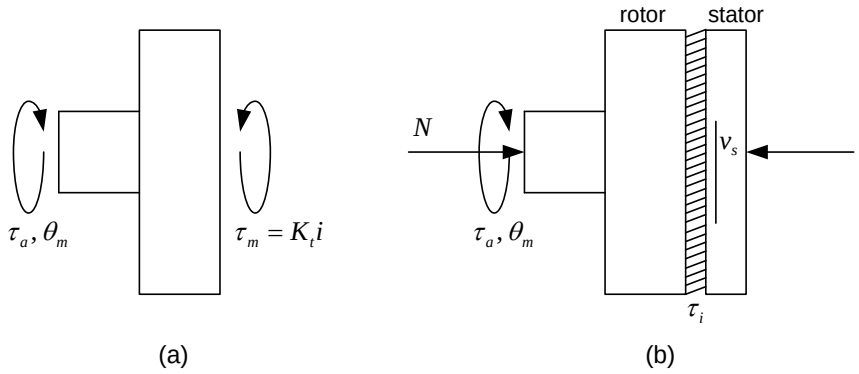

Figure 4-1. Comparison of the torque transmission for a DC motor and an ultrasonic motor: (a) the torque supplied by a DC motor is primarily dependent on the current; (b) torque transmission for the ultrasonic motor is based upon contact friction

The electromechanical conversion for the DC motor is fairly simple. Assuming the inductance is small, the output torque can be directly controlled by the input voltage. For example, the DC motor can mimic a spring damper system by letting

$$v = \frac{R}{K_t}(-b\dot{\theta} - k\theta) - K_e\dot{\theta} \tag{4.2}$$

where k and b are the chosen stiffness and damping. Note that there is no restriction on the torque that can be generated by the DC motor.

In contrast, the USM can generate torque only in the direction of motion and it is not capable of supplying any arbitrarily specified torque in force-feedback operation. This limitation of the USM is apparent when considering that basic operating principles. It can also be demonstrated by considering a simplified model. Consider a simple model of the interaction torque (τ_I) between the stator and rotor, given by

$$\tau_I = \mu N \operatorname{sgn}(v_s / R - \dot{\theta}_m) + c_R (v_s / R - \dot{\theta}_m) \tag{4.3}$$

where N is the compressive force between the stator and rotor, μ is a dynamic friction constant, and sgn denotes the signum function. The interaction torque is thus modeled by Coulomb and viscous terms, dependent on the relative velocities of the stator (i.e., the elliptical surface velocity at the circumference, previously given by Equation 2.3) and the rotor. The model is simplified approximation of the true behavior, but serves the purpose of this discussion. The interaction torque indicated in Equation 4.3 can be controlled by controlling the surface velocity of the stator. However, this is a difficult task because there is no direct measurement of the surface motion of the stator. Estimating the stator motion from measurable outputs such as rotor motion and the strain of the piezoelectric ceramic sensors is also difficult due to modeling difficulty. Hence, direct torque control is not a simple matter.

The basic nature of force-feedback using the USM is demonstrated. Suppose the rotor is moving in the positive direction (ω_m>0), and we would like to produce torque in the opposite direction of motion $\tau_m = -C$, where C is a positive constant, while θ_m is positive, the task is to find v_s such that

$$-C = \mu N \operatorname{sgn}(v_s / R - \dot{\theta}_m) + c_R (v_s / R - \dot{\theta}_m) \tag{4.4}$$

First, note that v_s and ω_m should always be in the same direction, for otherwise this would indicate a forced slipping between the stator and rotor. The situation would occur when an external load torque, τ_L, is applied that is greater than the torque produced by the USM, and in the opposite direction. In general operation this is not a desirable circumstance, resulting in wear of the contacting surfaces. The externally applied torque is thus assumed to be always smaller than the dynamic holding torque of the motor. Then, if the velocity and stator move in the same direction and the USM torque must be negative, it follows from Equation 4.4 that $0 < v_s / R < \omega_m$. However, for the case that $C < \mu N$, there is no v_s that provides the required torque. That is, the motor can only apply torque in direction of rotor motion; hence, τ_M cannot take any arbitrarily specified functional form.

4.2 Force Feedback Control Approach

As discussed in Chapter 2, modeling the torque produced by USM is a difficult task; and the models are not generally suitable for model based control design. The force-feedback control approach studied is shown in the Figure 4-2. The torque input $\tau_{L,}$ supplied by the user generates an interaction torque $\tau_I = \tau_L - \tau_M$, that is measured and input to a shaping function (or a reference model), which produces a reference angle of rotation. The reference signal is compared with the measured rotation angle to produce an error signal, which is input to the control. Although not considered here, in general it is often necessary to add extraneous inputs that are neither dependent on the user input nor the state (i.e., position and velocity) of the haptic interface. However, we will not consider extraneous inputs.

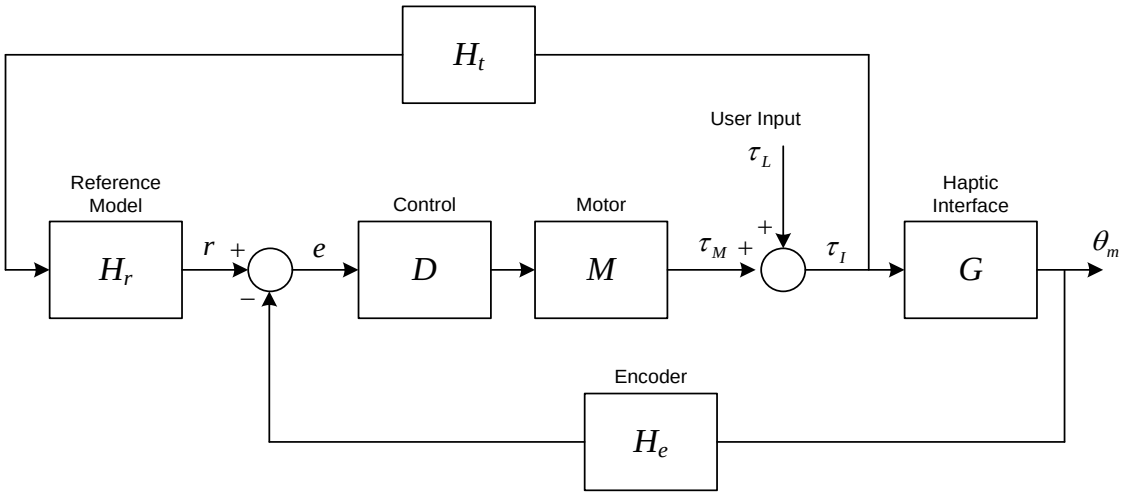

Figure 4-2. Force-feedback approach; input disturbance based position control

In the complex domain, where $L[\cdot]$ indicates the Laplace transform, the relationship between the load torque, $T_L(s) = L[\tau_L]$, and the motor rotation, $\Theta_m(s) = L[\theta_m]$, is given by

$$\Theta_m = \frac{G}{1 - MDH_rH_t + GMDH_e} T_L \tag{4.5}$$

Thus, D and H_r define the force feedback characteristics as a function of the input and the motor state. The system $H_r(s)$ represents the desired response to an externally applied torque, such that $T_L H_r(s) = \Theta_m(s)$ results in $H_r(s) = G(s)$. When M represents the dynamics of a DC motor, it is not difficult to show that the system of Equation 4.6 is non-minimum phase. However, since the torque of the DC motor is easily controlled, this type of model reference control is not necessary. For example, a DC motor with $H_r = 0$ and $D = k_P + k_D s$ would mimic the torque of a linear spring and damper. In contrast the direct torque control of the USM is a difficult task. For the case currently under consideration ($H_r \neq 0$), an input-output relationship between input torque and output position of the motor is examined using Equation 4.6 experimentally. A reference model

approach is utilized to provide force-feedback. Since the USM is considered to be a precise positioning device, this feature of the motor is used for this application.

Under normal operation, the closed loop performance is not based on any extraneous parameters. However, in some cases it is desirable to add additional dynamics to the system, dependent on external conditions. For typical control system architecture, disturbances are added at the junction between the load and the motor. For the current case, this disturbance is due to the input, and cannot be added at this point since it would not be an independent input. To act as an independent external disturbance, this input should be placed at the junction between the motor and the control input; thus, the disturbance is induced by the motor. As previously discussed, to generate an arbitrarily specified disturbance is a difficult task. In contrast, with the DC motor, the control input for a desired disturbance input can be determined from a model. Additionally, the control input for the USM contains several variables (amplitude, phase, frequency) that can be used to alter the disturbance.

4.3 Steady State Properties

Based on the discussion in Chapter 3 (Section 3.1.1), we assume that the steady state response of the USM will have more significant influence than the transient characteristics for haptic applications. With this assumption, we develop control algorithms based on the steady-state input-output characteristics of the USM.

To determine the steady-state characteristics, the control inputs given to the USM are two high-voltage, high-frequency signals of the form

$$v_1 = A\cos(2\pi ft), \quad v_2 = A\cos(2\pi ft + \theta) \tag{4.6}$$

where A is the voltage amplitude (held fixed at 130 Vrms), f is the frequency (in the range of 40 KHz), and θ is the phase difference between the two signals. The effect of these parameters on the steady state torque-speed characteristics are illustrated in the following sections. Based on the discussion in Chapter 2 (Section 2.4), we do not examine the effects of varying amplitudes on the motor's performance.

4.3.1 Effects of frequency modulation

The steady-state no-load operation of the motor is shown in Figure 4-3, when A=130V, θ=90˚, and frequency f ranges between 40-45KHz. The nature of response is indicative of the vibration near resonance. A frequency input near resonance generates the largest vibration amplitude of the stator. When the frequency shifts away from the resonance, there is a reduction in vibration amplitude and hence a reduction in elliptical surface velocity of the stator, which results in decreased speed of the motor. We can also notice a hysteresis in the motor's behavior, when the frequency is increased and then brought back to a lower value. This hysteresis can be attributed either to temperature effects and/or the nonlinearity of the motor. The motor's response can be significantly affected by the operating temperature, but its effects are not examined because it can be accounted for by feedback control. Below 40 KHz, the motor stops suddenly due to the anti-resonance. Hence, the operating range of the motor is between 40 KHz and 45 KHz.

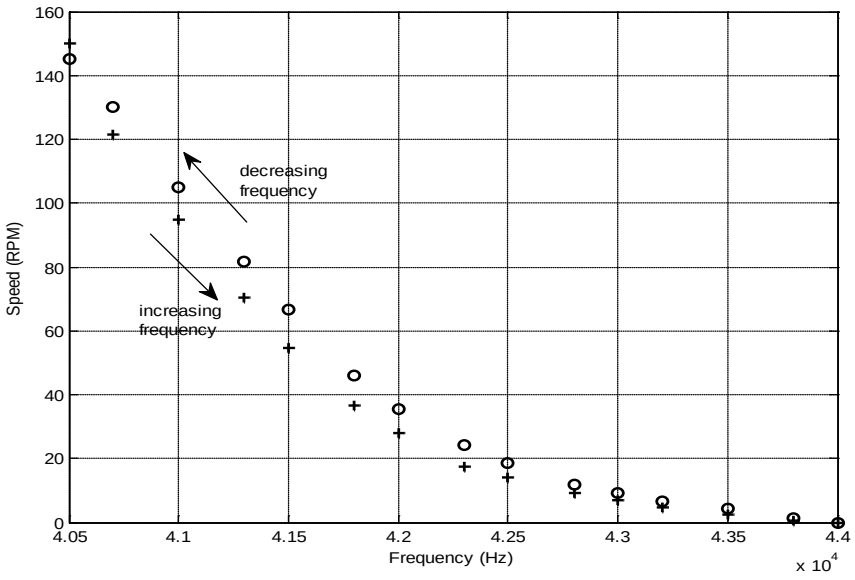

Figure 4-3. Speed Vs Frequency

4.3.2 Torque Speed Characteristics for Various Frequencies

Torque-speed characteristics for various excitation frequencies are shown in Figure 4-4. Both positive and resistive torque is applied to the motor. A resistive torque is applied to the motor by using a mechanical brake, while a positive torque is applied by the DC motor. The positive numbers on the figure indicate that the torque is resistive and the negative numbers indicates positive torque. Figure 4-4 demonstrates that the motor can generate any counteractive steady state torque, within a range of 1 N-m. The speed-torque characteristics of the motor also show that the behavior is fairly predictable. In general, to increase the output motor torque, the frequency should be decreased and vice versa.

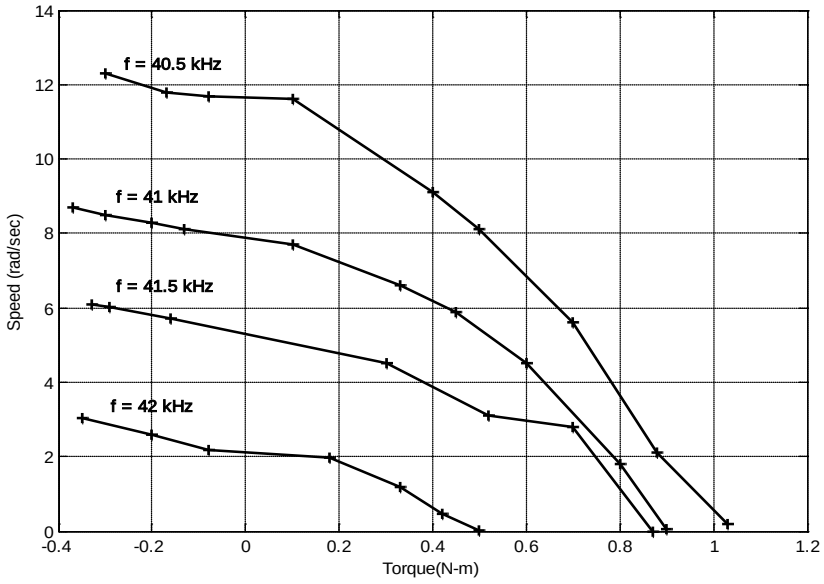

Figure 4-4. Speed Vs Torque curves for various frequencies

4.3.3 Effects of phase modulation

It is well known that the surface velocity of the stator is maximum when a perfect traveling wave is generated; hence, this will also generate the maximum torque and the maximum motor speed. As discussed, a perfect traveling wave is generated when the excitation signals are supplied exactly 90° out of phase. When the phase difference between the two excitation signals is not exactly 90°, a perfect traveling wave is not generated, and the surface velocity of the stator is reduced. This in turn reduces the motor's speed. The phase control algorithm is developed based on these basic characteristics.

The steady-state operation of the motor when A = 130V, and f = 41.5 kHz, and θ is varied between ±90° is shown in Figure 4-5. For a large region, there is an approximate linear relationship between the phase and the motor speed. However, there is a "dead-zone" on each side of the zero-degree phase shift in which there is no motion. A zero-degree phase shift implies that the stator exhibits purely standing wave motion, in which case the surface transmits no

momentum in the transverse direction; this phenomenon is sometimes referred to as the stick slip error [41]. As the phase shift is increased, both standing wave and traveling wave motion is present. Apparently, the energy required to overcome the interaction friction between the rotor and stator is not exceeded until the surface motion reaches a sufficient velocity, characterized by the traveling wave motion, and thus characterized by the phase shift. From Figure 4-4, it is clear that the dead zone increases with external load. It is expected that control of motor using phase modulation is more complicated, relative to frequency modulation, due to the presence of the dead zone.

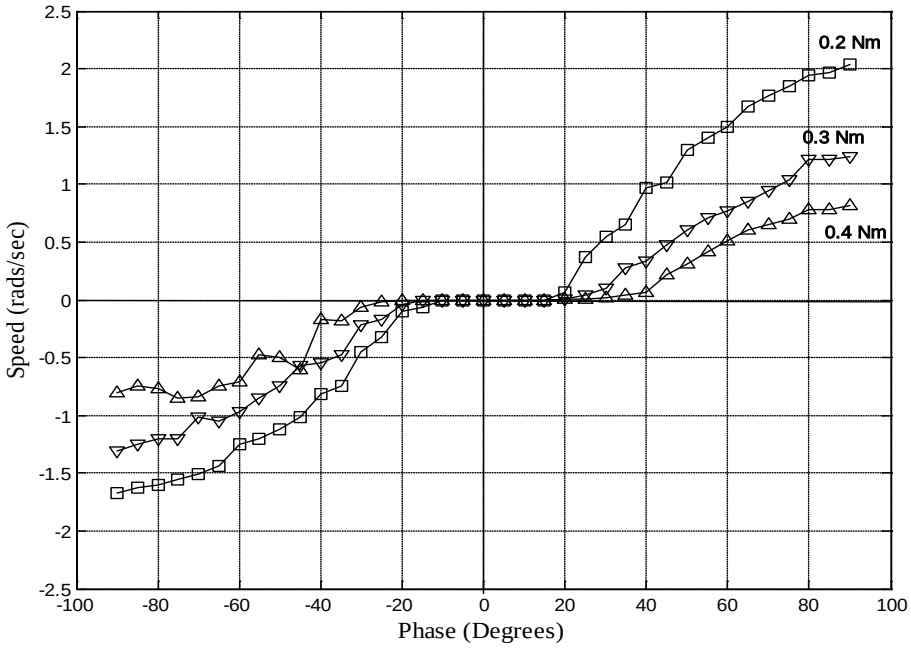

Figure 4-5.Speed Vs Phase for various Torque

The steady state torque-speed curves of the motor is measured while operating the motor between ± 90°, at different frequencies (40.5 KHz, 41 KHz, 41.5 KHz), A=130 V, as shown in

Figure 4-6, Figure 4-7, and Figure 4-8, respectively. Similar results can be found in Ref. 35. From the figures, the speed of the motor decreases with increase in frequency. The curves above the zero-speed represent the resistive torque values, while the curve below the zero represents the negative torque values. Note that the curves are mirror images each for both positive and negative phase difference. The plots also indicate that the torque speed curves follow a similar trend for different phase shifts.

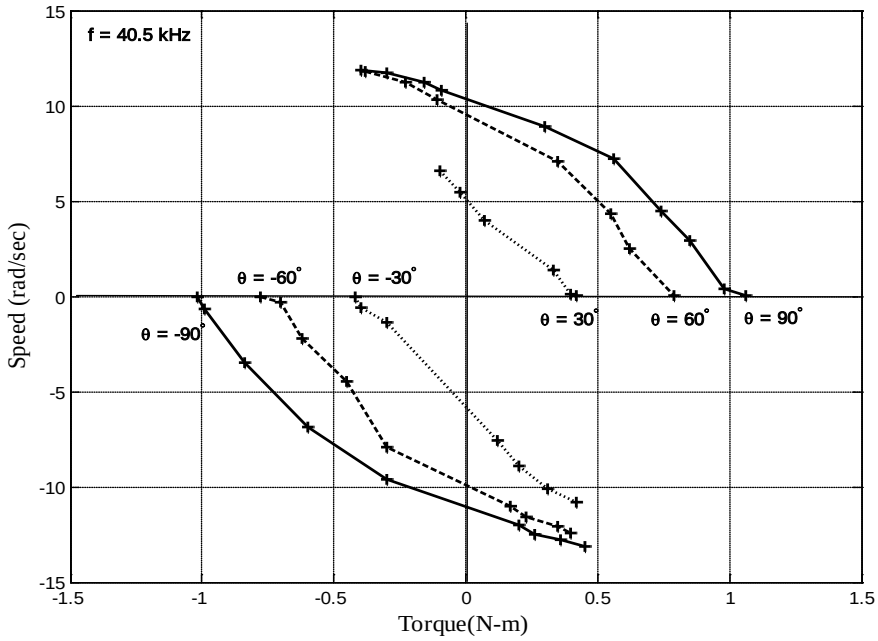

Figure 4-6.Speed Vs Torque curves for a phase range at 40.5K Hz

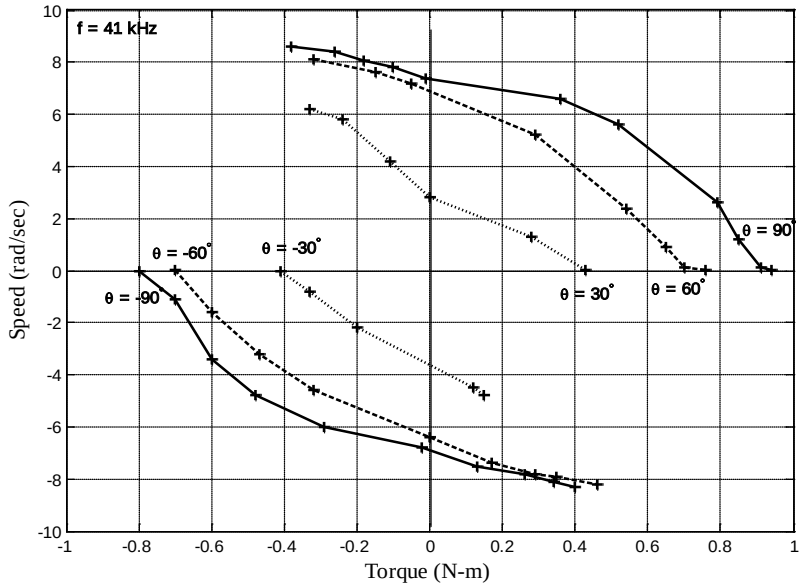

Figure 4-7.Speed Vs Torque curves for a phase range at 41K Hz

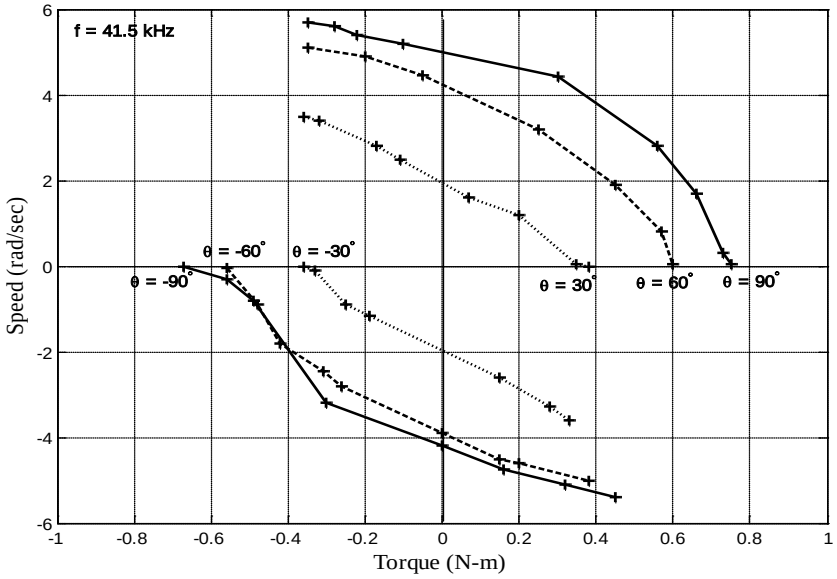

Figure 4-8. Speed Vs Torque curves for a phase range at 41.5K Hz

4.4 Control Formulation

Based on the steady state properties, it is clear that the torque of the motor can be varied by varying the frequency or the phase. The motor torque increases with a decrease in frequency. The motor torque is increased with an increase in phase. Subsequent experimental analysis of force-feedback operation is limited to simple control formulations based on these steady state observations. The following sections detail the control algorithms based on the two parameters frequency and phase.

4.4.1 Frequency Control

Position error is defined as $e(t)=r(t)-\theta(t)$, where $r(t)$ is the reference position and $\theta(t)$ is the measured position. The frequency is modulated based on the relation

$$u_f = \begin{cases} f_{\max} - (k_P e + k_I \int e + k_D \dot{e}), e > 0 \\ f_{\max} + (k_P e + k_I \int e + k_D \dot{e}), e < 0 \end{cases} \tag{4.7}$$

where, f_{max} is the upper limit in frequency where the velocity becomes approximately zero and f_{min} is the lower frequency limit corresponding to the upper motor speed. A limit is set on the lower frequency because there is an abrupt increase in speed when the resonance is passed. The voltage amplitude is controlled by

$$A = \begin{cases} A_n, e > 0 \\ -A_n, e < 0 \end{cases} \tag{4.8}$$

where A_n =130V, change in amplitude is required to change the direction of motor. Note that the direction of the motor depends on the sign of the error and not the sign of the control input.

4.4.2 Phase Control

Holding the driving frequency constant $f=f_o$, we define the phase control law

$$\theta = k_p e + k_I \int e\,dt + k_d \dot{e} \tag{4.9}$$

The amplitude of input voltage is same as given is Equation 4.4. Recalling the stick-slip phenomenon shown in Figure 4-3, there is a potential that the output motion is zero even when phase is non-zero. We expect that a high integral term should be useful in accounting for this dead-zone nonlinearity.

The Simulink block diagram for frequency control and phase control are presented in the Appendix B.

4.5 Summary

The limitations of the USM such as, incapability of generating torque in the opposite direction of motion and difficulty of generating an arbitrarily specific torque are the main reasons for resorting to an indirect control approach. For force feedback applications developing an input-output relationship between input torque and output motion is desired. Hence, we developed a model reference control approach to perform force-feedback operations. Since the motor's response is faster when compared to human motor action, it is assumed that the steady state properties of the USM influence its performance in haptic applications. The steady-state input-output properties of the motor are determined experimentally from the experimental setup. These results are further used to develop control algorithms.

5 Experimental Evaluations

Since our force-feedback approach is based on position control, basic performance without externally applied torque is first investigated. These results are followed by force-feedback experiments to evaluate the motor's performance in simulating the input-output response of simple second-order systems, i.e. a spring and damper.

5.1 Position Reference Tracking

This section demonstrates the position tracking performance of the USM for the frequency modulation technique (Section 5.1.1) and the phase modulation technique (Section 5.1.2). A block diagram of these experiments is shown in Figure 5-1. This is identical to the block diagram of Figure 4-2, but with no interaction torque feedback.

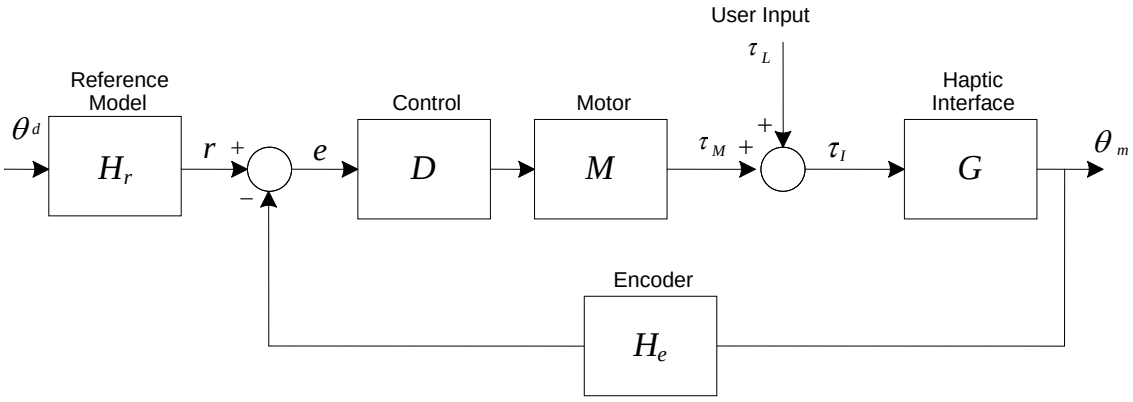

Figure 5-1. Constant Reference Tracking

We tested three types of reference inputs: a step input, a filtered step input, and sinusoidal inputs.

For the filtered step input, two systems are considered: a first order system of the form

$$H_r = \frac{K}{s + 1/\tau} \tag{5.1}$$

and a second-order system

$$H_r = \frac{K\omega_n^2}{s^2 + 2\zeta\omega_n s + \omega_n^2} \tag{5.2}$$

The responses due to these inputs will be referred to as the *first-order input response*, and *second order input response*, respectively. The first-order input response is used in cases where the step input resulted in an erratic response of the motor; a smooth input is typically required for nonlinear systems. The following subsection present position tracking results for the three types of reference inputs. The results are intended to demonstrate the basic effects of the control parameters.

5.1.1 Frequency Control

In case where the position is controlled by monitoring the frequency, the upper limit (f_{max}) plays a vital role in precise position control. At very low frequency values, the steady state oscillations become greater in tracking control. In contrast, the steady state oscillation amplitude at f_{max} was found to be around 0.0075°. Hence the upper limit of the excitation frequency is set to 45 KHz. Figure 5-2 demonstrates the effect of frequency on the steady-state oscillations.

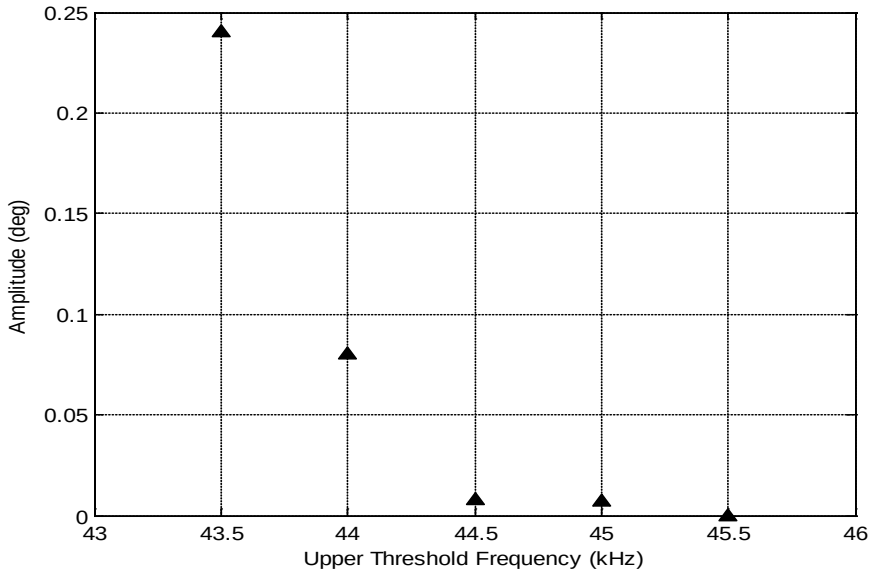

Figure 5-2. Effects of upper frequency (f_{max}) on steady-state tracking performance

The following results demonstrate the first-order input response under frequency control. The effect of proportional gain on motor's tracking ability is shown in Figure 5-3 and Figure 5-4 . As expected, the closed-loop response time increases with an increase in the proportional gain. Figures Figure 5-5 to Figure 5-8, show the effect of derivative and integral gain on the motor's tracking. While the integral gain does drive the error to zero, the time this takes is typically on the order of 10 seconds. For K_I >3.5, the system became unstable. From Figure 5-7 it is observed that with an increase in differential gain the damping in response increases as expected. These tracking experiments indicate that proportional gain plays a predominant role when compared to integral and derivative gains in achieving better tracking response.

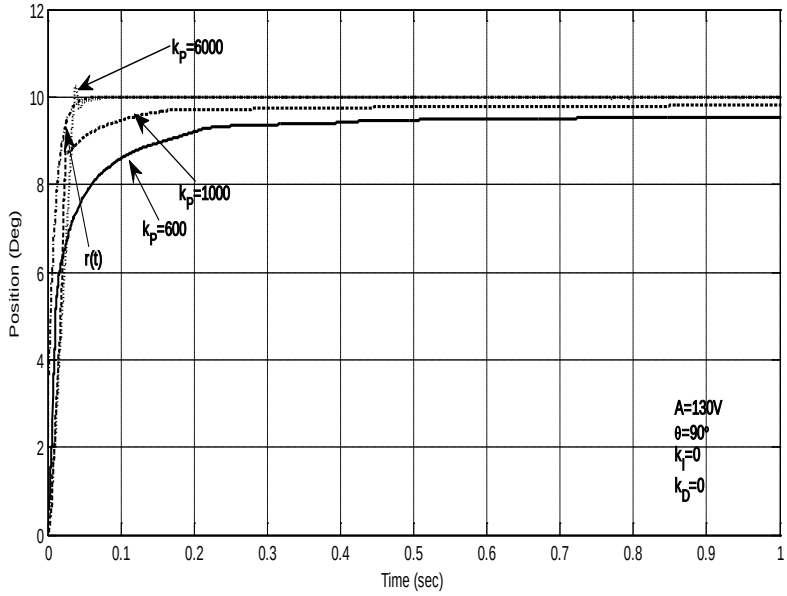

Figure 5-3. Effects of proportional gain on constant reference tracking frequency control; $r(t) = 10°$

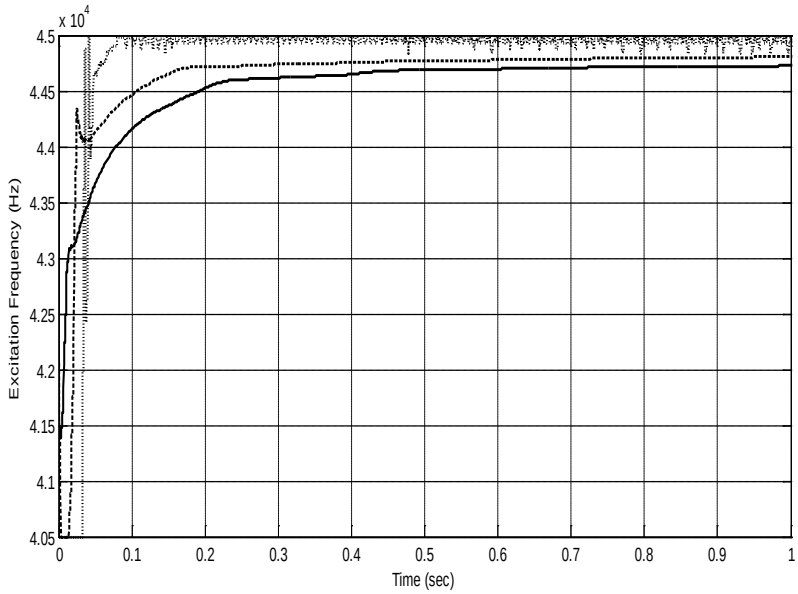

Figure 5-4. Commanded excitation frequency corresponding to Figure5-3

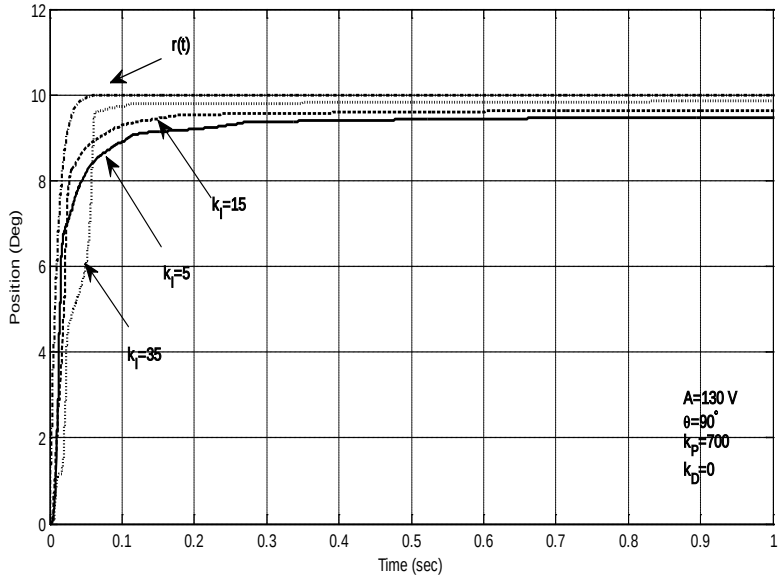

Figure 5-5. Effects of integral gain on constant reference tracking frequency control; $r(t) = 10°$

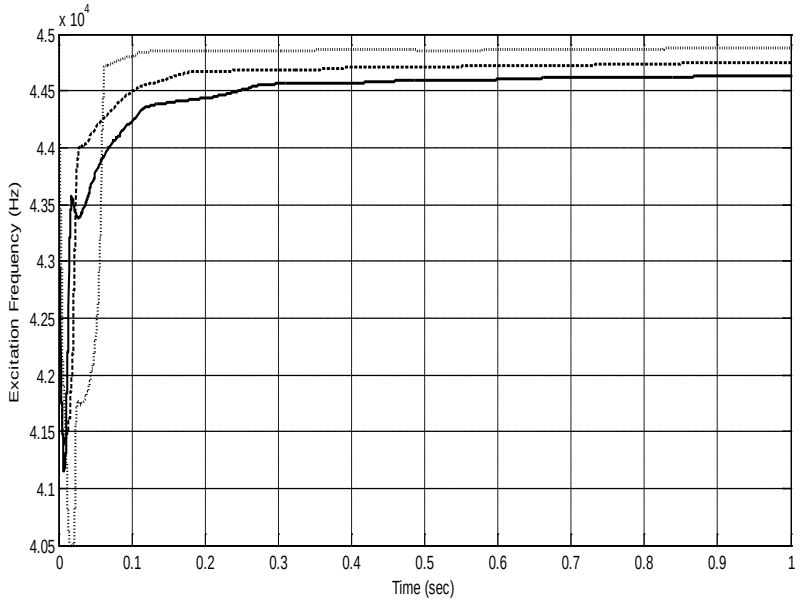

Figure 5-6. Commanded excitation frequency corresponding to Figure5-5

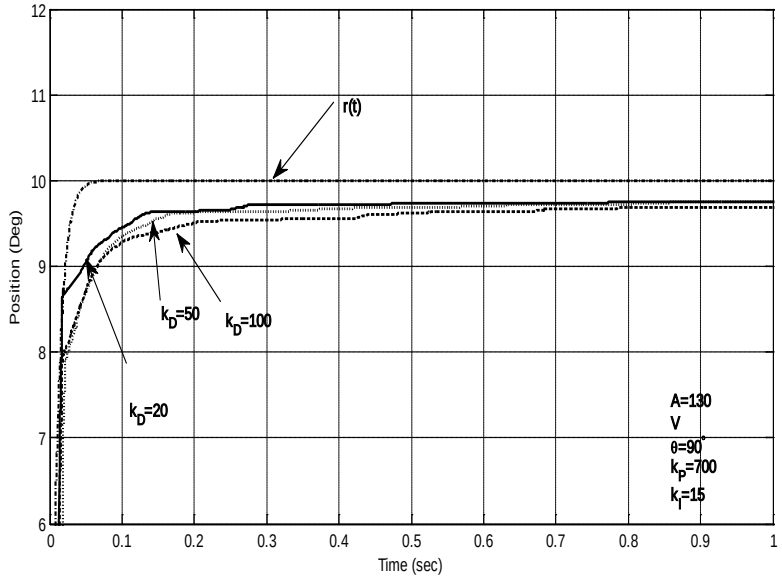

Figure 5-7. Effects of derivative gain on constant reference tracking frequency control; $r(t) = 10°$

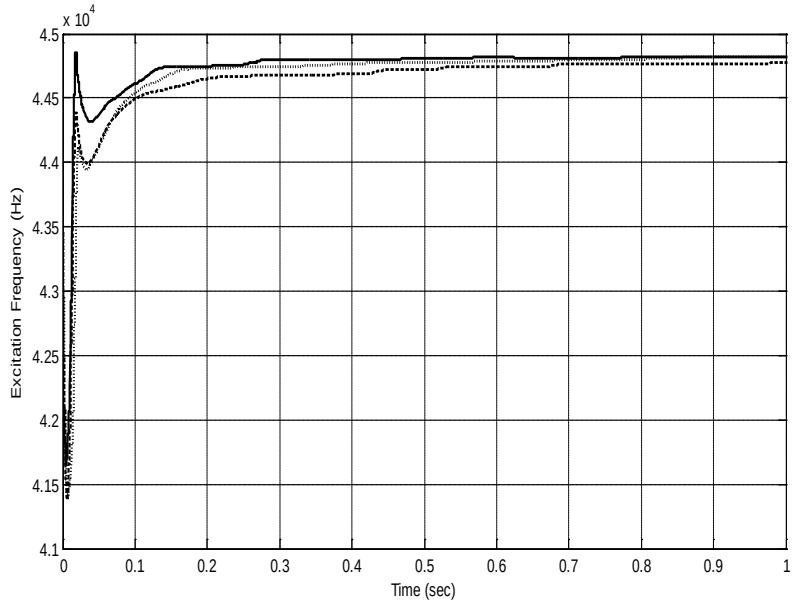

Figure 5-8. Commanded excitation frequency corresponding to Figure5-7

Figure 5-9 to Figure 5-12 show the second-order input response for varying proportional and integral gains. The reference input is of the form given by Equation 5.5 where ω_n, the natural frequency is set to 18 rad/sec and the damping ratio is ζ=0.7. The derivative gain had a minimal effect on the tracking results; these results are included in Appendix A.

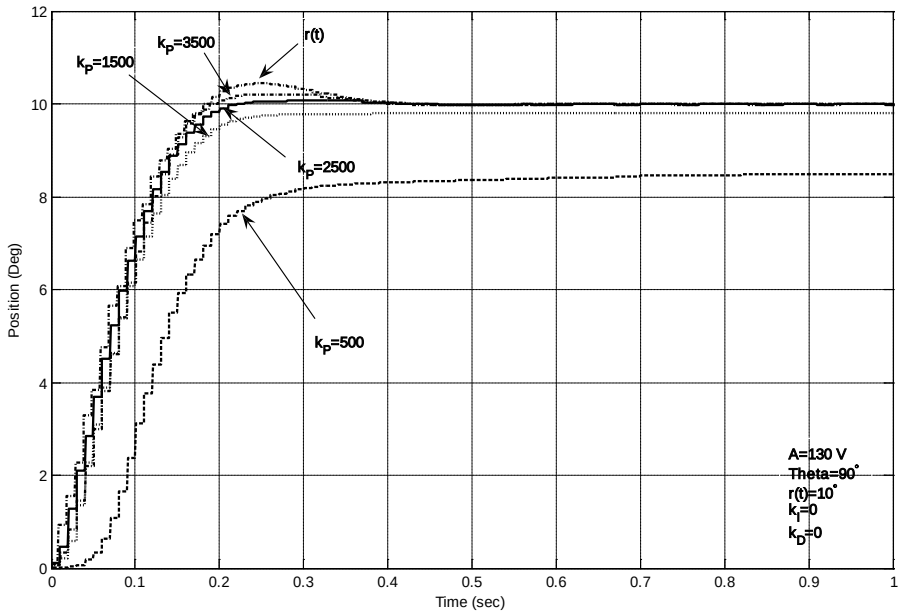

Figure 5-9. Effects of proportional gain on model reference tracking frequency control

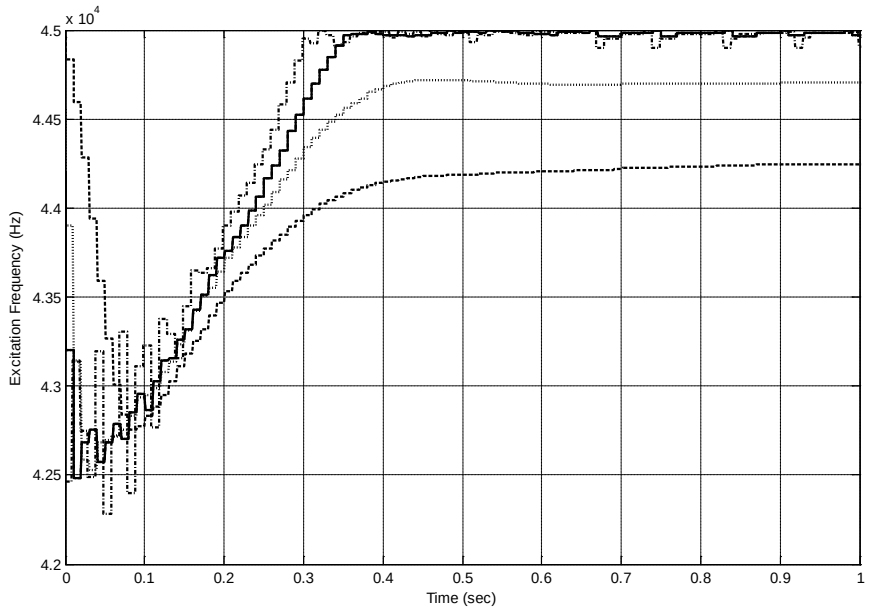

Figure 5-10. Commanded excitation frequency corresponding to Figure 5-9

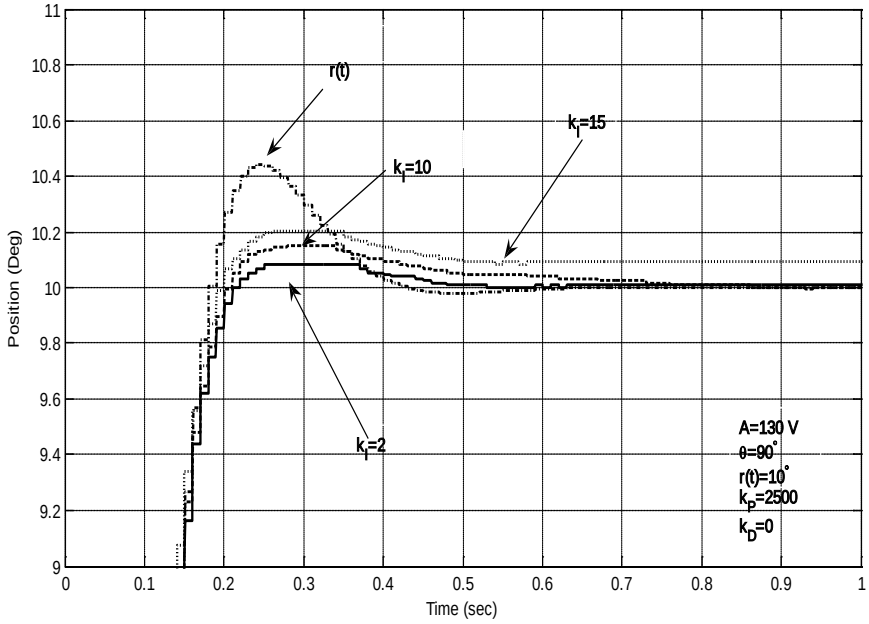

Figure 5-11. Effects of integral gain on model reference tracking frequency control

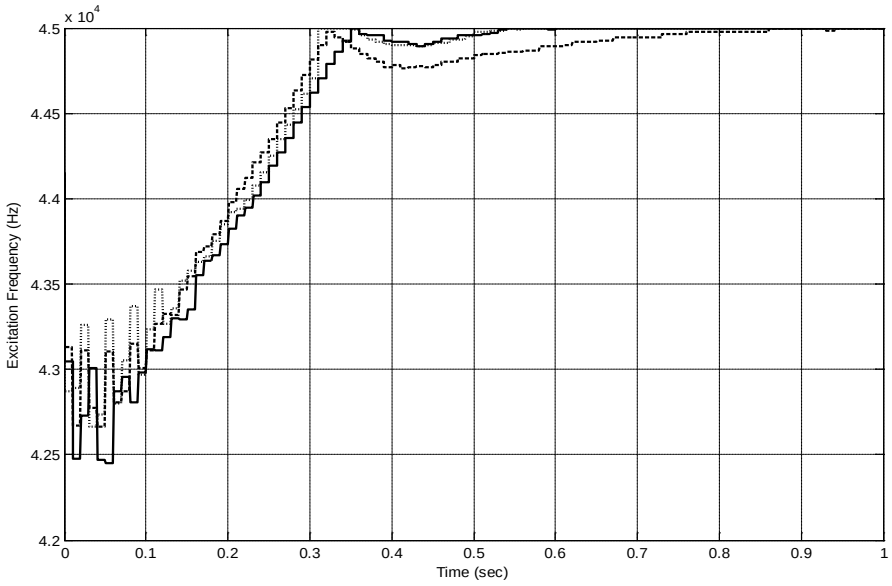

Figure 5-12.Commanded excitation frequency corresponding to Figure 5-11

Position tracking performance for sinusoidal inputs $r(t)=10\sin\omega t$ deg, is shown in Figure 5-12 in the form of a closed-loop frequency response. The chosen reference model (Equation 5.2) indicates a desire that that $\Theta(i\omega)/\ r(t)$, exhibit a second order response, identical to a spring damper system. Frequency response plot helps in analyzing the behavior of the closed-loop system. The frequency response, is of course, a function of the control gains; the results are for k_P = 1000, k_D = 1, k_I = 20. As shown, the closed-loop system for these control gains has a bandwidth frequency of approximately 20 Hz. Note that the closed-loop response appears similar to a second-order system.

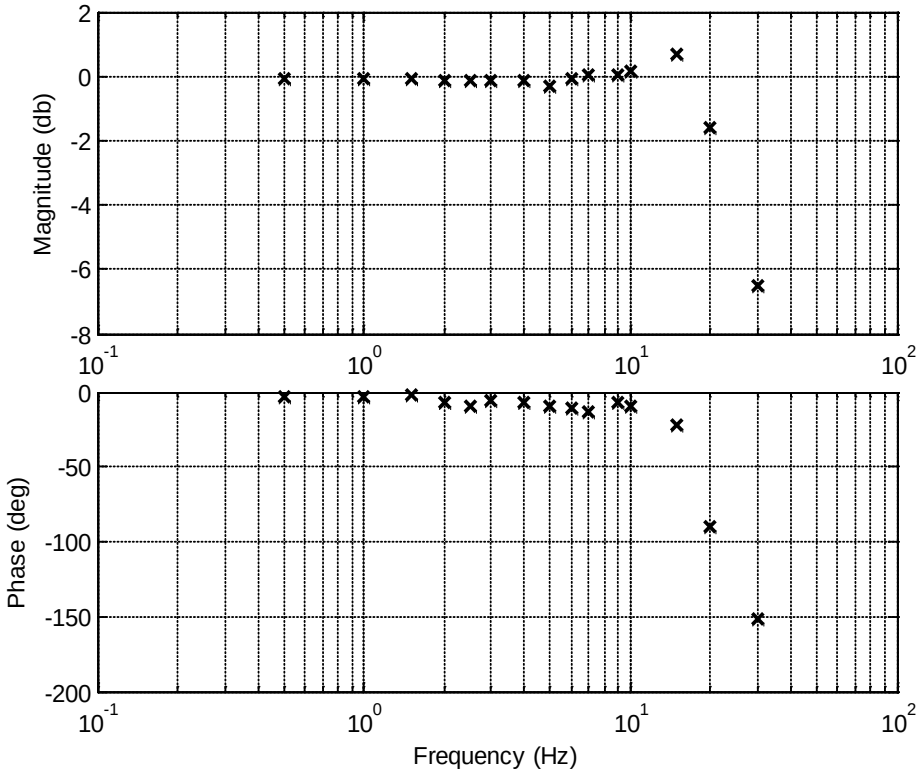

Figure 5-13. Experimental closed-loop frequency response of position reference tracking.

5.1.2 Phase Control

The frequencies at which these experiments are conducted at f_o= 41.5 KHz and 42.5 KHz. It was observed that 41.5 KHz frequency enabled the required speeds for model reference tracking. In case of position tracking with phase control, the primary challenge is to control the motor near the dead zone region (refer to the discussion of stick-slip in Section 4.2.3). In particular for proportional gains, when the error becomes small, the phase shift also becomes small. At some error value the phase shift will be non-zero, but not large enough to drive the motor. These experiments were conducted to demonstrate the effects of the gains on the system's step response. Figure 5-13 and Figure 5-14 show the effect of proportional gain on the closed-loop response of the motor using phase control. For K_p = 7 the steady-state error is relatively large.

The reason for this is shown in Figure 5-15, which shows a commanded phase of approximately 10 degrees. This phase is within the dead-band region of the steady-state speed/phase response (cf. Figure 4.). Hence, the motor stops rotating within this region. For proportional gain K_p=15, the position of the motor overshoots from the desired position and the steady-state error does not go to zero, once again, due to dead-zone effect.

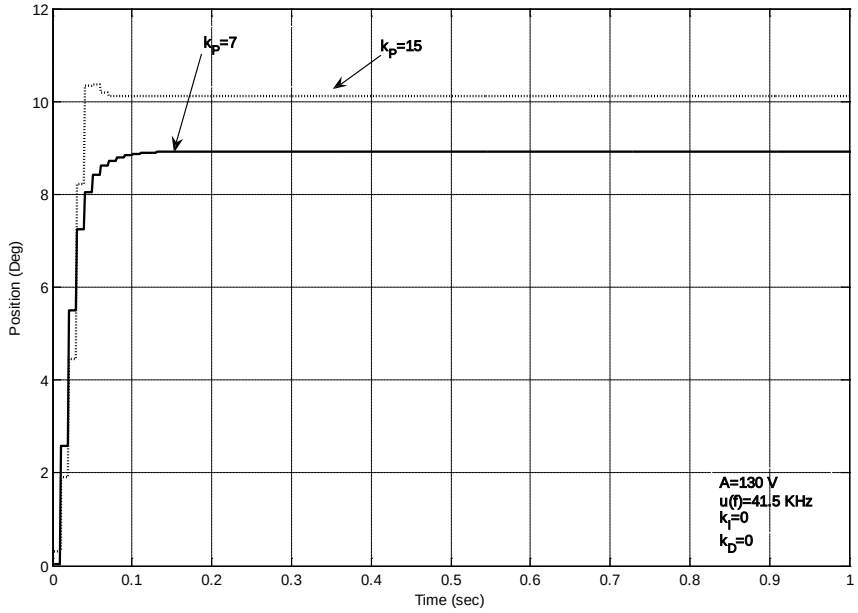

Figure 5-14. Effects of proportional gain on constant reference tracking phase control.

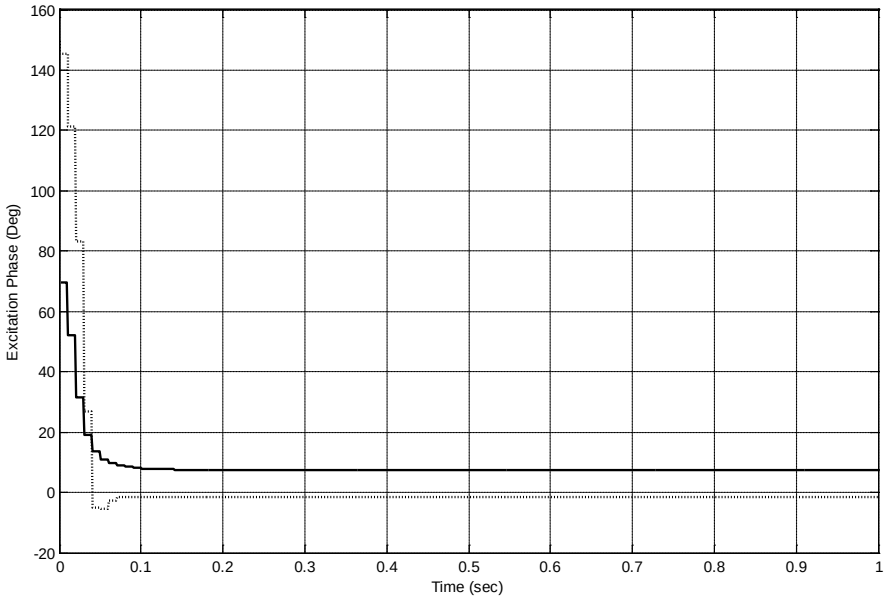

Figure 5-15. Commanded excitation phase corresponding to Figure5-14

Inclusion of an integral gain improves tracking performance, which is shown in Figure 5-15 and Figure 5-16. While the integral gain does drive the error to zero, the time this takes is typically large, on the order of 100 seconds. However, it is not possible to make the integral gain large, as it produces unstable motion. For $K_I > 10$, the system becomes unstable. The effects of the derivative gain are minimal; they are provided in Appendix A.

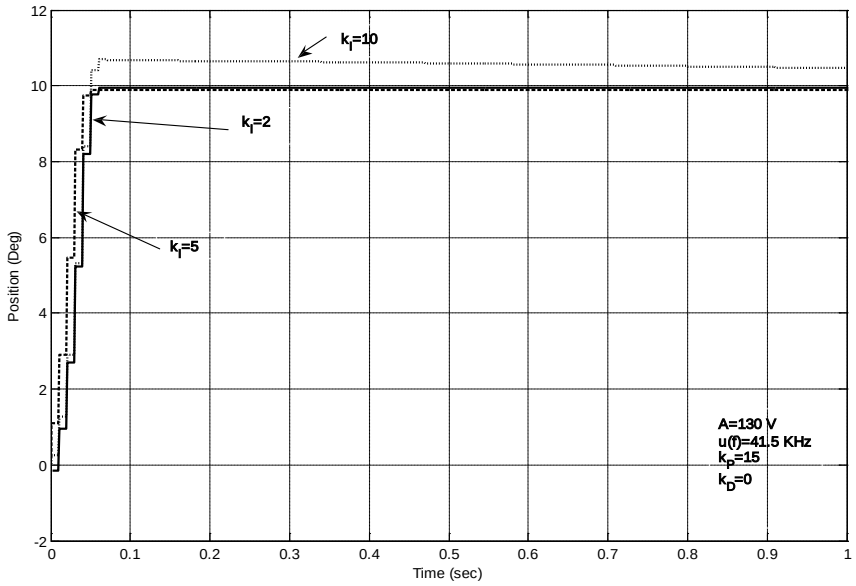

Figure 5-16. Effects of integral gain on constant reference tracking phase control.

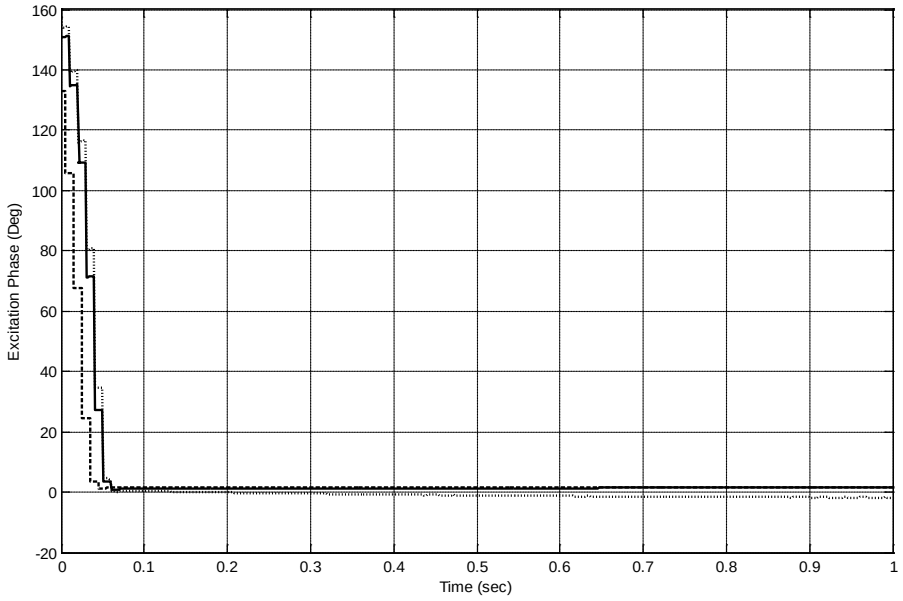

Figure 5-17. Commanded excitation phase corresponding to Figure5-16

Second-order input tracking with phase control is shown in Figure 5-17 to Figure 5-20. The tracking with phase control was less effective than frequency modulation, primarily due to the low phase dead-zone. Higher proportional gains than those shown produce unstable motions

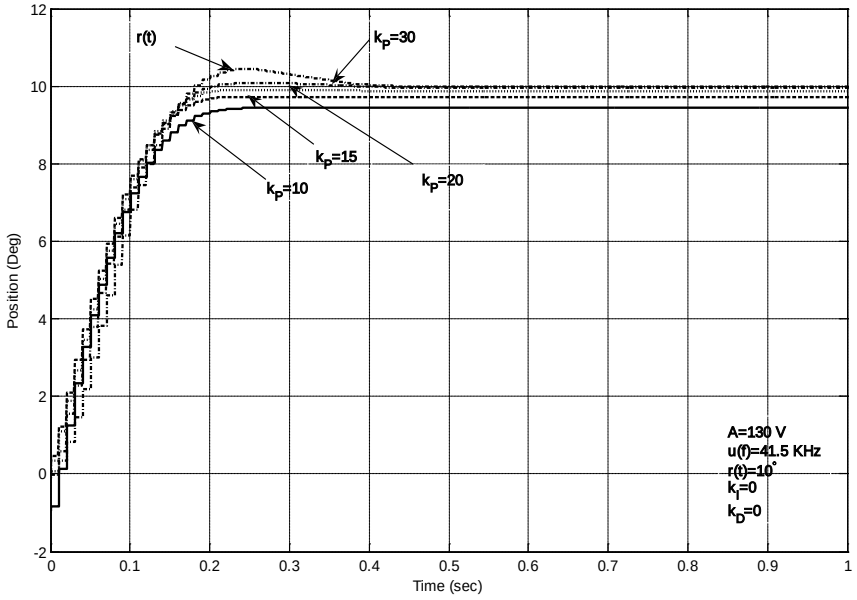

Figure 5-18. Effects of proportional gain on model reference tracking frequency control

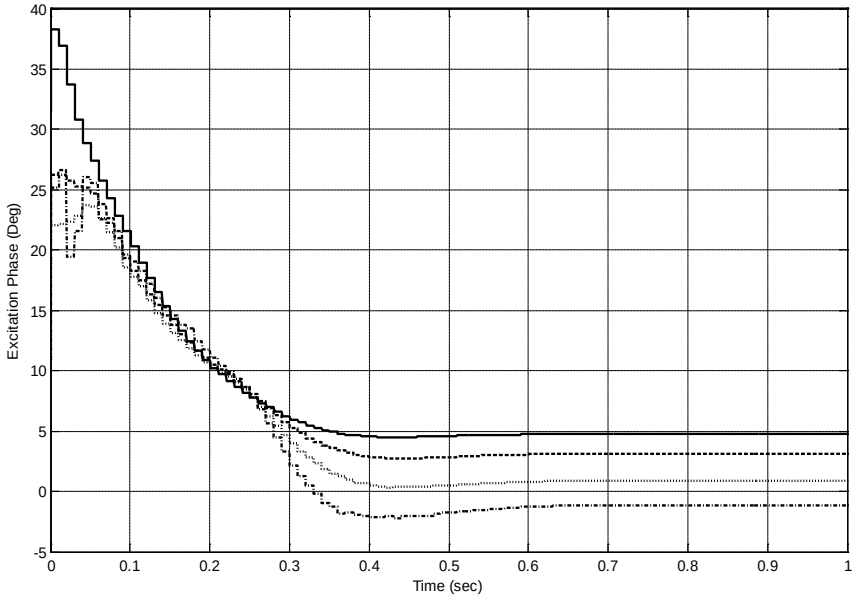

Figure 5-19. Excitation phase corresponding to Figure 5-18

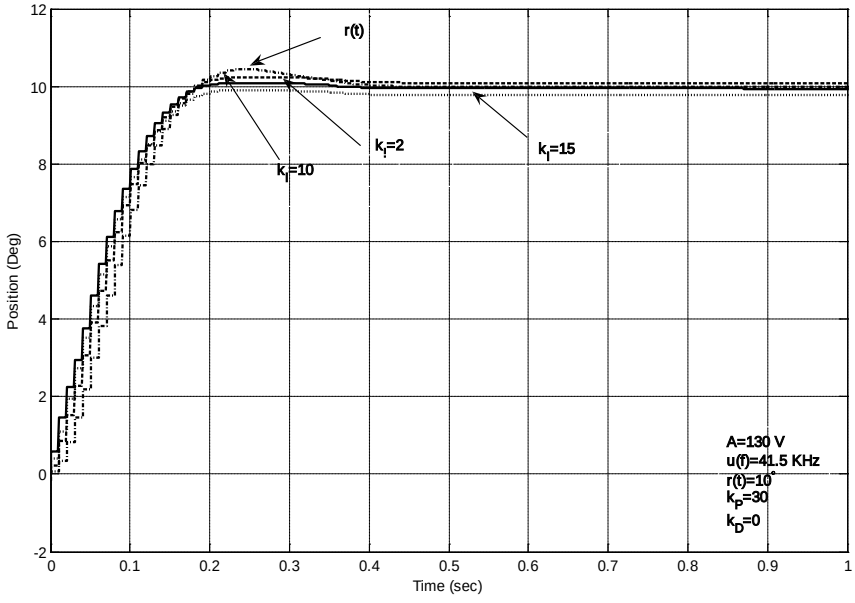

Figure 5-20. Effects of integral gain on model reference tracking frequency control.

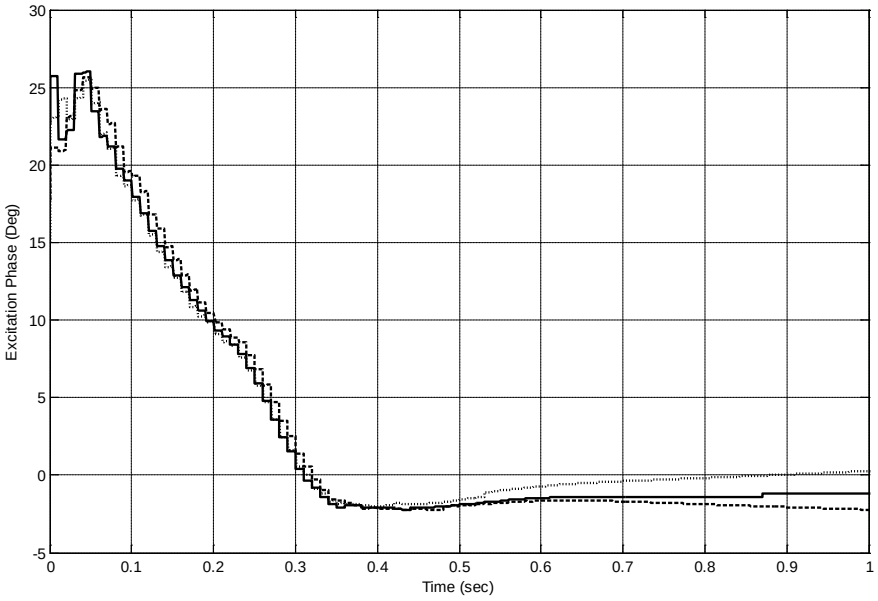

Figure 5-21. Excitation phase corresponding to Figure 5-20

Before evaluating the motor's closed-loop response for force-feedback application, disturbance rejection experiments were conducted. These experiments were performed by applying a constant torque input, and with $H_r = 0$. The results of these experiments are presented in Appendix A.

5.2 Force Feedback

As previously mentioned, the force-feedback control approach is designed to produce a specified input-output relationship, indicated by H_r, between input torque and the output motion. From Figure 4-2, the system $H_r(s)$ represents the desired response to an externally applied torque, such that $T_L H_r(s) = \Theta_m(s)$ results in $H_r(s) = G(s)$. That is, when the output rotation is equal to the reference $r(t)$, the closed-loop system behaves as the reference model. The chosen reference model indicates a desire that that $\Theta(i\omega)/\ T_L(i\omega)$ exhibit a second order response, identical to a

linear spring-damper system. As discussed in the previous section, we do not expect that the motor can produce such a torque. Rather, we seek to determine if an approximation to the input-output relation can be obtained.

For the following experiments, we set H_r equal to the second-order system given by Equation 5.2. Two types of user inputs are evaluated: a second order input of the form

$$T_L(s) = \frac{A\omega_L{}^2}{s(s^2 + 2\zeta\omega_L + \omega_L{}^2)} \tag{5.3}$$

and a sinusoidal user input of the form

$$T_L(s) = \frac{A}{s^2 + \omega_L^2} \tag{5.4}$$

As before, second-order inputs are supplied instead of step inputs because step inputs resulted in erratic response of the motor.

5.2.1 Force Feedback-Pulse Input

Second order user inputs of A =0.05 N-m torque, with natural frequencies ω_L =2 Hz and 3 Hz and a damping ratio ζ=0.5 are supplied. Force-feedback performance under frequency control (Equations 4.7 and 4.8) is shown in Figure 5-22 and Figure 5-24. In these figures $\theta(t)$ indicates the rotational response of the motor and $r(t)$ is the reference. Figure 5-22 show position tracking for a 2 Hz input torque when the gains are K_P=250, K_I=1.75 and K_D=30. Inclusion of integral gains improves the tracking for K_I <1.75. Figure 5-24 show position tracking for a 3 Hz input torque, when the gains are K_P=400, K_I=30 and K_D=0. For this case, the output response becomes unstable for K_I >30.

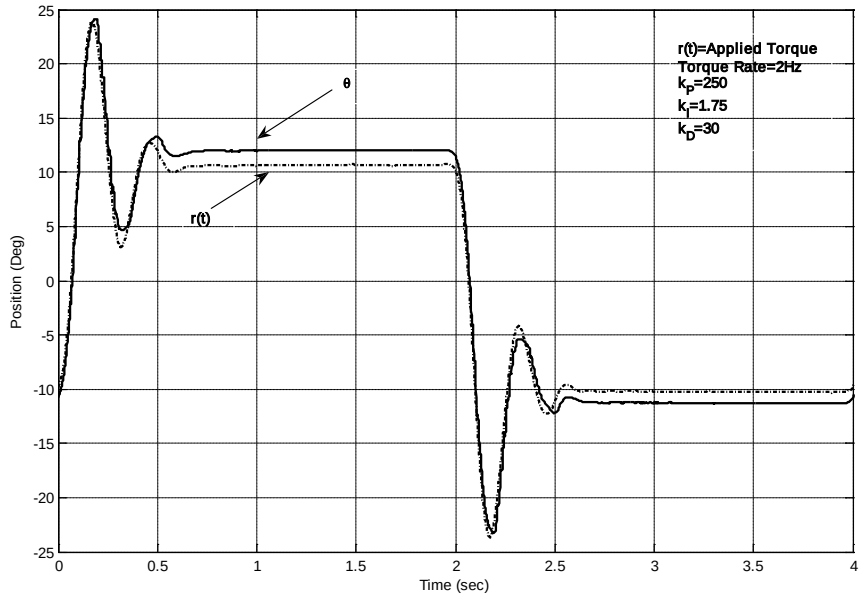

Figure 5-22. Position tracking for varying torque-2Hz user input

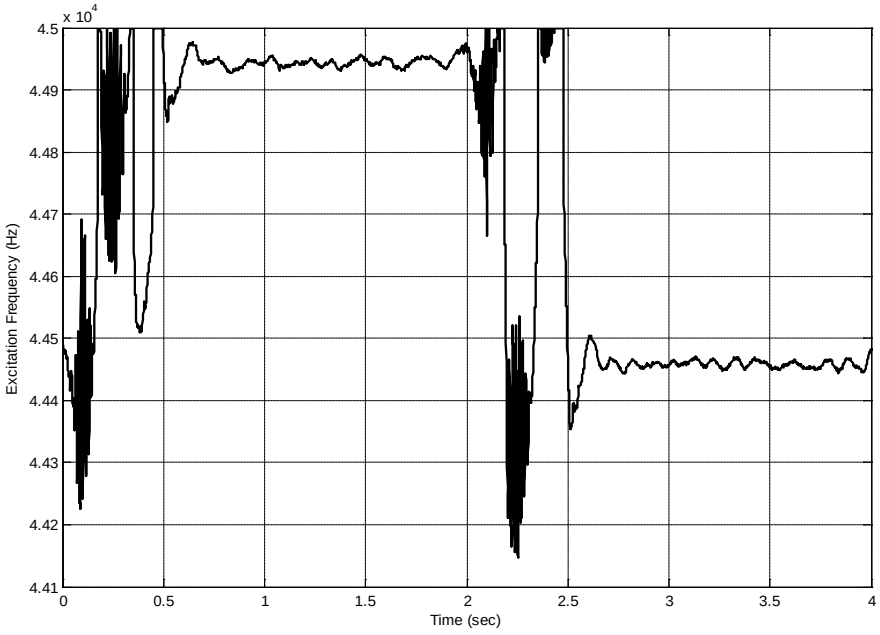

Figure 5-23. Commanded excitation frequency corresponding to Figure 5-22

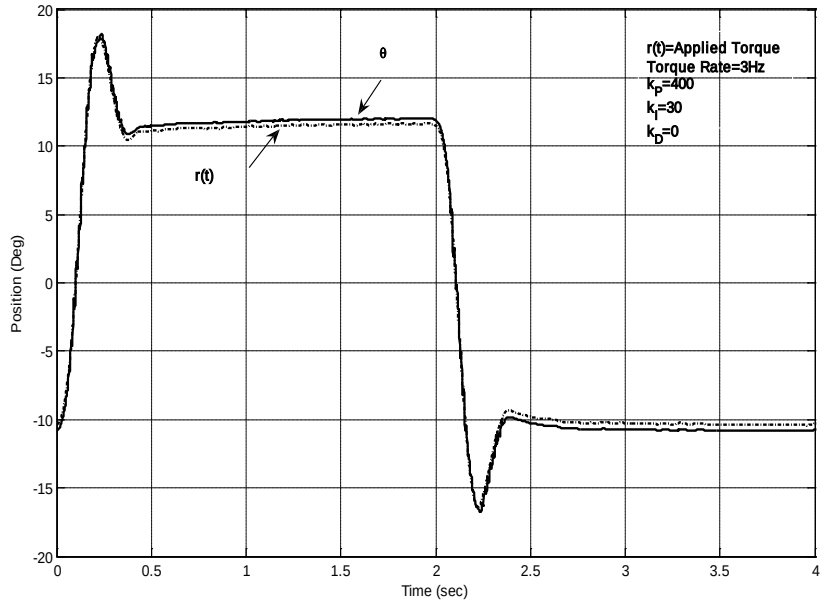

Figure 5-24. Position tracking for varying torque-3Hz

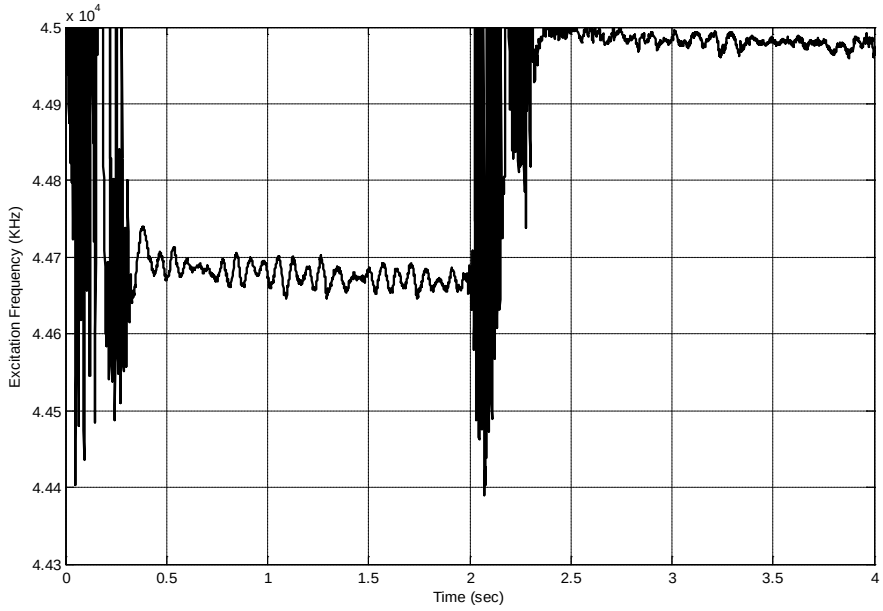

Figure 5-25. Commanded excitation frequency corresponding to Figure 5-24

Figure 5-26 and Figure 5-28 demonstrate phase control (Equation 4.9) for the same second-order torque inputs. As expected, the steady state error is higher compared to the frequency control results, which is due to the dead zone effect. It was expected that a high integral gain would help to correct for this dead-zone effect. However, as previously stated, there is limit on the integral gain that can be used due to instability. From Figure 5-26 and Figure 5-28, the presence of steady state oscillations suggest that the closed-loop system is marginally stable. The reason for this effect is the constant frequency setting for phase control, f_o (Equation 4.9). In general, f_o must be set to a low value to achieve a sufficient response time (cf. Figure 4-4). However, as f_o is decreased the control sensitivity to error becomes large. In effect, lowering f_o increases the control gain of the closed-loop system. It is well-known that typical systems can only support a limited control gain before instability. Thus, for phase control, there is exists a tradeoff between response time and magnitude of steady-state oscillation.

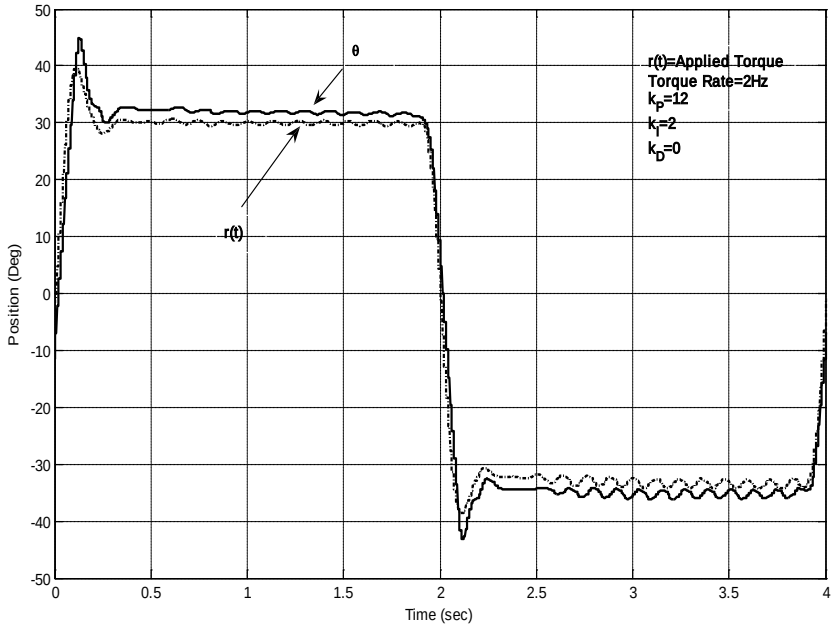

Figure 5-26. Position tracking for varying torque-2Hz user input

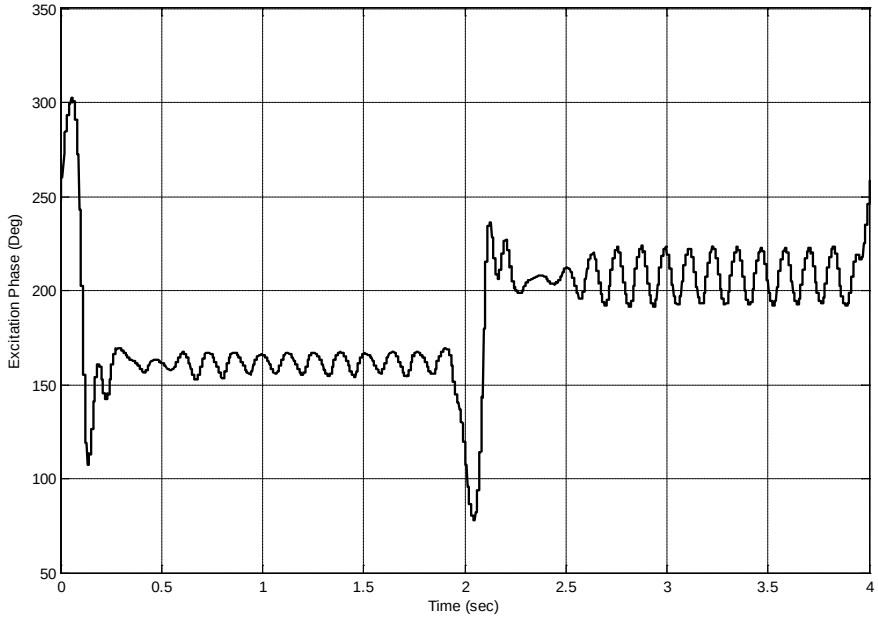

Figure 5-27. Commanded excitation phase corresponding to Figure 5-26

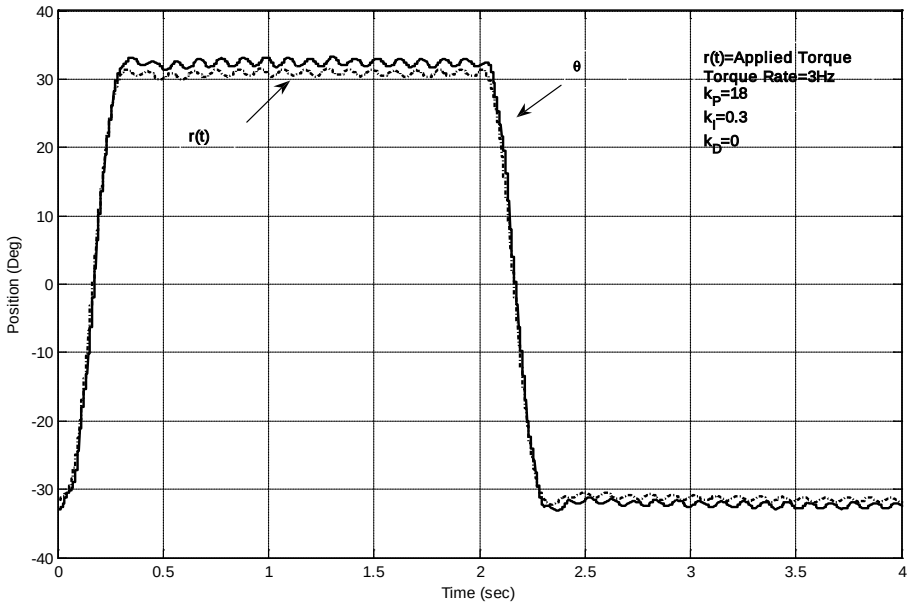

Figure 5-28. Position tracking for varying torque-3Hz user input

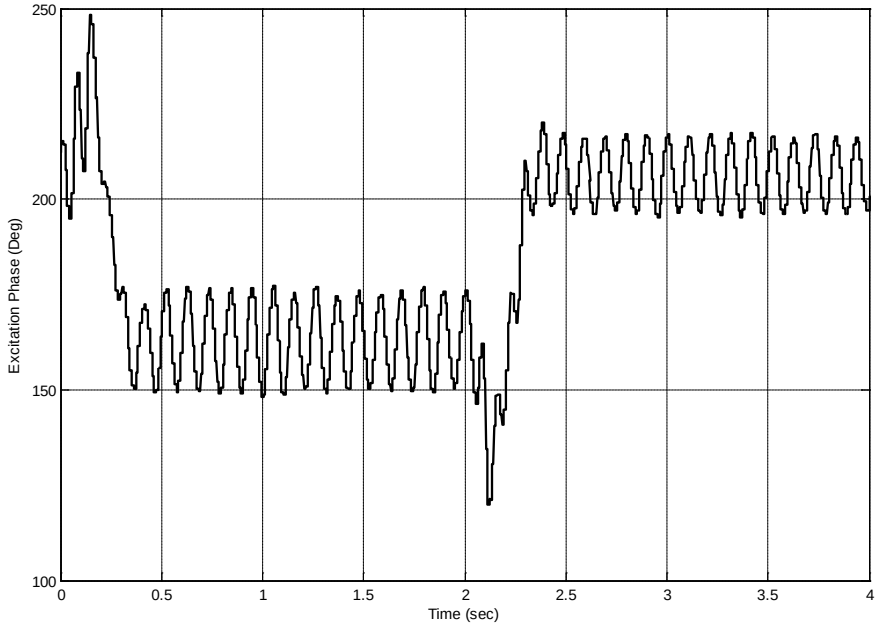

Figure 5-29. Commanded excitation phase corresponding to Figure 5-28

5.2.2 Force Feedback for Sinusoidal Inputs

As discussed in Chapter 2, the USM cannot exactly mimic the torque of a spring and damper. Here we determine if an *approximate* second-order input-output relationship can be achieved.

Figure 5-30 and Figure 5-32 show the closed-loop response for ω_L =1Hz and 2Hz sinusoidal input signals, respectively, using frequency control, for input torque of A = 0.05N-m. Since the closed-loop system is nonlinear, the motor response is not necessarily expected to be a periodic signal. From Figure 5-30, the output response obviously contains frequency content other than 1 Hz. This implies that the closed-loop system is nonlinear. In contrast, Figure 5-32 shows frequency content primarily at 2 Hz.

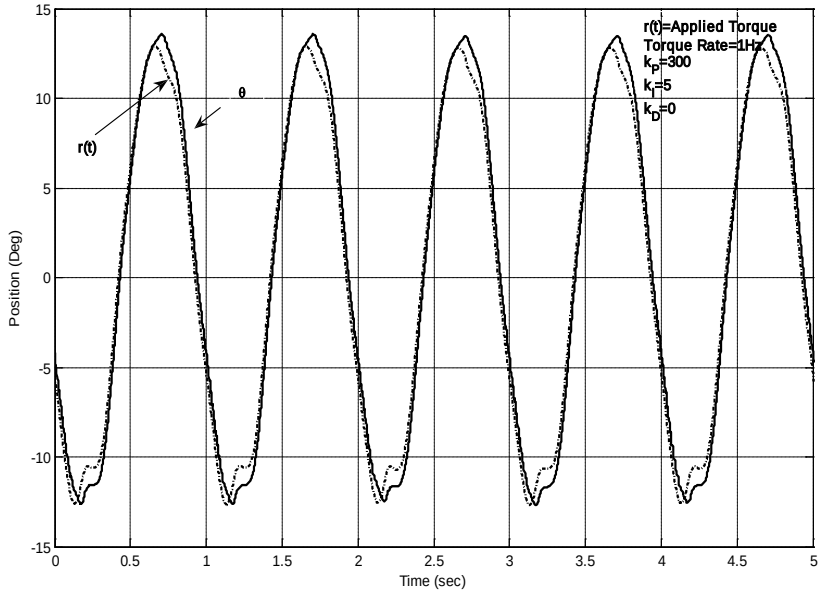

Figure 5-30. Position tracking for varying torque-1 Hz user input

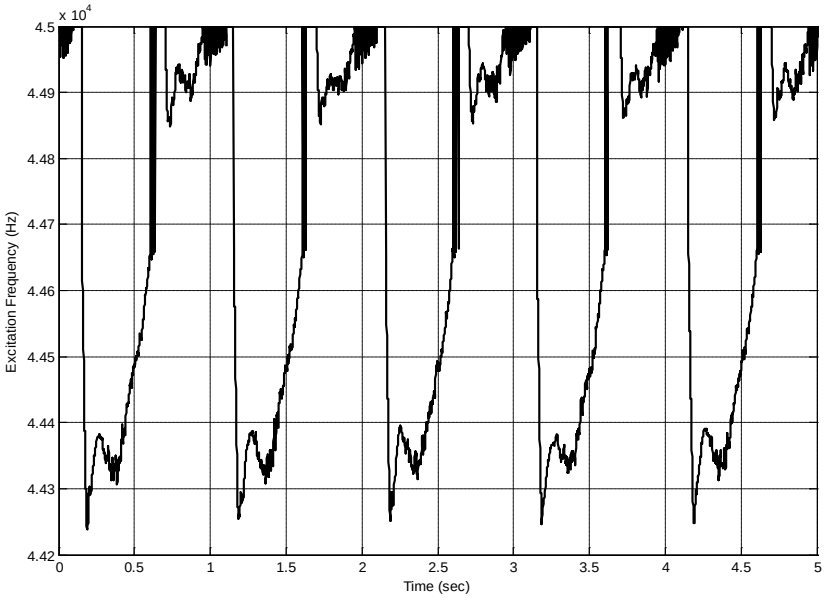

Figure 5-31. Commanded excitation frequency corresponding to Figure 5-30

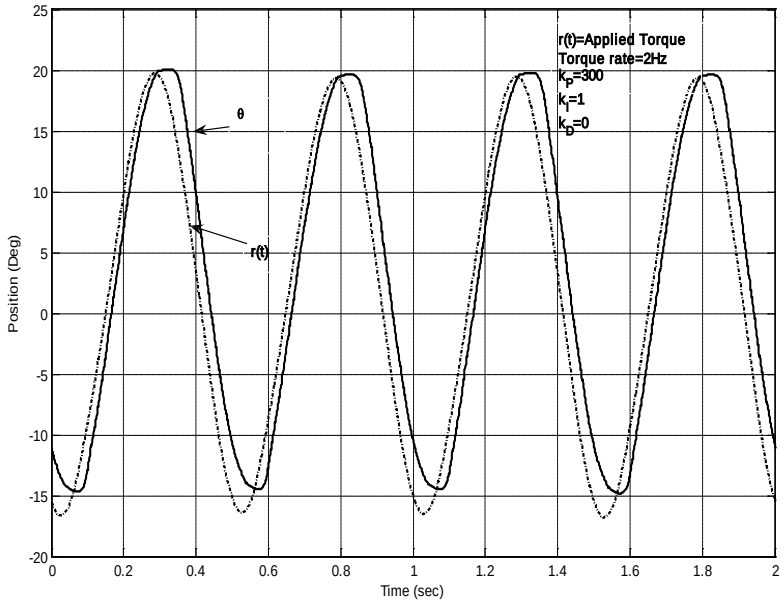

Figure 5-32. Position tracking for varying torque-1Hz user input

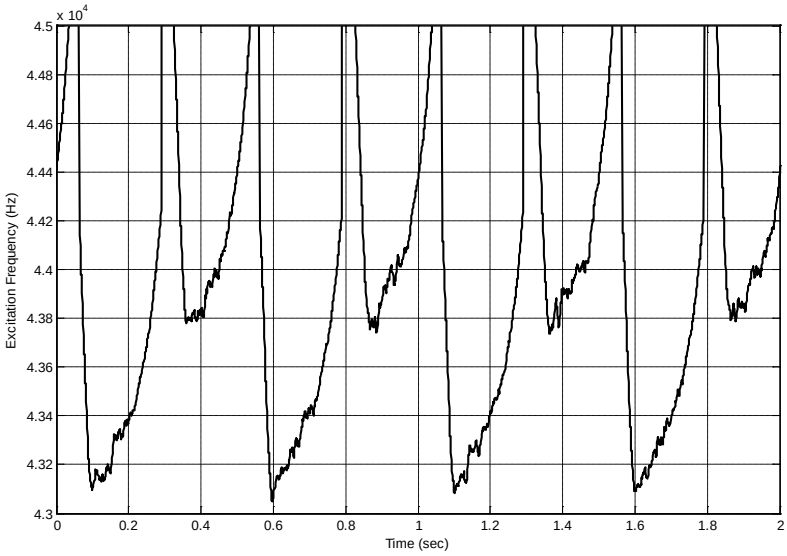

Figure 5-33.Commanded excitation frequency corresponding to Figure 5-32

In general, the closed-loop response demonstrates more linear behavior as ω_L becomes larger. However, the frequency content at lower frequencies is assumed to negligible. Considering this assumption an input-output relationship was determined over the frequency range of interest ($0.1 \leq \omega_L \leq 5$Hz). This can be analyzed by performing standard frequency response tests, which are conducted over a range of natural frequencies 0.5Hz-5Hz and damping ratios on the range of 0.05-0.7. The following results are representative of USM's performance with force feedback control approach for $\omega_{L=}$ 2Hz. The magnitude and phase of $\Theta(i\omega)/T_L(i\omega)$,is shown in the Figure 5-34 and Figure 5-35 for $\zeta = 0.1$ and $\zeta = 0.5$ respectively. The results approximate the second order behavior with the exception of phase lag.

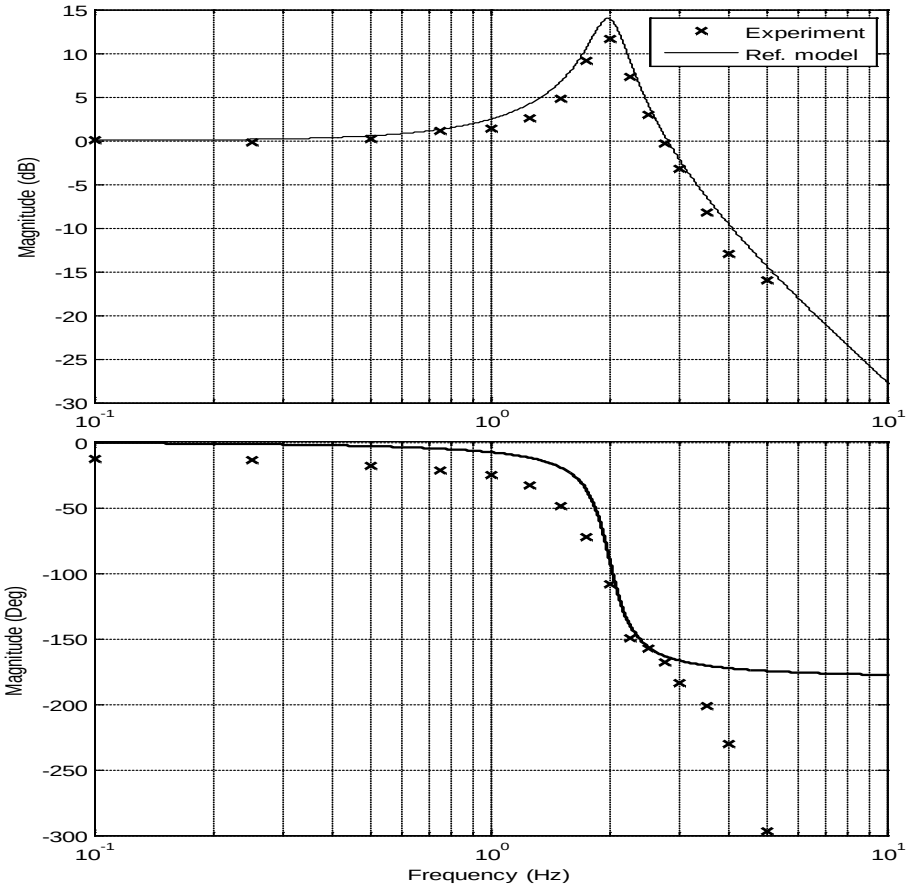

Figure 5-34. Closed-loop frequency response $\Theta(i\omega)/T_L(i\omega)$ for reference model parameters $\omega_n = 4\pi$ rad/s and $\zeta = 0.1$.

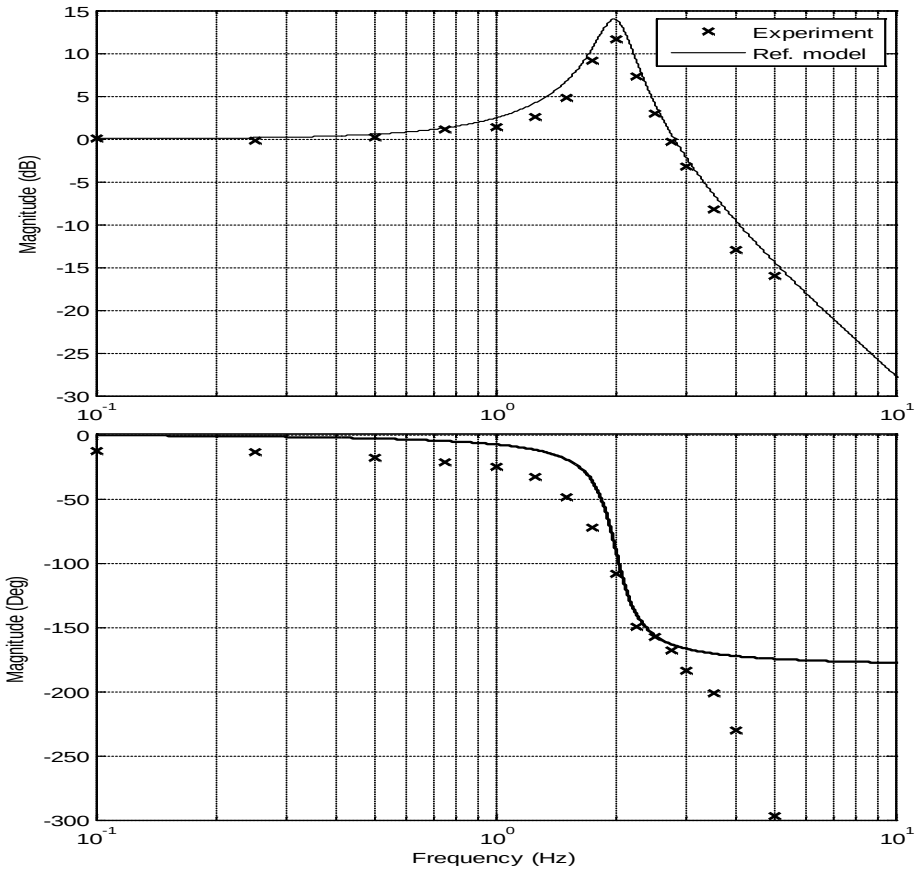

Figure 5-35. Closed-loop frequency response $\Theta(i\omega)/T_L(i\omega)$ for reference model parameters $\omega_n = 4\pi$ rad/s and $\zeta = 0.5$

From Figure 5-34 and Figure 5-35, with higher damping of the reference model the controller generally performs less favorably in that the closed-loop damping is slightly higher than desired value, and the high frequency roll-off is steeper. As was the case for lower damping, the phase lag continues to fall at high frequencies. The results indicate that the spring like input-output relationship can be obtained if the input frequency is smaller than the natural frequency of the reference model.

The final experimental results demonstrate phase control for a periodic user input. Here we only show some representative plots. It was our experience that phase control resulted in extensive wear of the motor. Hence, a frequency response, as was constructed for frequency control was not similarly performed for phase control.

Again the frequency is set to f_o = 41.5 KHz. Figure 5-36 and Figure 5-38 indicate the response of the motor for 1Hz and 2 Hz user sinusoidal inputs. With an increase in the user input frequency, the tracking ability of the motor reduces. The inclusion of integral gain improved the performance, for k_I<3.5.

Similar to the frequency control results, the closed-loop response for phase control also exhibits primarily linear behavior. Since frequency modulation technique and phase modulation technique are two different mechanisms to control the surface velocity of the stator, we expect these two methods to produce similar output. Hence, we can expect that a frequency response, similar to Figure 5-34 and Figure 5-35, will produce similar results.

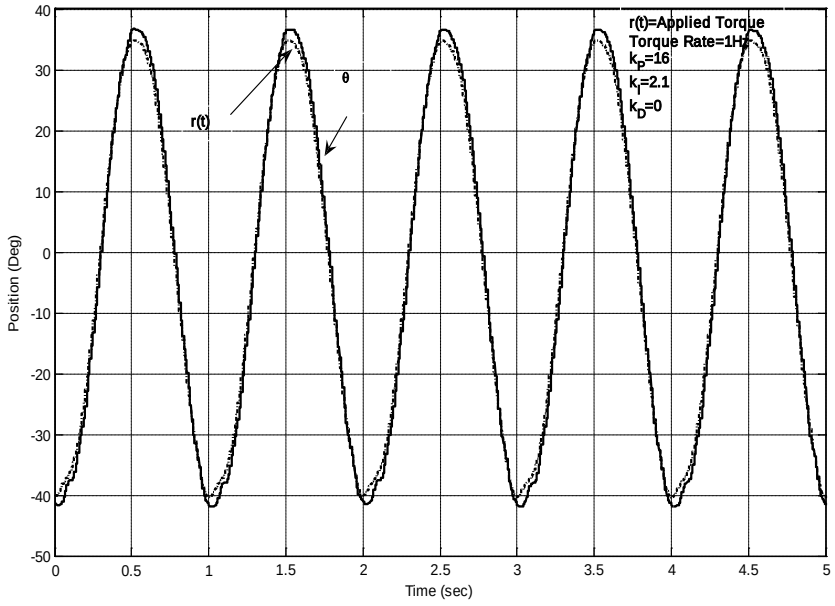

Figure 5-36. Position tracking for varying torque-1Hz user input

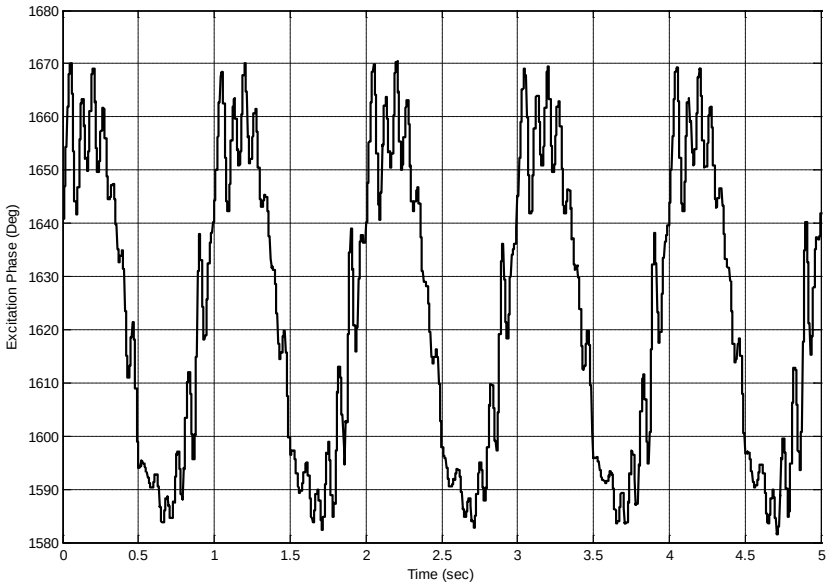

Figure 5-37. Commanded excitation phase corresponding to Figure 5-36

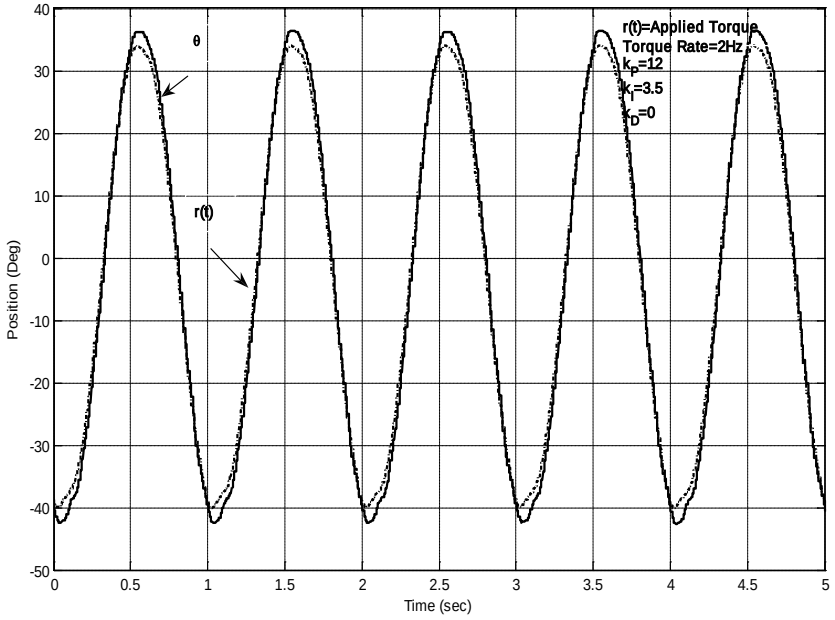

Figure 5-38. Position tracking for varying torque-2 Hz user input

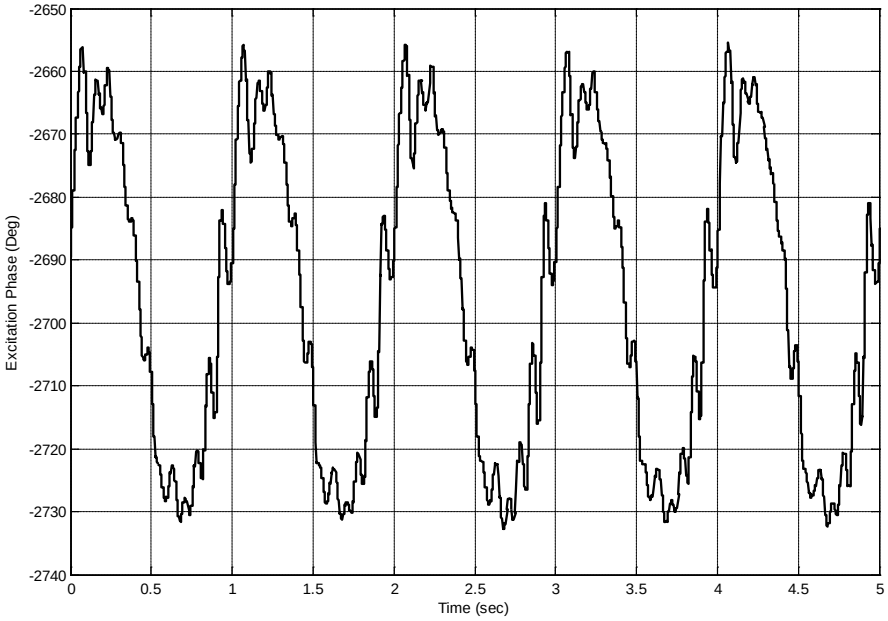

Figure 5-39. Commanded excitation phase corresponding to Figure 5-38

6 Conclusions and Future Work

This chapter presents a summary of the thesis work and suggestion for future work.

6.1 Conclusion

We have considered the USM for use as a torque source in haptic devices where a particular input-output (input torque – motion) response is desired. Historically DC motors have been the standard choice for this purpose. Owing to some of the unique features, the USM has been considered as an alternative. With the DC motor, since the output torque is simple to control, likewise the input-output properties of a DC motor based haptic device are simple to control. In a similar manner we would like to control the output torque of the USM. Various mathematical models were surveyed to determine a simple relationship between input parameters and the output torque of the motor. This was done in order to develop a model-based control approach for force-feedback applications. Although, several researchers developed model-based torque control technique based on steady state parameters, to determine a relationship between the input parameters and the motor's output torque was a difficult task. Additionally, they did not consider the limitations of the USM while developing the torque control approach. To accommodate for these limitations we developed a model reference control approach that gives an input-output relationship (input torque –output motion). Force-feedback experimental results conducted using model-reference control approach indicates that closed-loop response mimics a second-order spring damper system. The extent of which the closed-loop response is distinguishable from a true spring/damper is debatable, particularly at input frequencies below the natural frequency of the reference model.

6.2 Future Work

Only simple position control techniques, based on frequency modulation and phase modulation, were considered; and no extensive effort was made to optimize the control parameters. We speculate that more advanced techniques of position control would provide better tracking performance and thus a better approximation of the desired reference model. Hence, a further refinement in model reference control approach can be performed. Apart from frequency and phase modulation techniques, a more optimized control approach combining the effect of the input parameters (frequency, phase and amplitude) can be developed.

As mentioned before under normal operation, the closed loop performance is not based on any extraneous parameters. However, in some cases it is desirable to add additional dynamics to the system, dependent on external conditions. Hence, an investigation to determine how a disturbance torque can be simulated and how the torque can be controlled might be an interesting research area. In addition, our experiments were performed using a second-order reference model. The possibility of reproducing the feel of a higher order system could be investigated further. Capability of the USM to behave like a non-linear spring damper system and possibility of simulating other input/output relationships can also be the focus of future research

APPENDIX A

Supplementary results for Position Control-Frequency Control

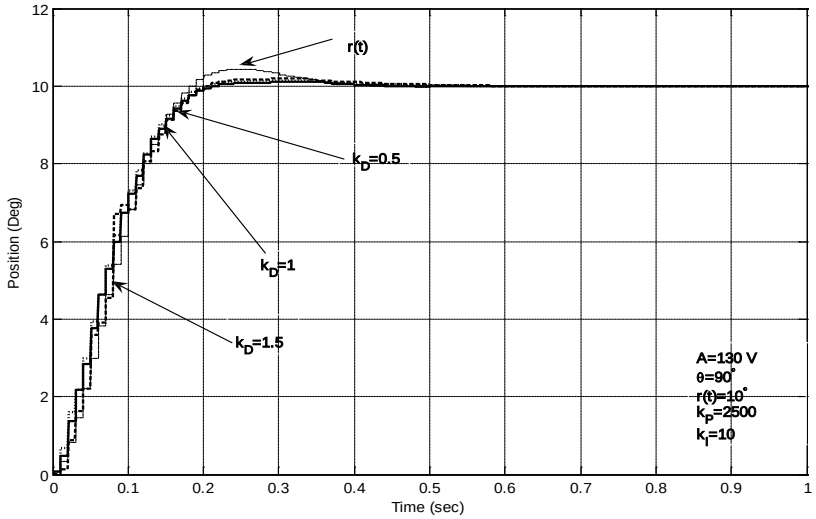

Figure A-1. Effect of derivative gain on model reference tracking-frequency Control

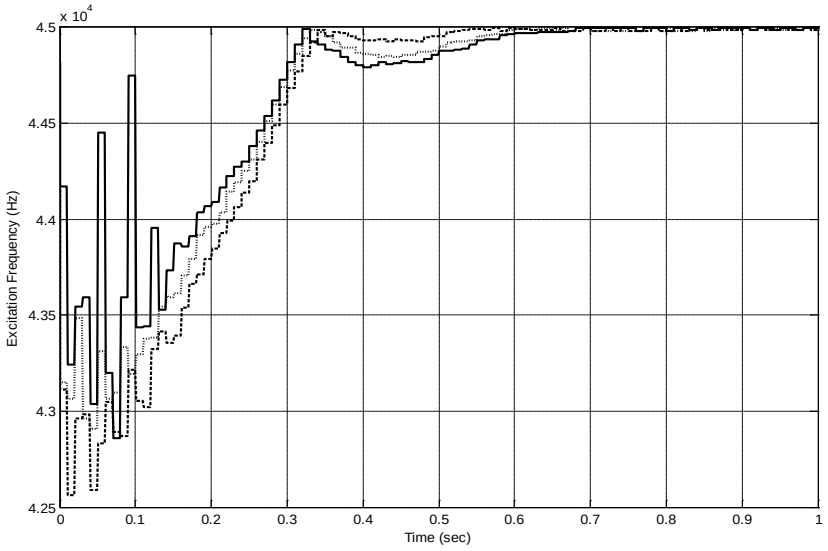

Figure A-2.Commanded excitation frequency corresponding to Figure A-1

Supplementary results for Position Control-Phase Control

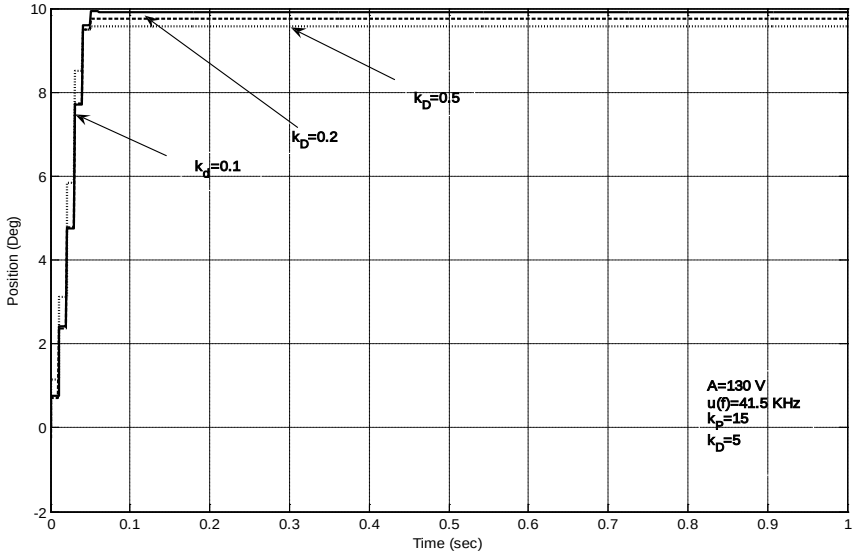

Figure A-3. Effects of derivative gain on constant reference tracking phase control-41.5 KHz

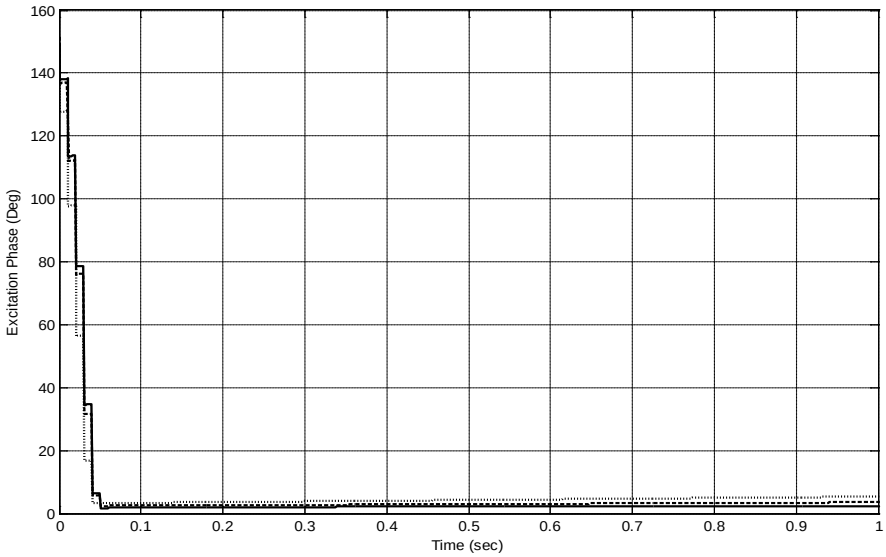

Figure A-4. Commanded excitation phase corresponding to Figure A-3

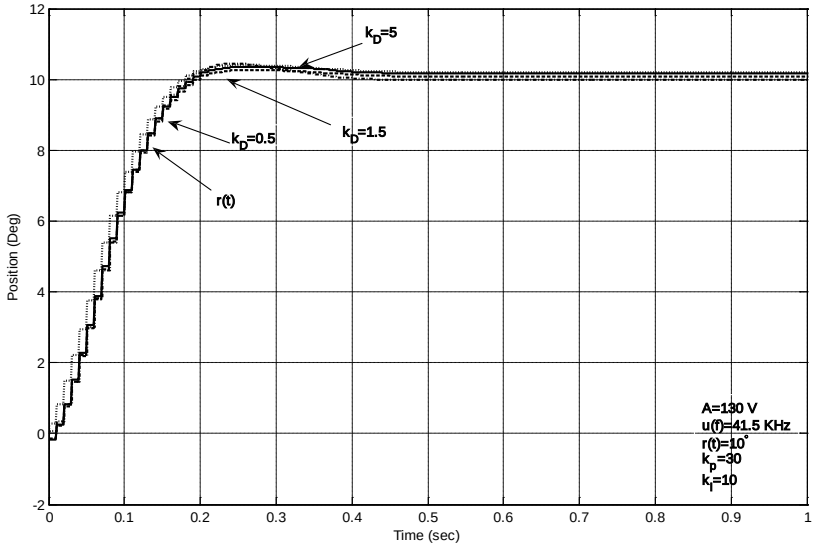

Figure A-5. Effect of derivative gain on model reference tracking phase control at 41.5 KHz.

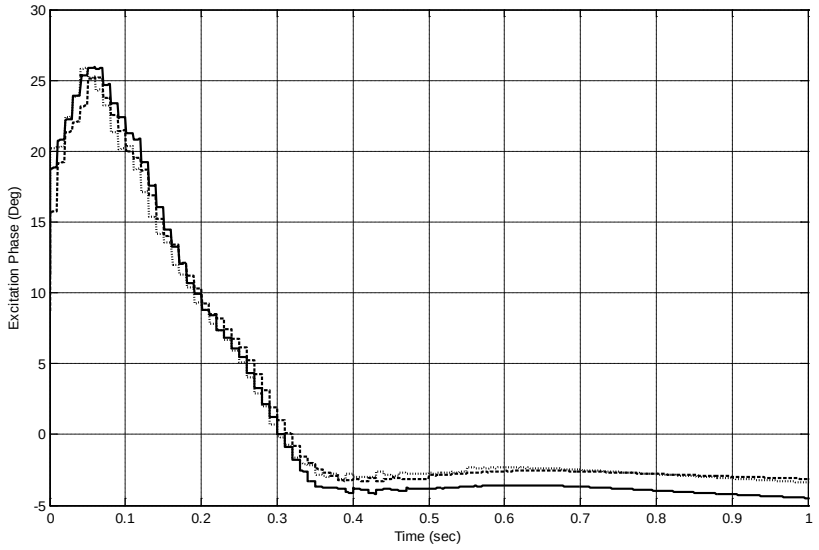

Figure A-6.Commanded excitation phase corresponding to Figure A-5

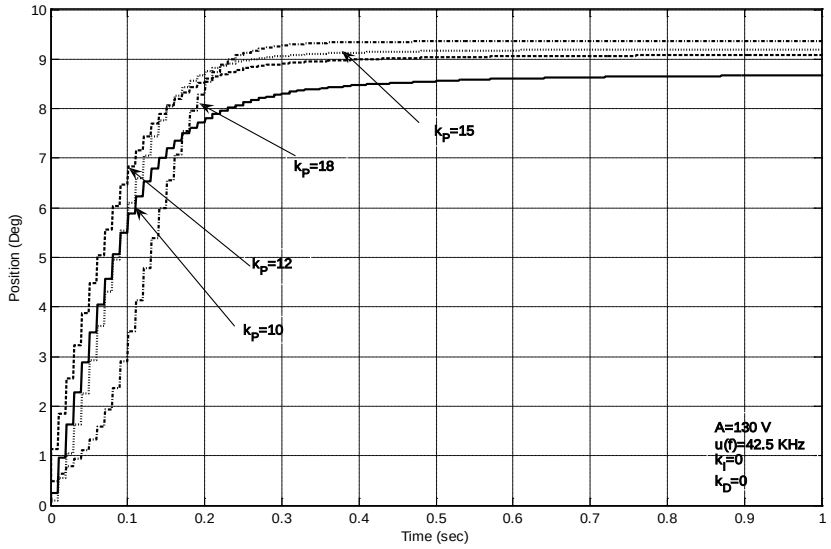

Figure A-7. Effect of proportional gain on constant reference tracking using phase control at 42.5 KHz

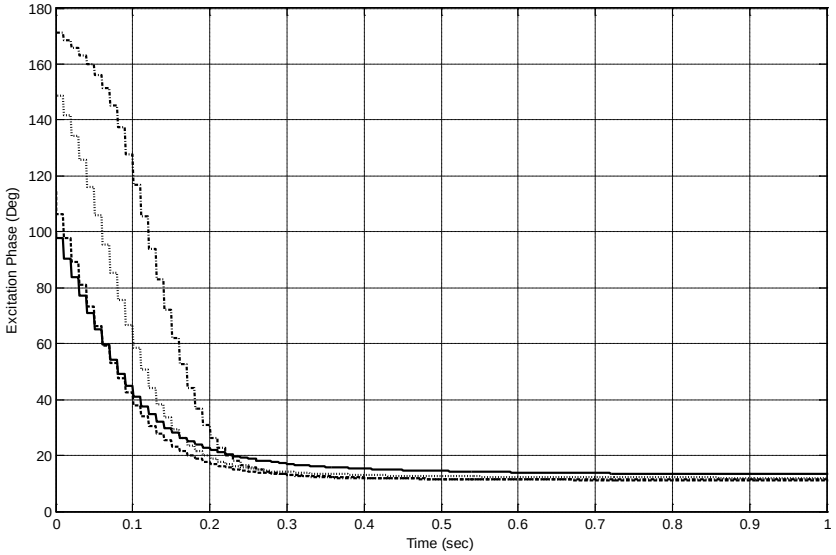

Figure A-8. Commanded excitation phase corresponding to Figure A-7

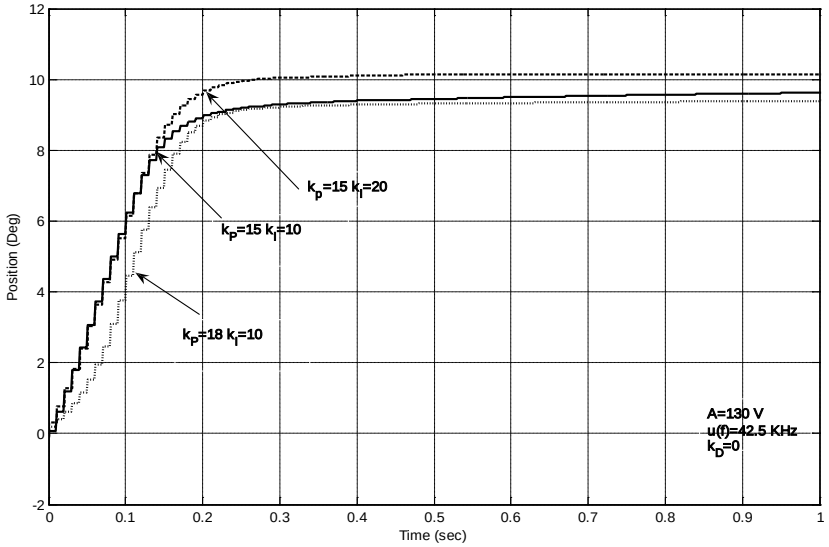

Figure A-9. Effect of integral gain on constant reference tracking using phase control at 42.5 KHz.

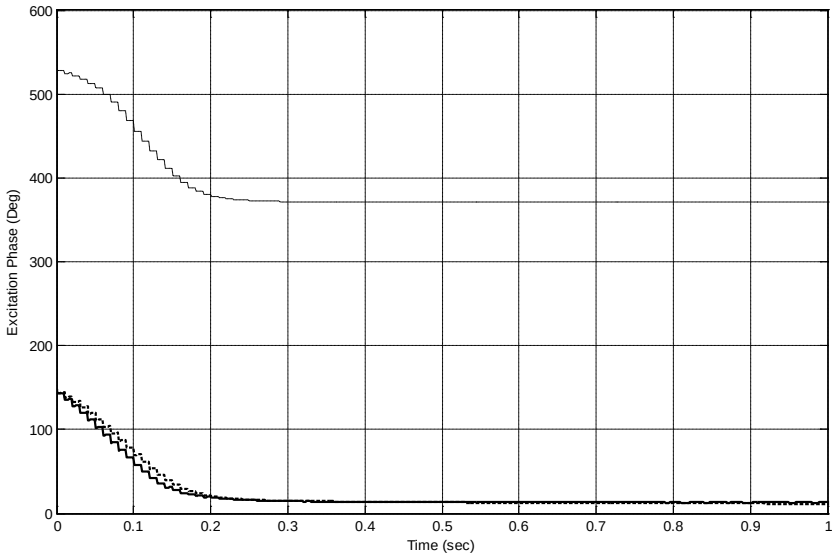

Figure A-10. Commanded excitation phase corresponding to Figure A-9

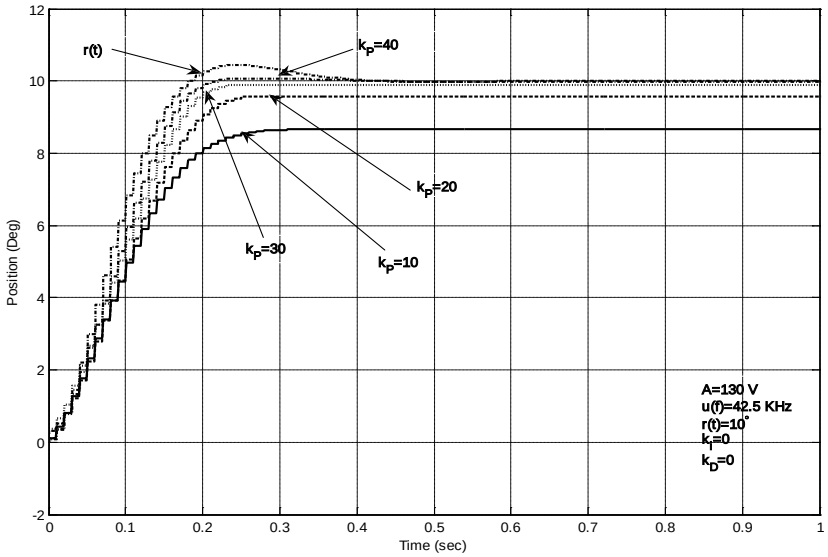

Figure A-11. Effect of proportional gain on model reference tracking phase control at 42.5 KHz.

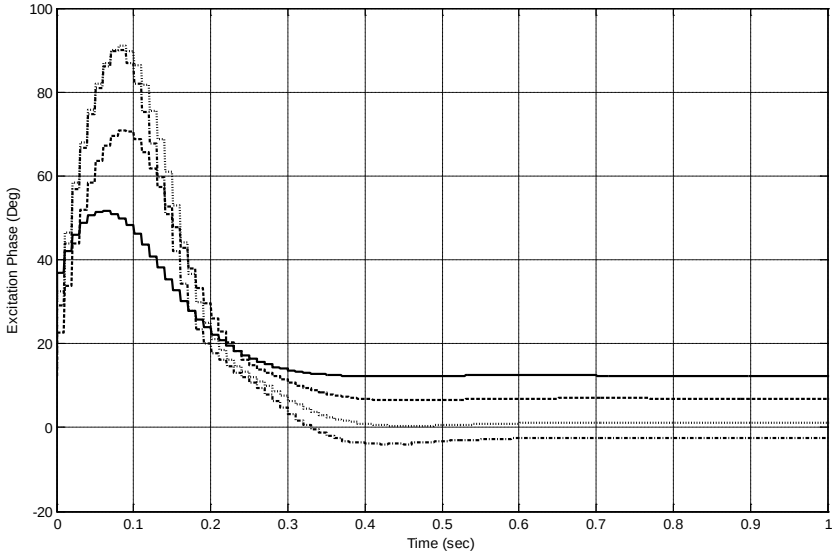

Figure A-12. Commanded excitation phase corresponding to Figure A-11

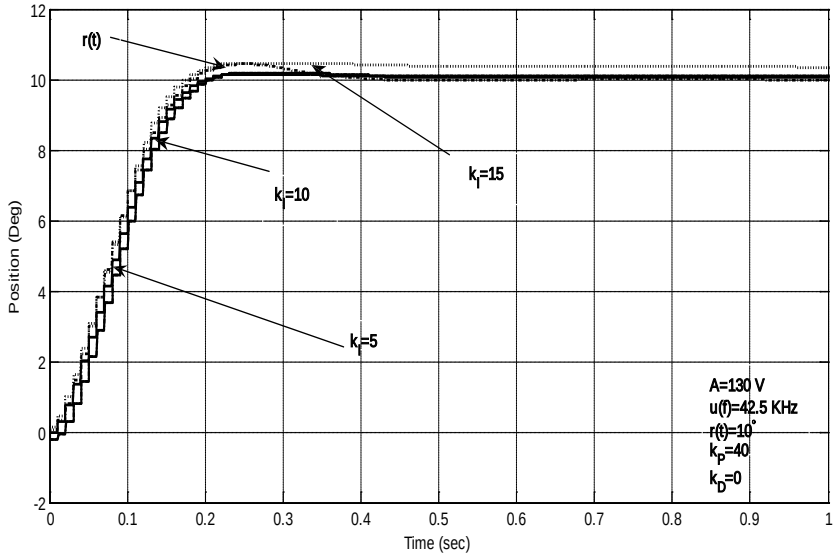

Figure A-13. Effect of integral gain on model reference tracking using phase control at 42.5 KHz.

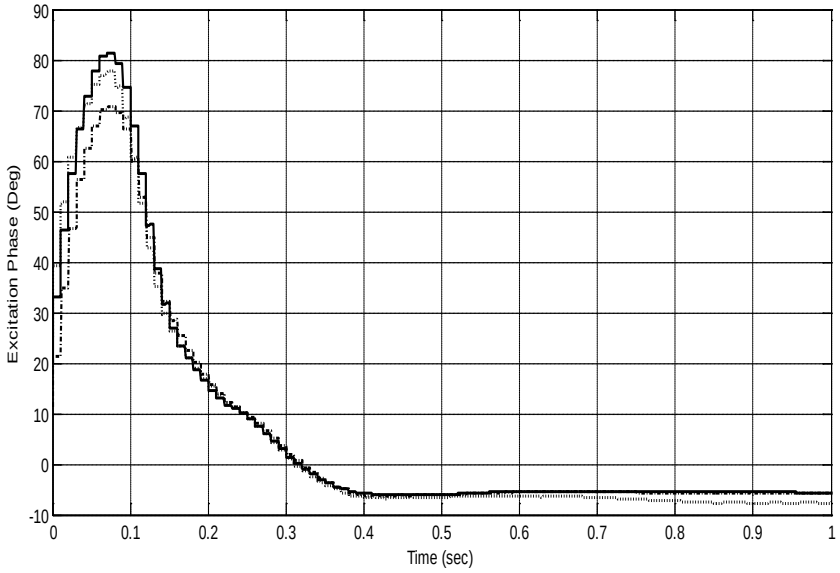

Figure A-14. Commanded excitation phase corresponding to Figure A-13.

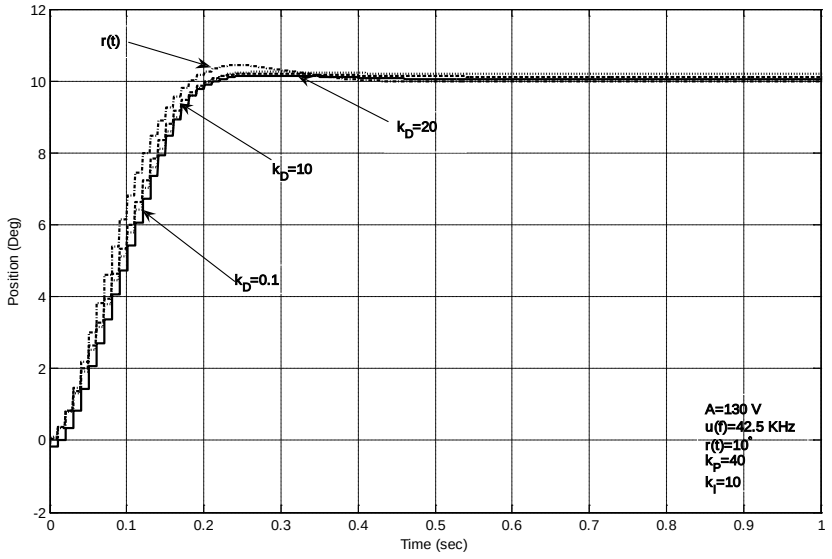

Figure A-15. Effect of derivative gain on model reference tracking using phase control at 42.5 KHz.

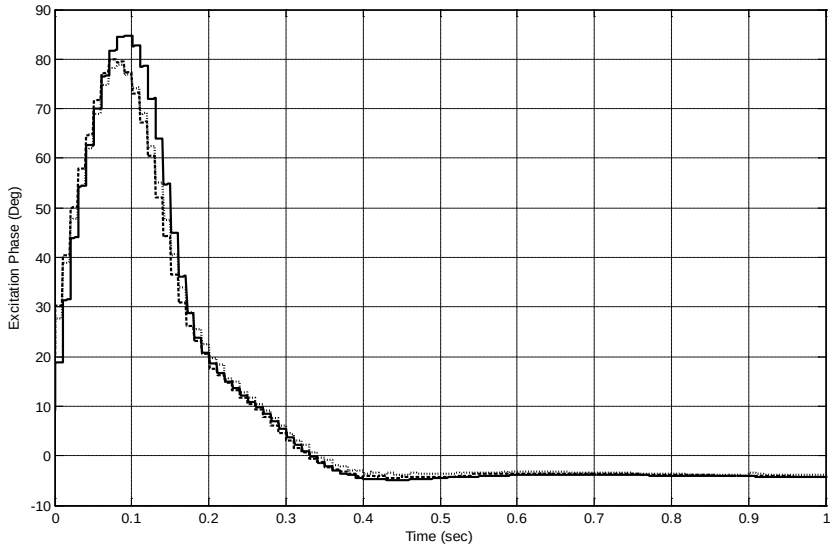

Figure A-16. Commanded excitation phase corresponding to Figure A-15

Disturbance Rejection Experiments

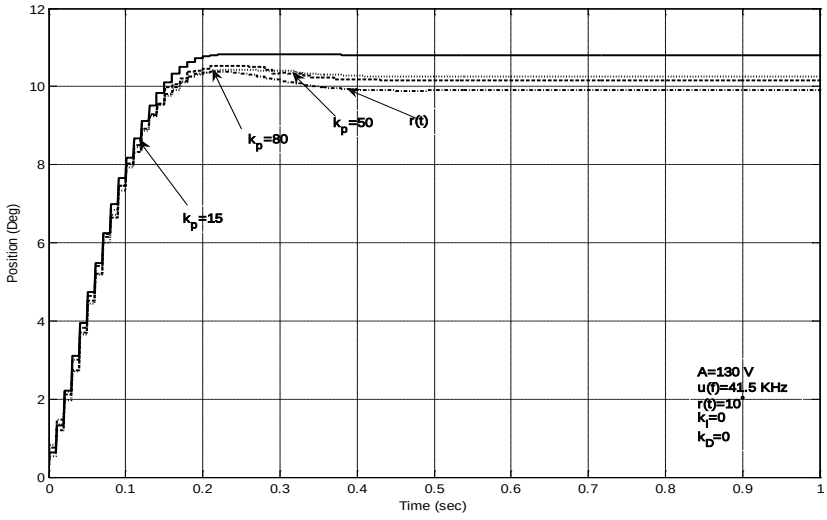

Figure A-17. Effect of proportional gain when constant user torque is applied

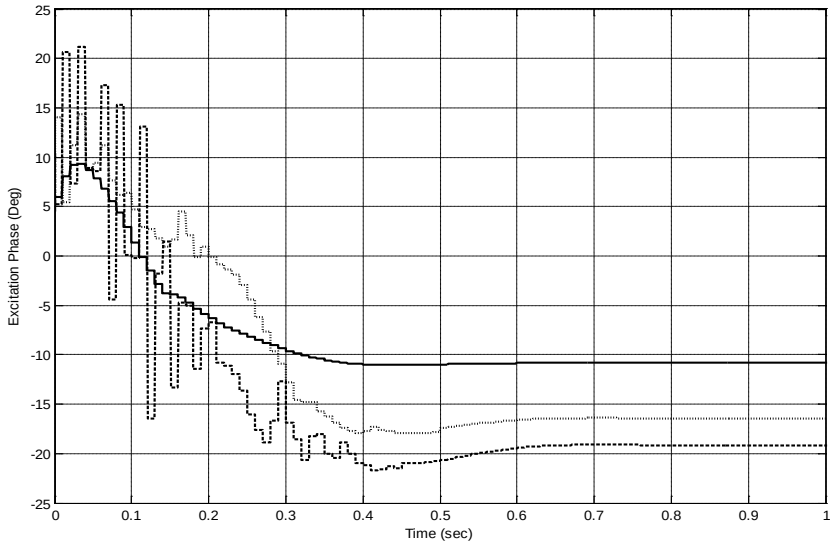

Figure A-18. Commanded excitation frequency corresponding to Figure A-17

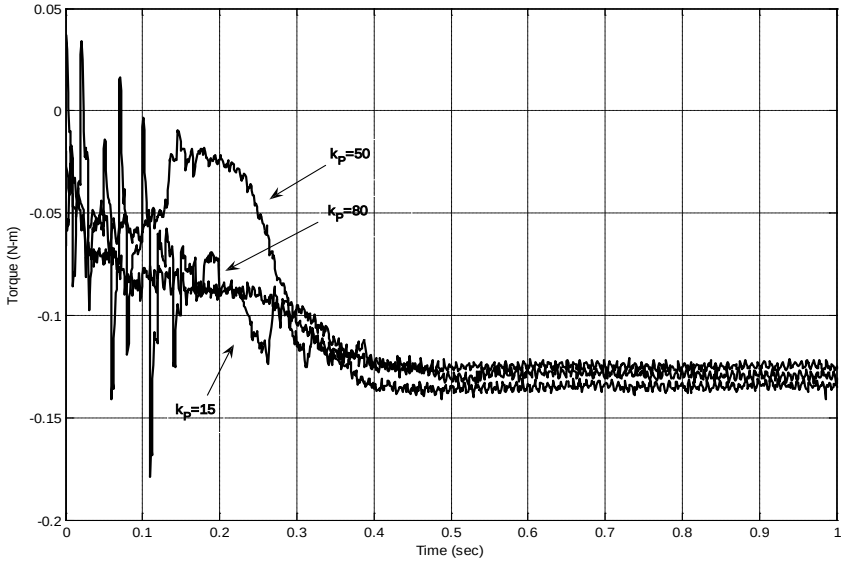

Figure A-19. Measured interaction torque corresponding to Figure A-18

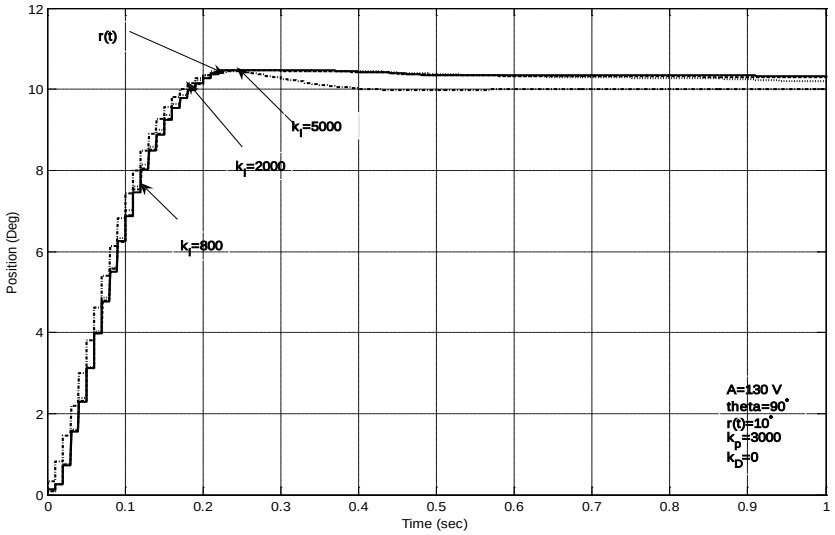

Figure A-20. Effect of integral gain when constant user input torque is applied

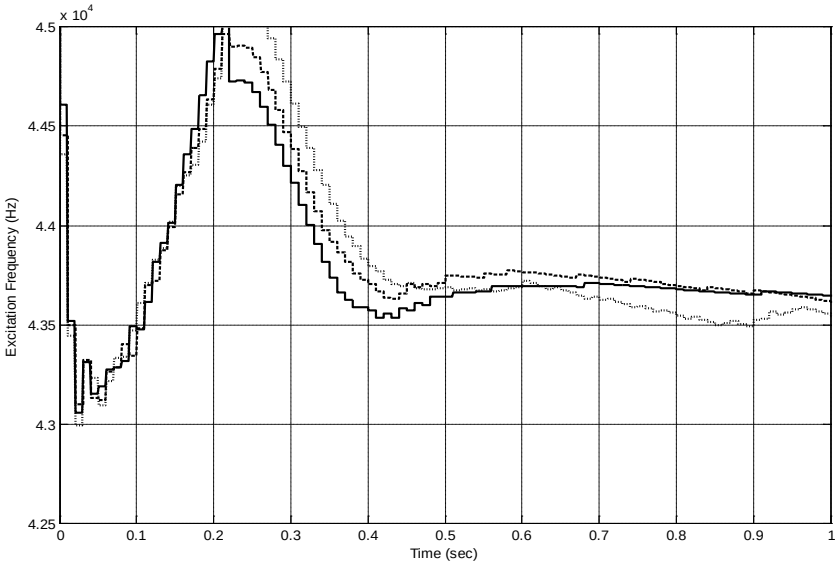

Figure A-21. Commanded excitation frequency corresponding to Figure A-20

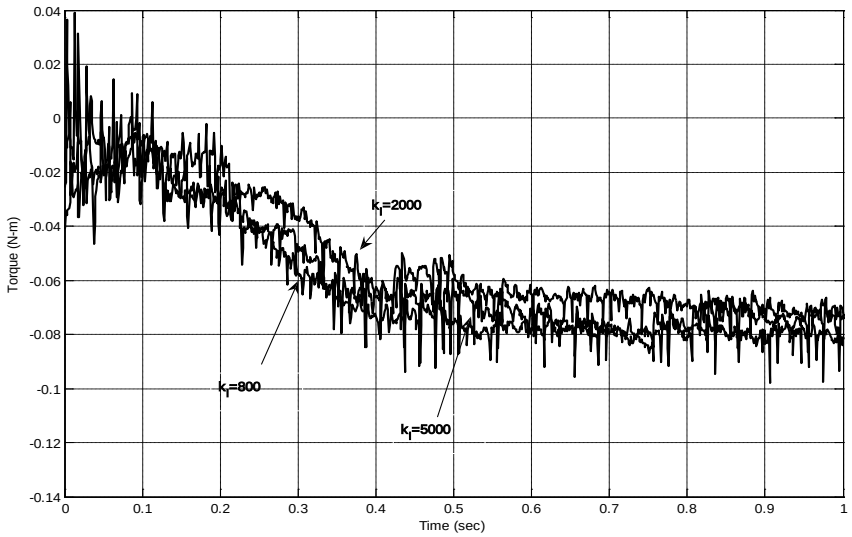

Figure A-22. Measured interaction torque corresponding to Figure A-20

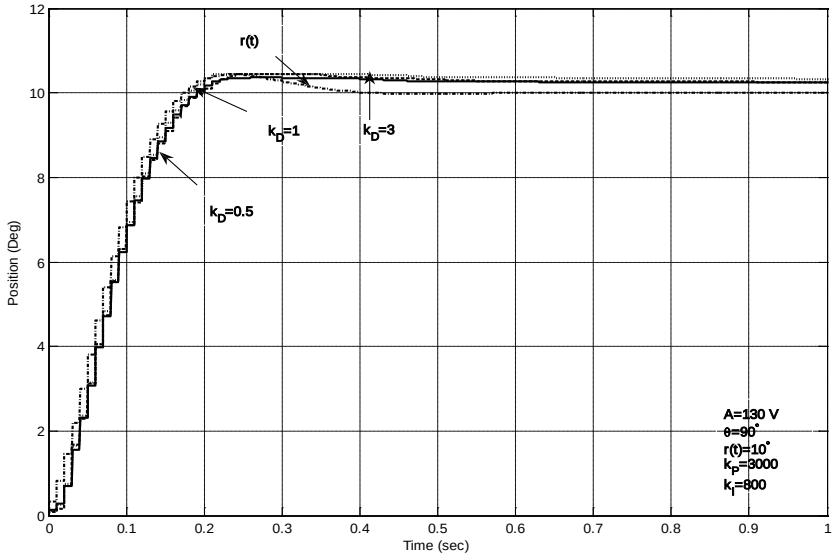

Figure A-23. Effect of derivative gain when constant user input torque is applied

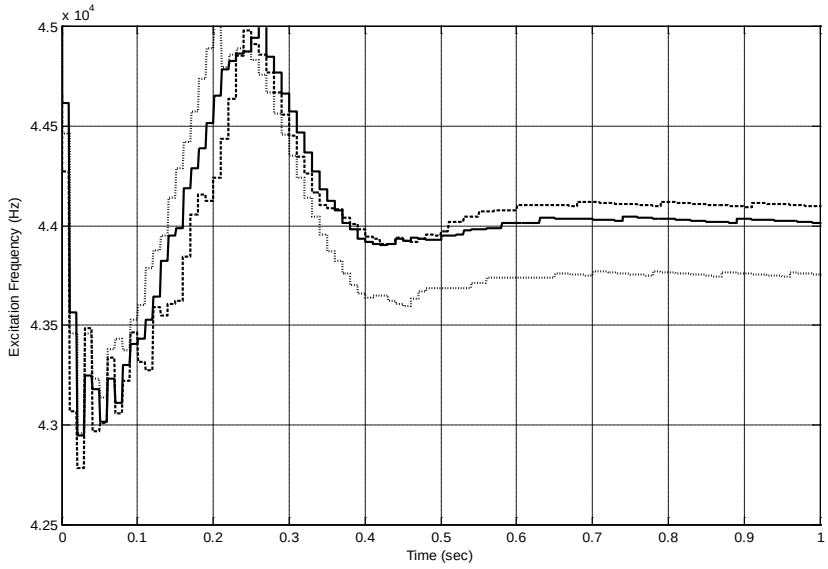

Figure A-24. Commanded excitation frequency corresponding to Figure A-23

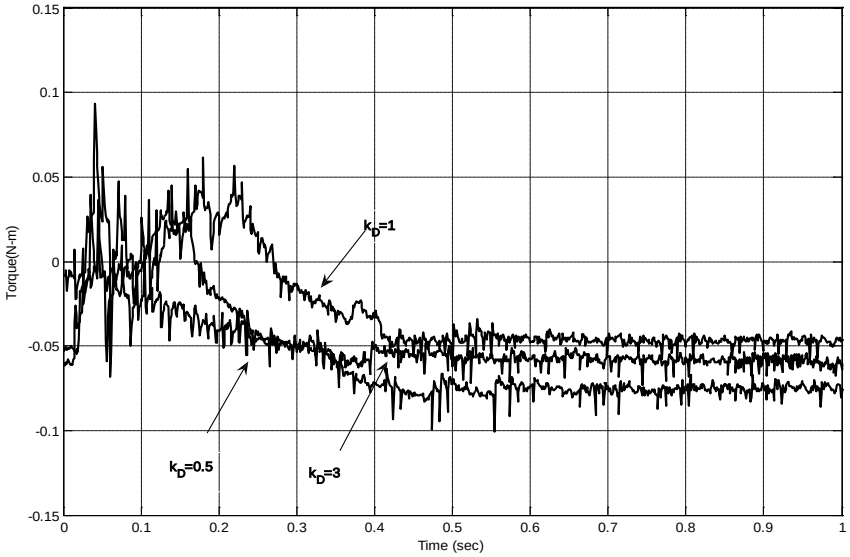

Figure A-25. Measured interaction torque corresponding to Figure A-23

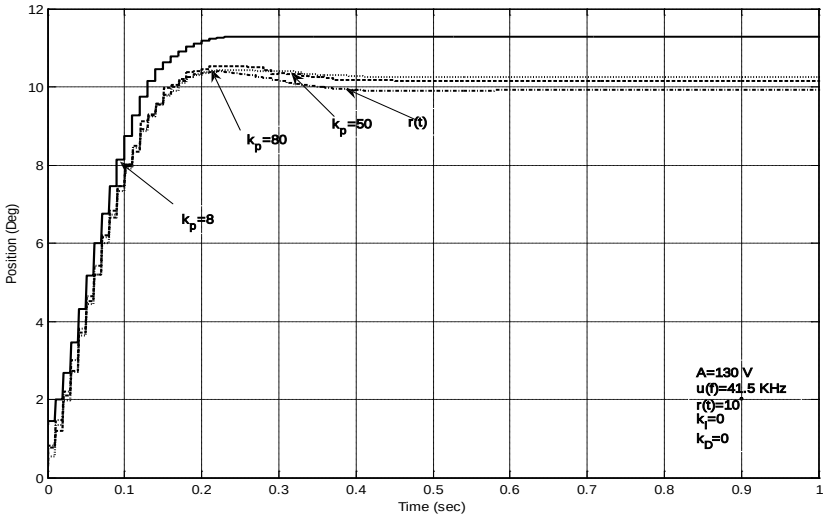

Figure A-26. Effect of proportional gain when constant user input torque is applied - 41.5 KHz

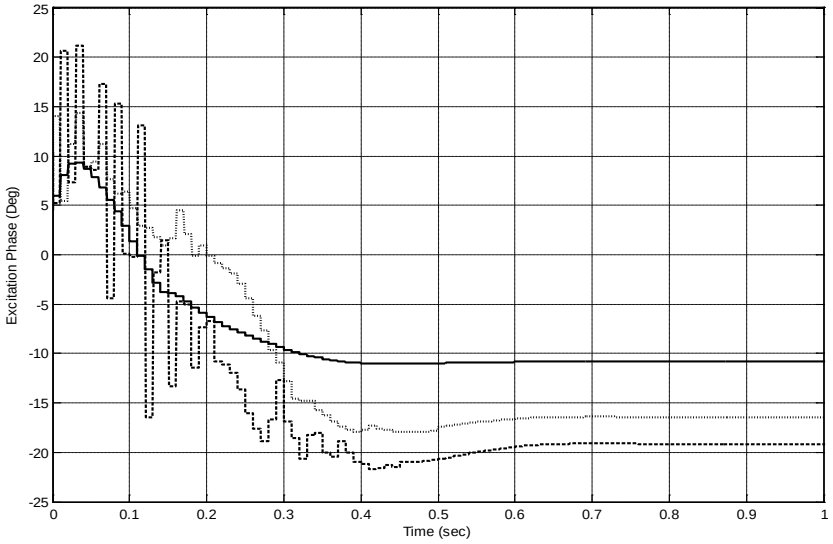

Figure A-27. Commanded excitation phase corresponding to Figure A-26

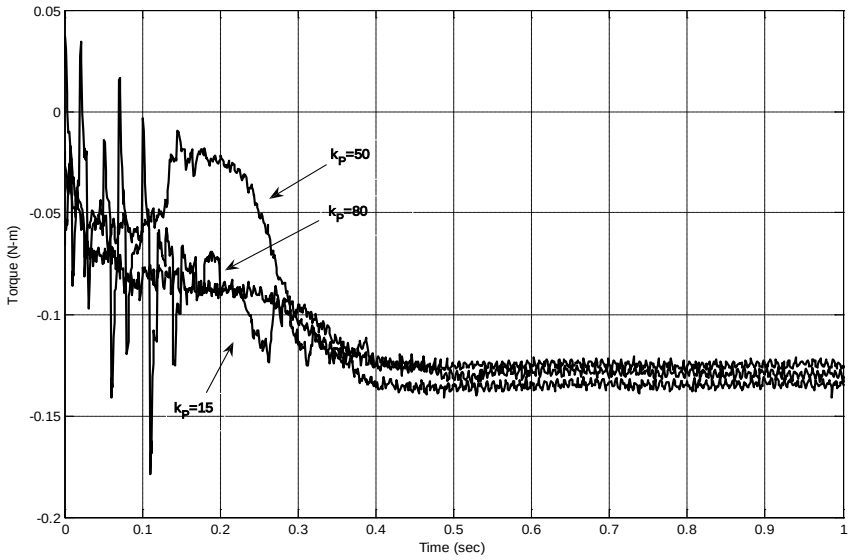

Figure A-28. Measured interaction torque corresponding to Figure A-26

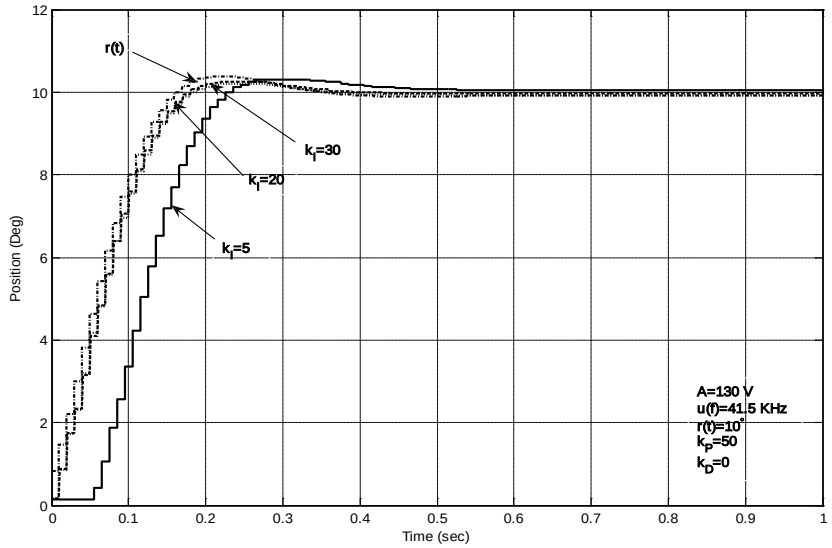

Figure A-29. Effect of integral gain when constant user input torque is applied-41.5 KHz

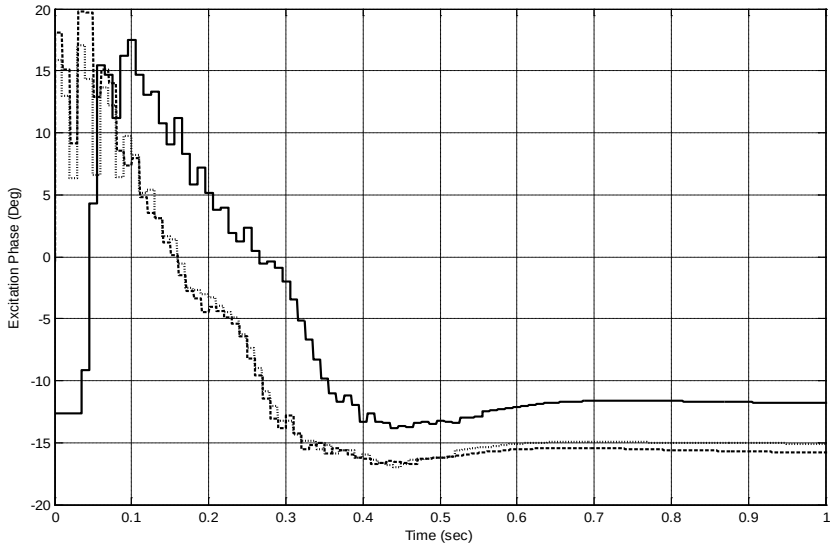

Figure A-30. Commanded excitation phase corresponding to Figure A-29

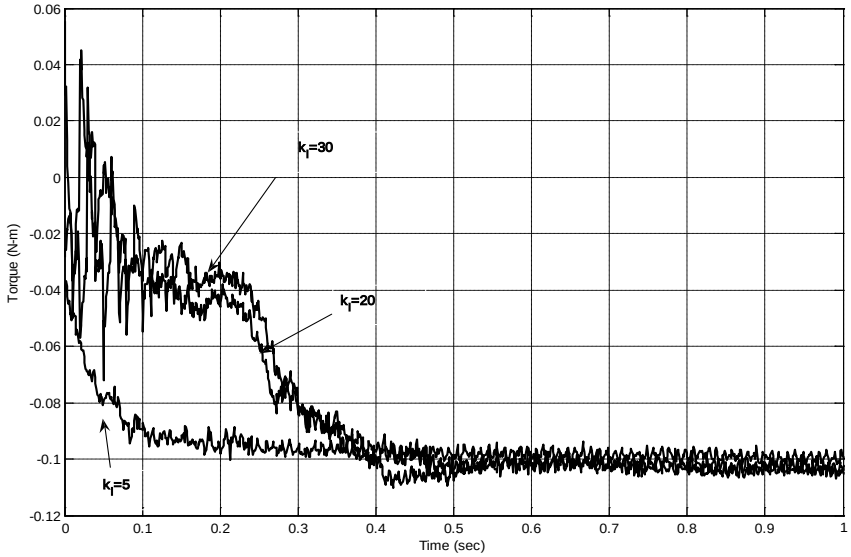

Figure A-31. Measured interaction torque corresponding to Figure A-29

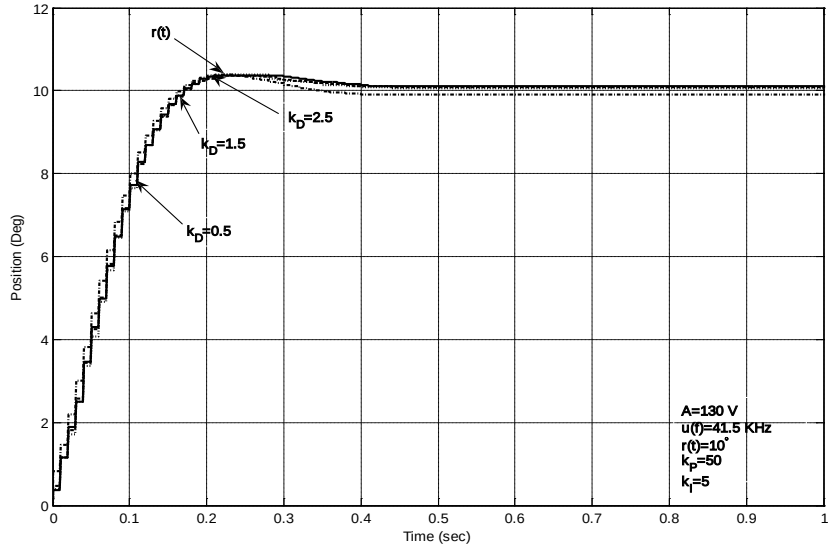

Figure A-32. Effect of derivative gain when constant user input torque is applied- 41.5 KHz

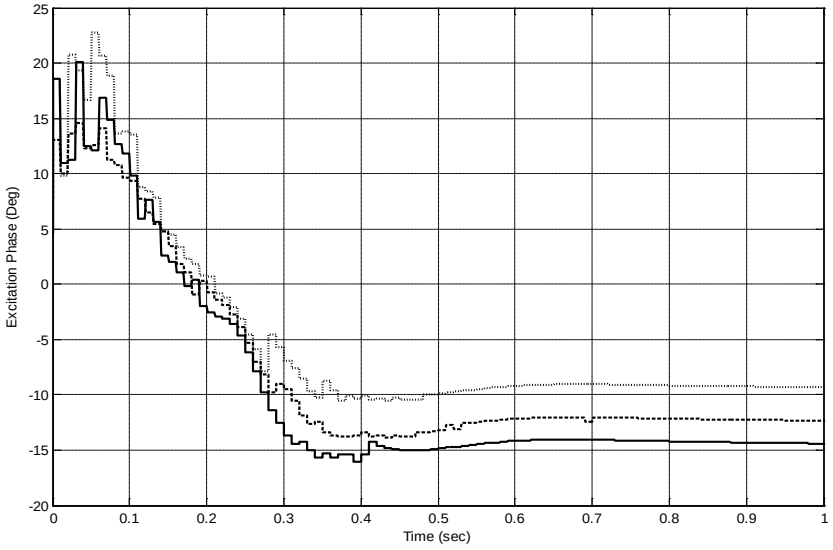

Figure A-33. Commanded excitation phase corresponding to Figure A-32

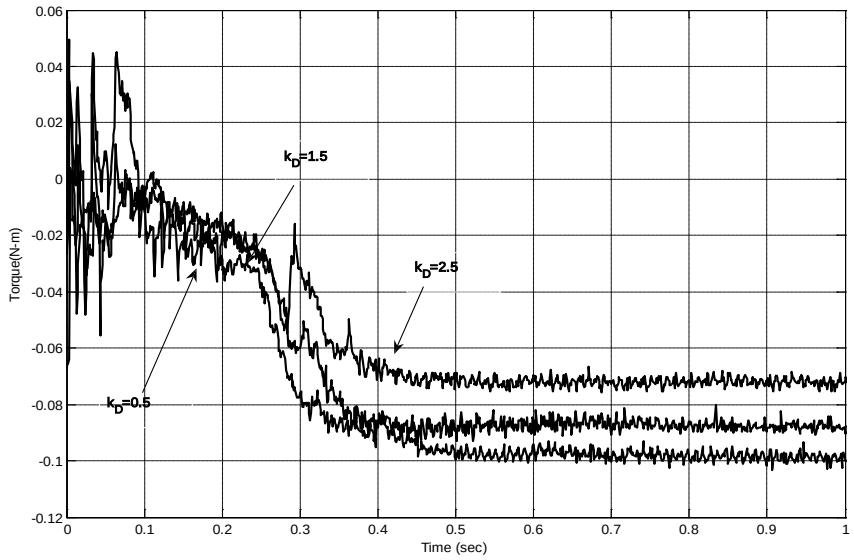

Figure A-34. Measured interaction torque corresponding to Figure A-32

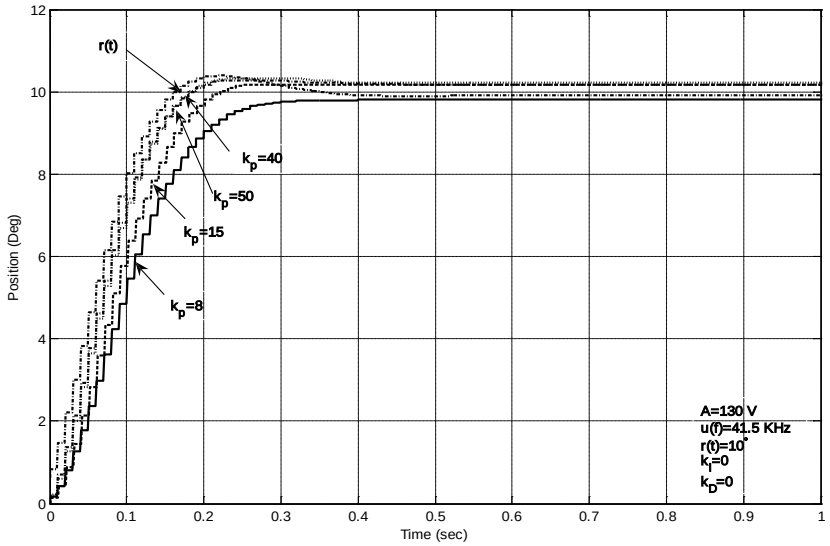

Figure A-35. Effect of derivative gain when constant user input torque is applied-42.5 KHz

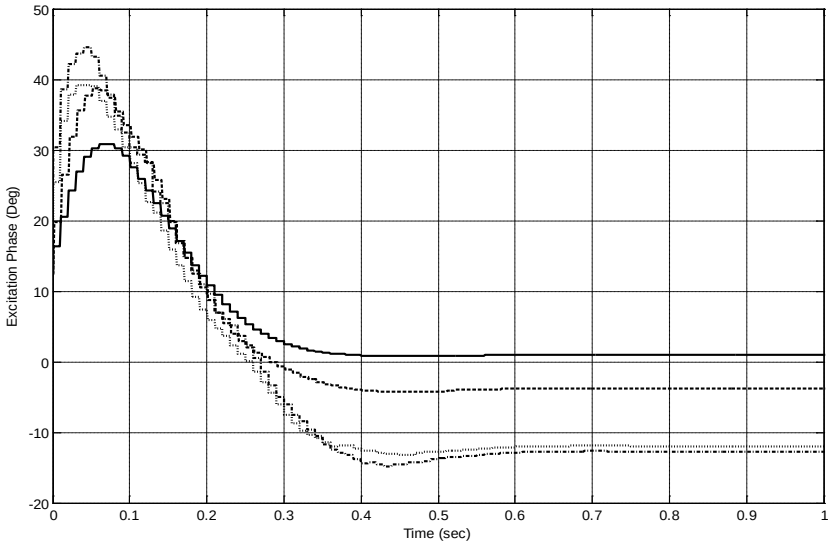

Figure A-36. Commanded excitation phase corresponding to Figure A-35

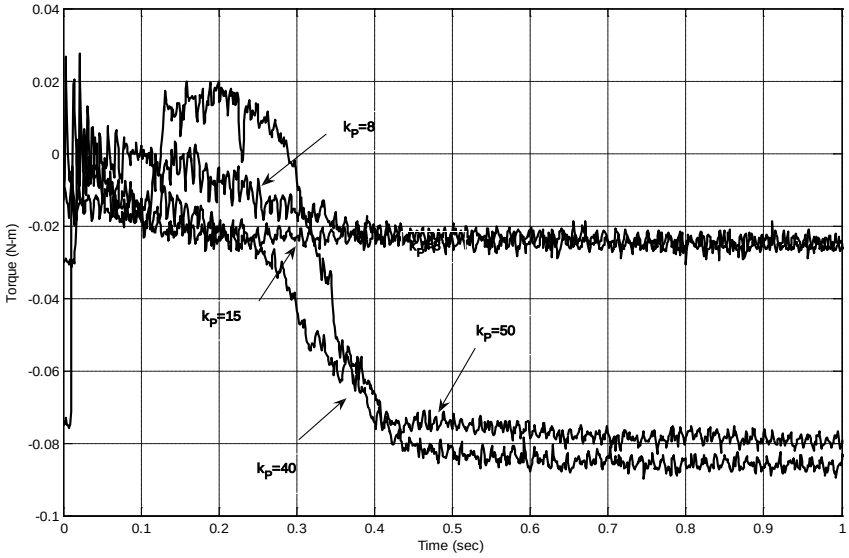

Figure A-37. Measured interaction torque corresponding to Figure A-35

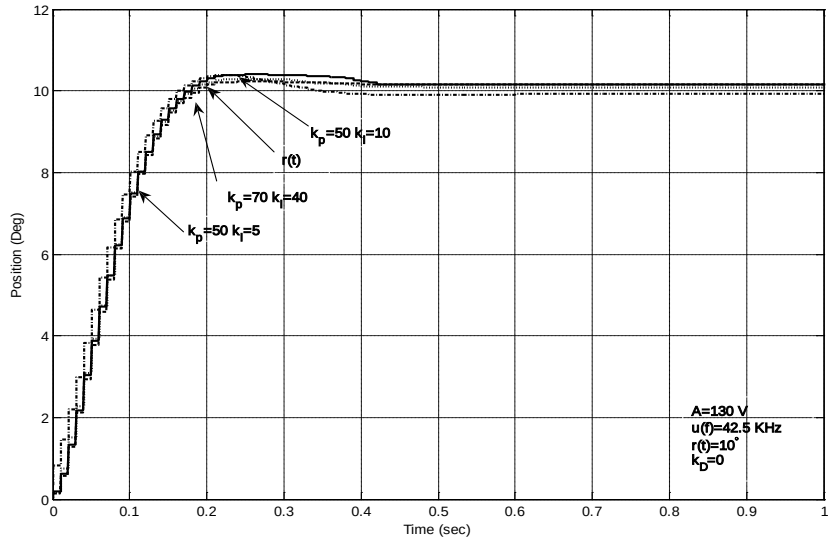

Figure A-38. Effect of integral gain when constant user input torque is applied- 42.5 KHz

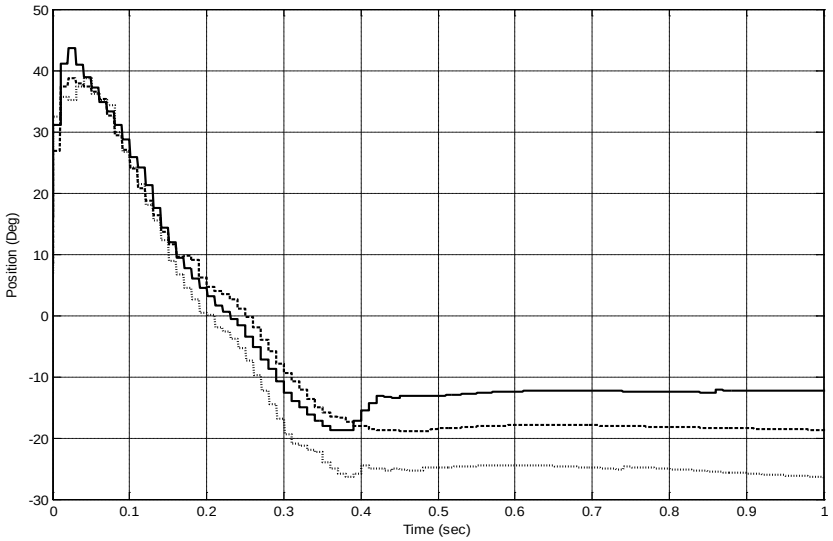

Figure A-39. Commanded excitation phase corresponding to Figure A-38

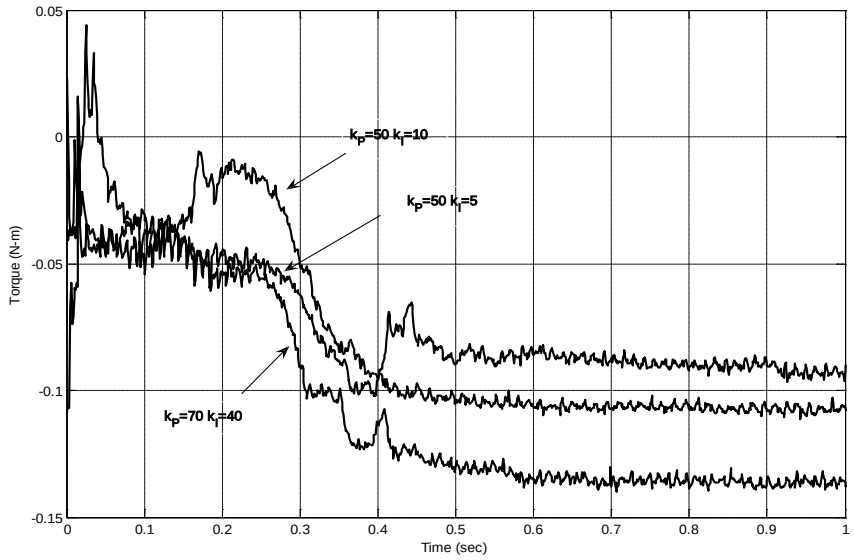

Figure A-40. Measured interaction torque corresponding to Figure A-38

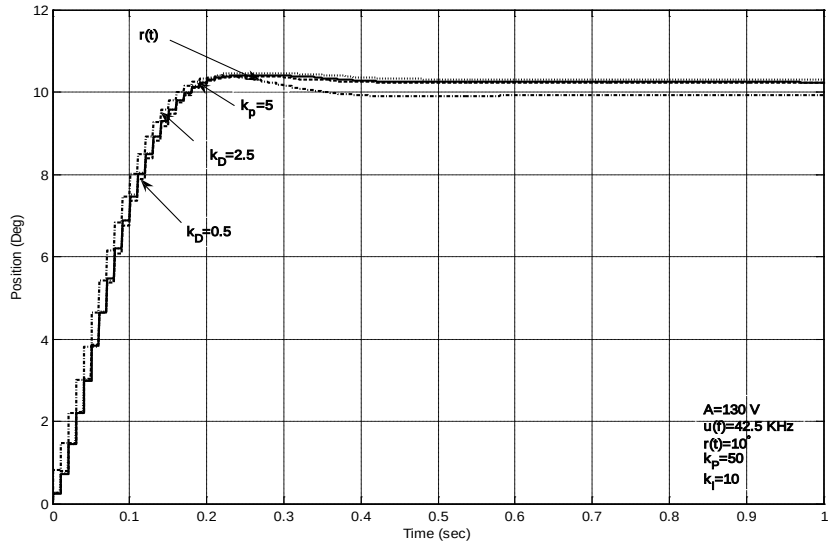

Figure A-41. Effect of derivative gain when constant user input torque is applied-42.5 KHz

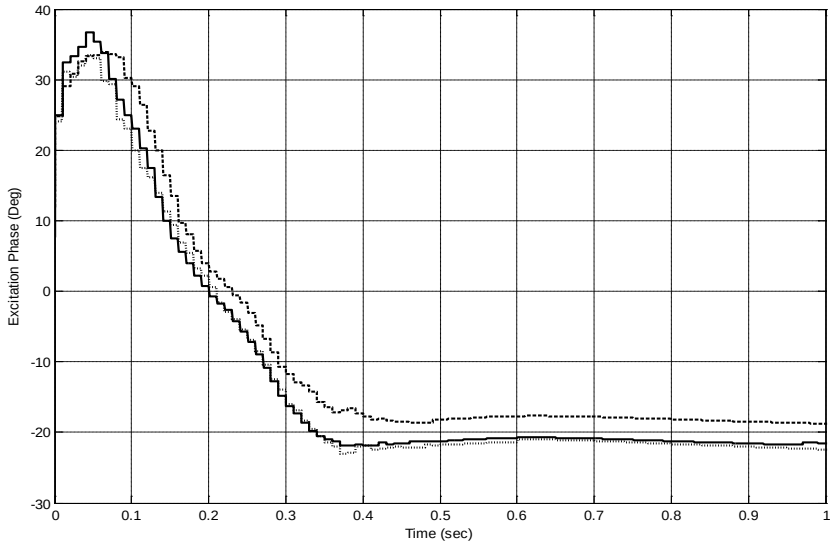

Figure A-42. Commanded excitation phase corresponding to Figure A-41

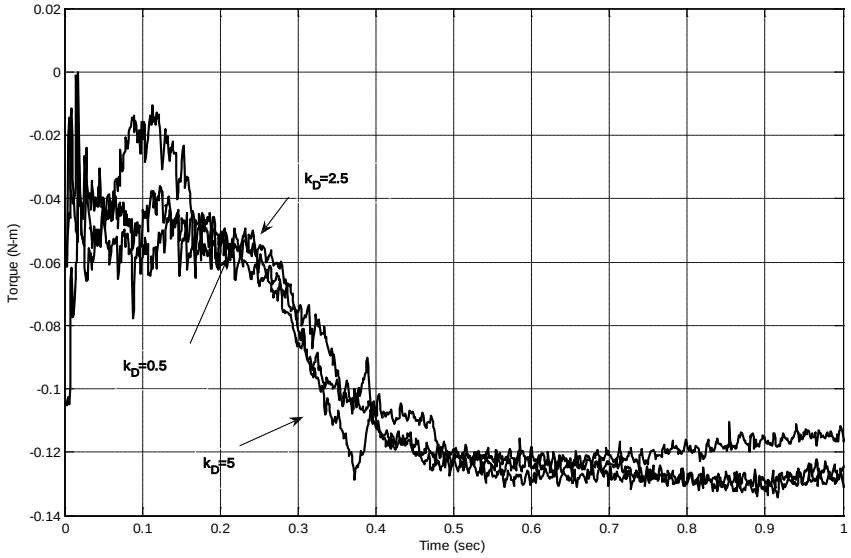

Figure A-43. Measured interaction torque corresponding to Figure A-40

Supplementary Results for Frequency Response

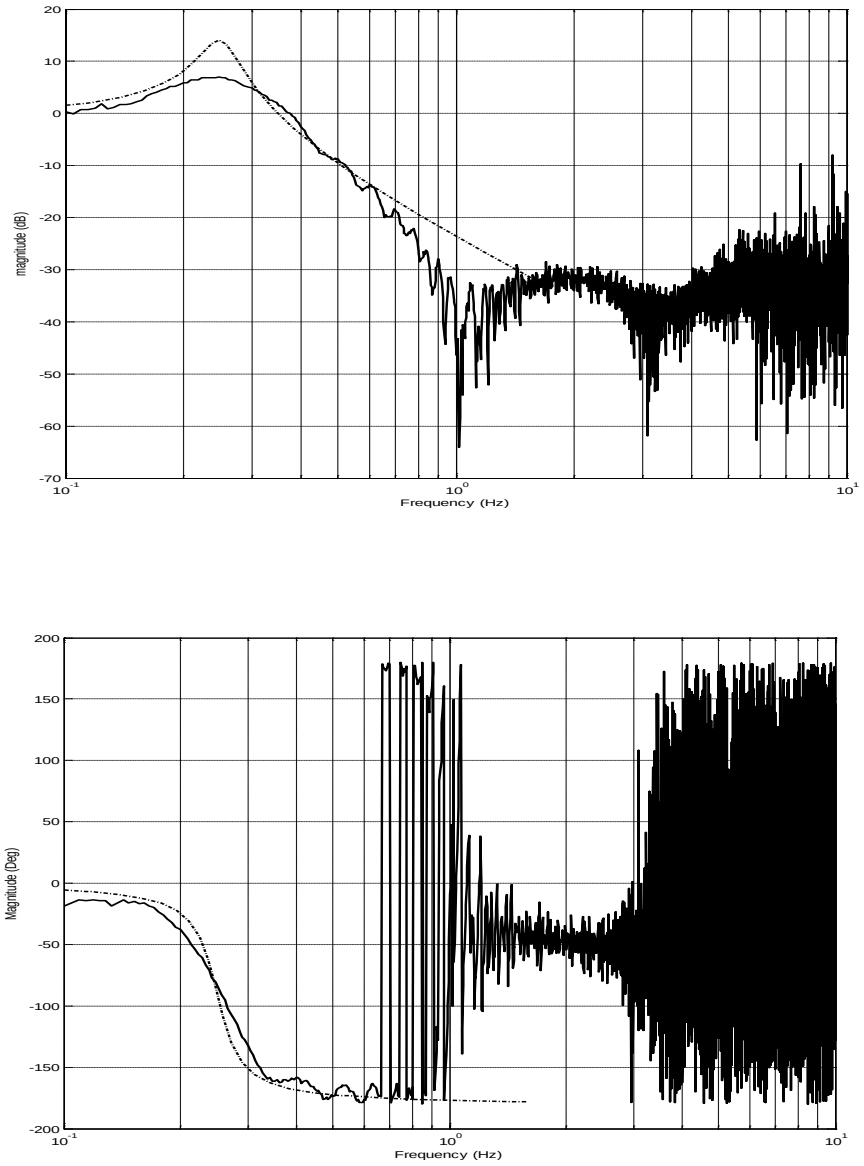

Figure A-44. Closed-loop frequency response $\Theta(i\omega)/T_L(i\omega)$ for reference model parameters $\omega_n = 0.5\pi$ rad/s and $\zeta = 0.1$.

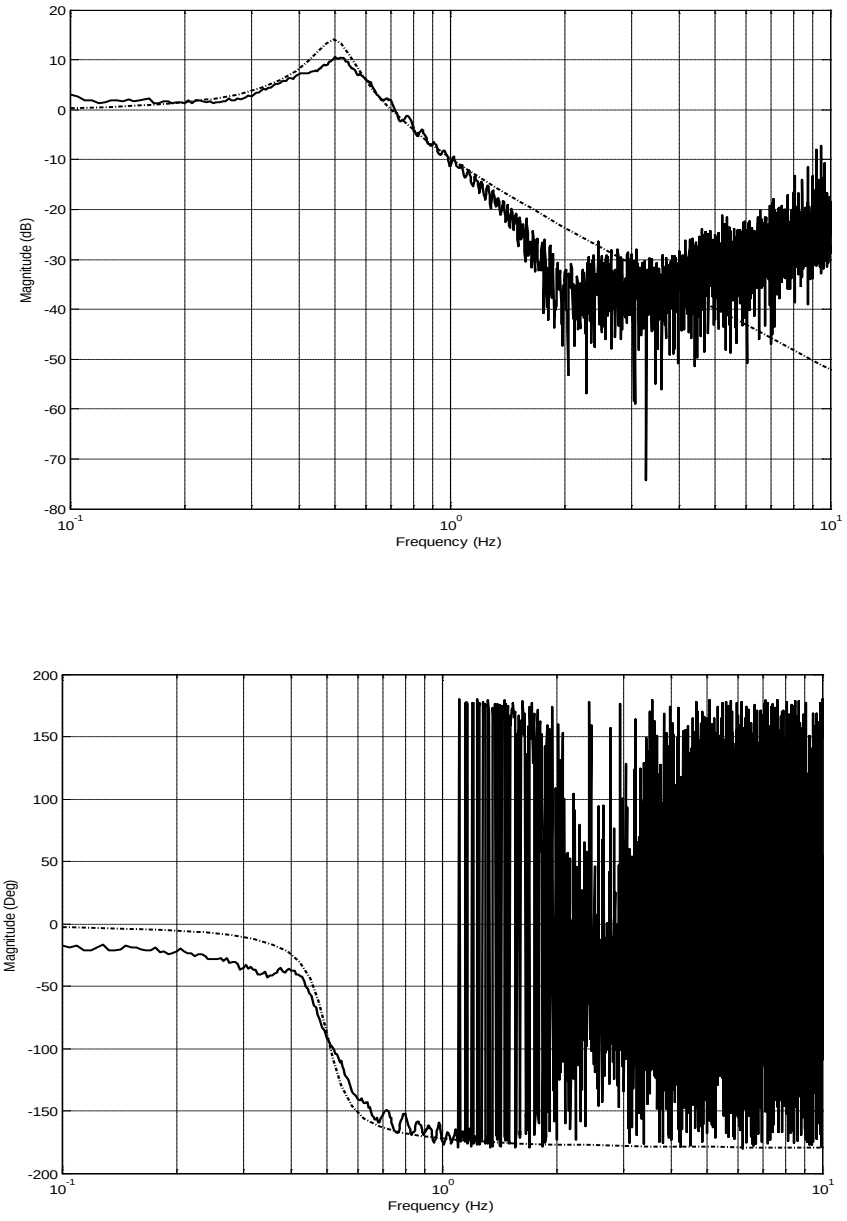

Figure A-45. Closed-loop frequency response $\Theta(i\omega)/T_L(i\omega)$ for reference model parameters $\omega_n = \pi$ rad/s and $\zeta = 0.1$.

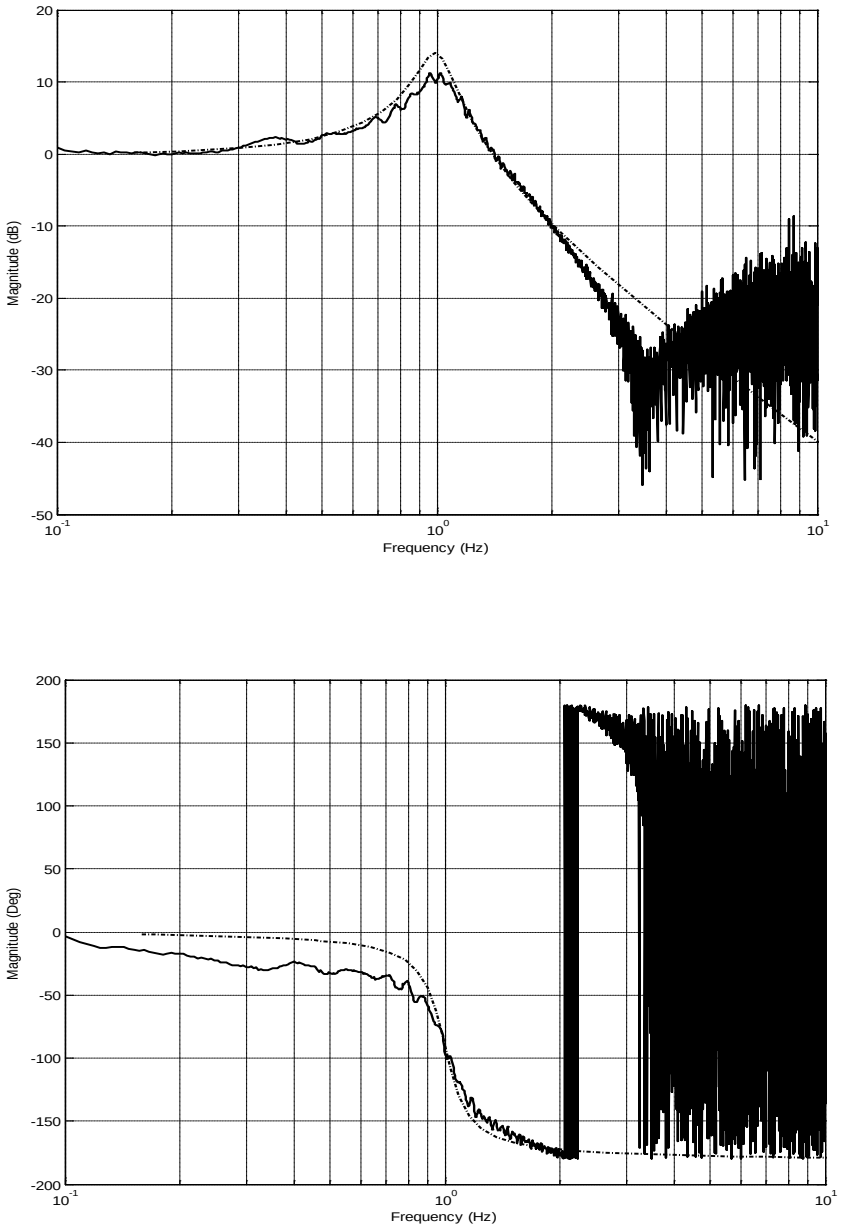

Figure A-46. Closed-loop frequency response $\Theta(i\omega)/T_L(i\omega)$ for reference model parameters $\omega_n = 2\pi$ rad/s and $\zeta = 0.1$.

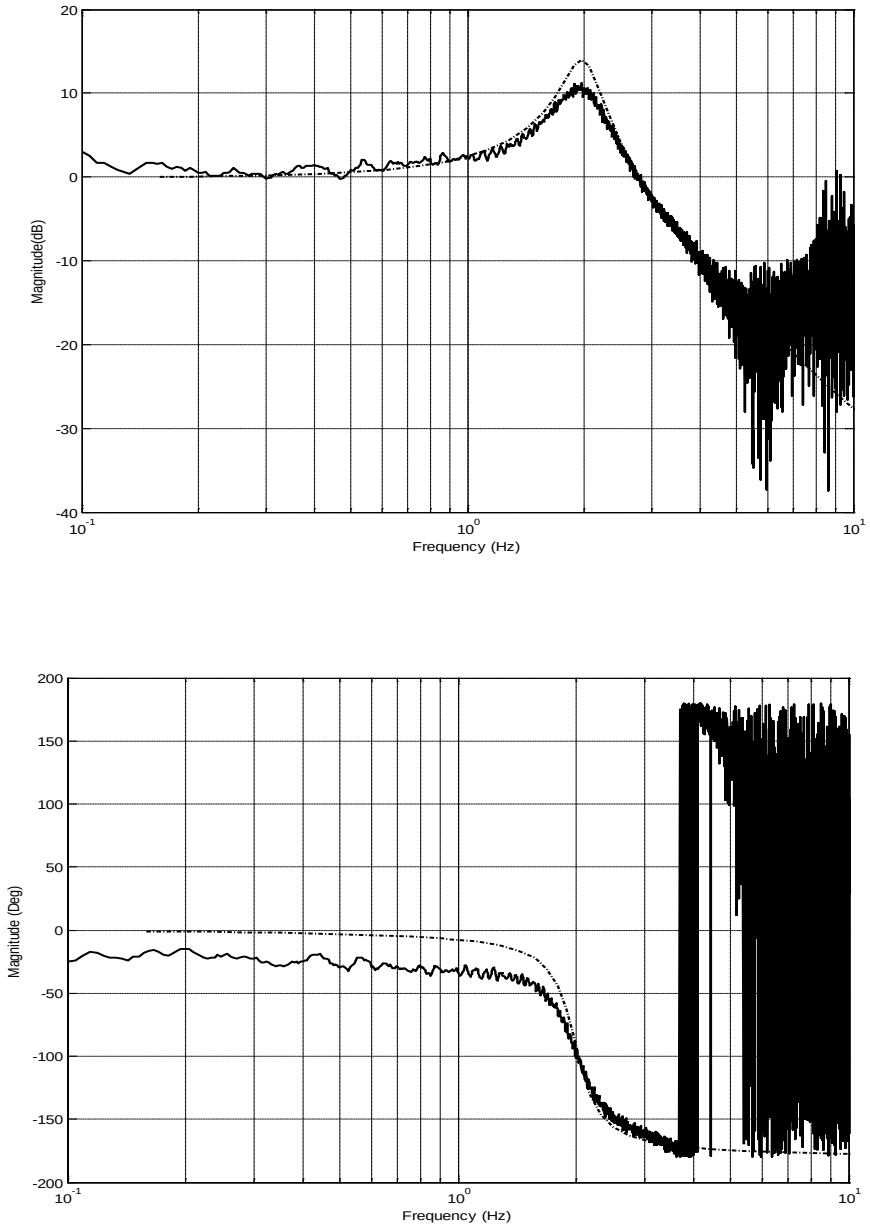

Figure A-47. Closed-loop frequency response $\Theta(i\omega)/T_L(i\omega)$ for reference model parameters $\omega_n = 4\pi$ rad/s and $\zeta = 0.1$.

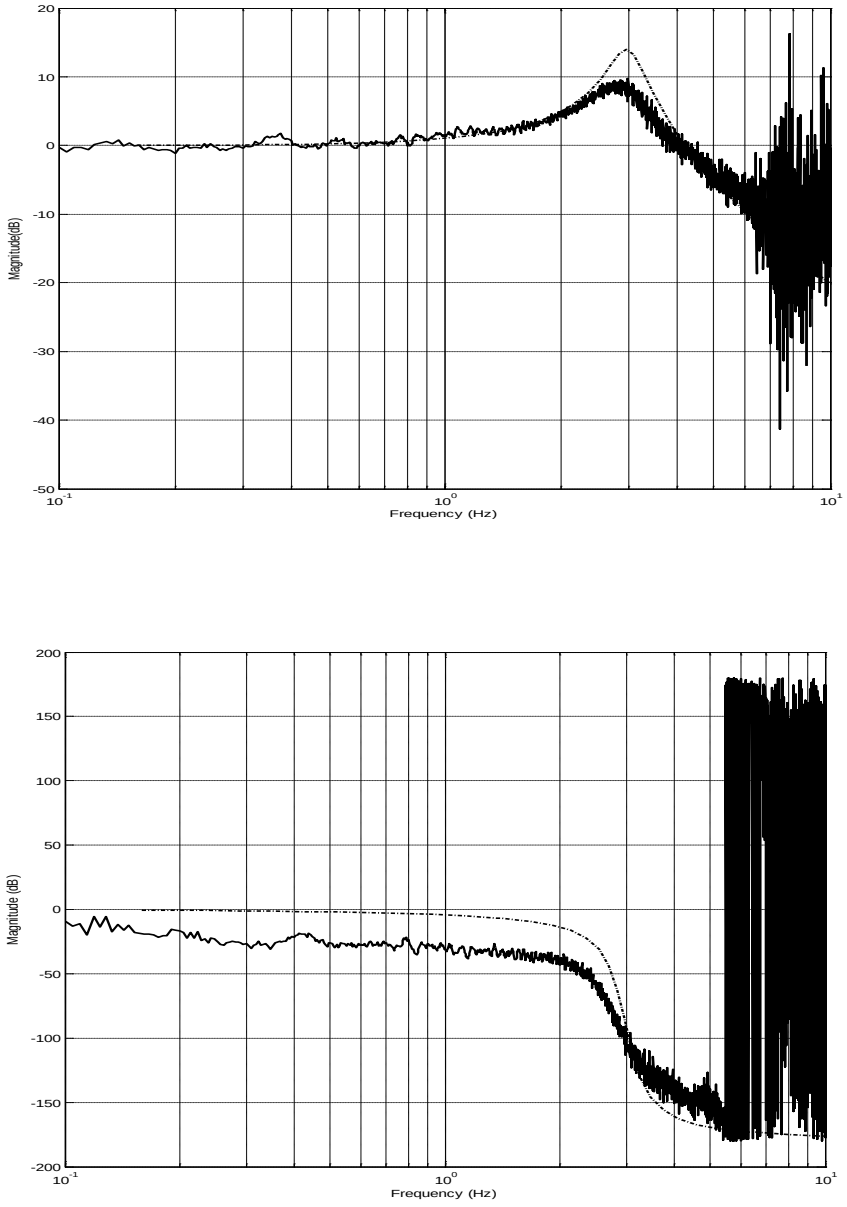

Figure A-48. Closed-loop frequency response $\Theta(i\omega)/T_L(i\omega)$ for reference model parameters $\omega_n = 6\pi$ rad/s and $\zeta = 0.1$.

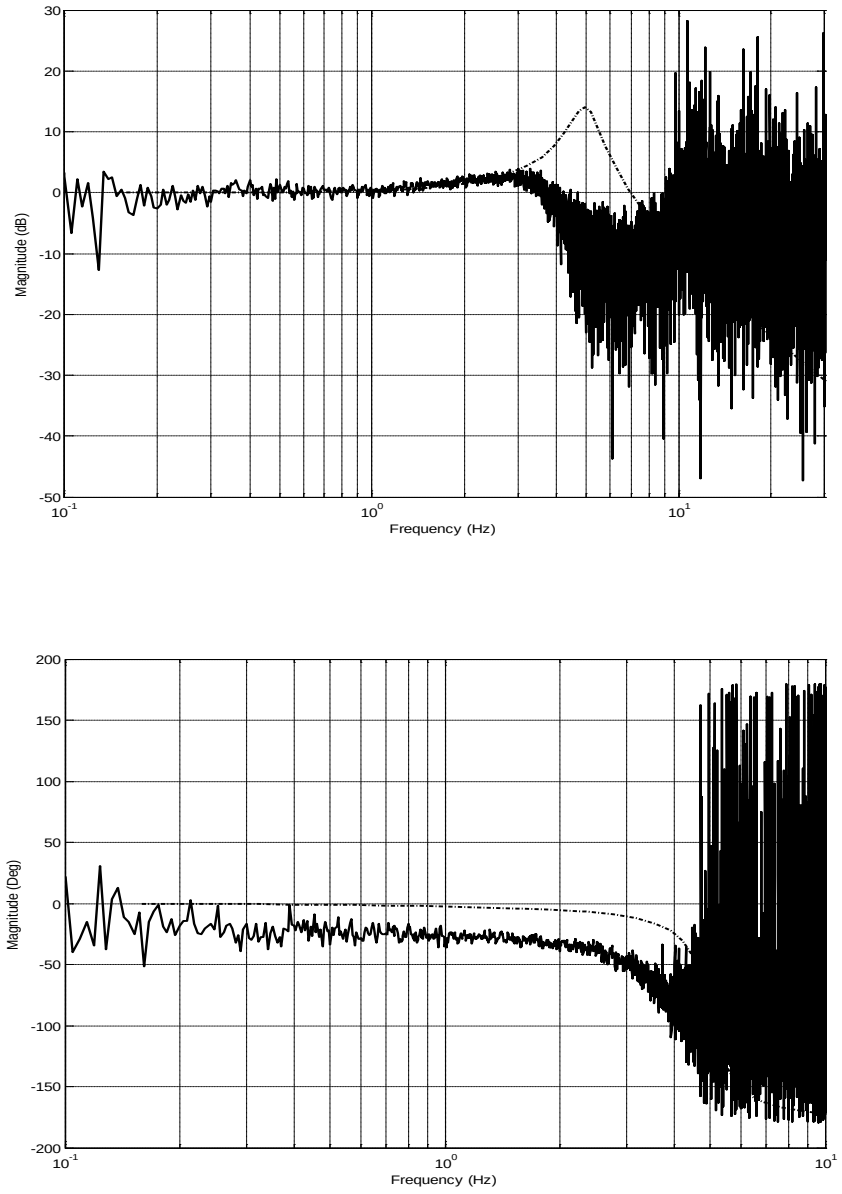

Figure A-49. Closed-loop frequency response $\Theta(i\omega)/T_L(i\omega)$ for reference model parameters $\omega_n = 10\pi$ rad/s and $\zeta = 0.1$.

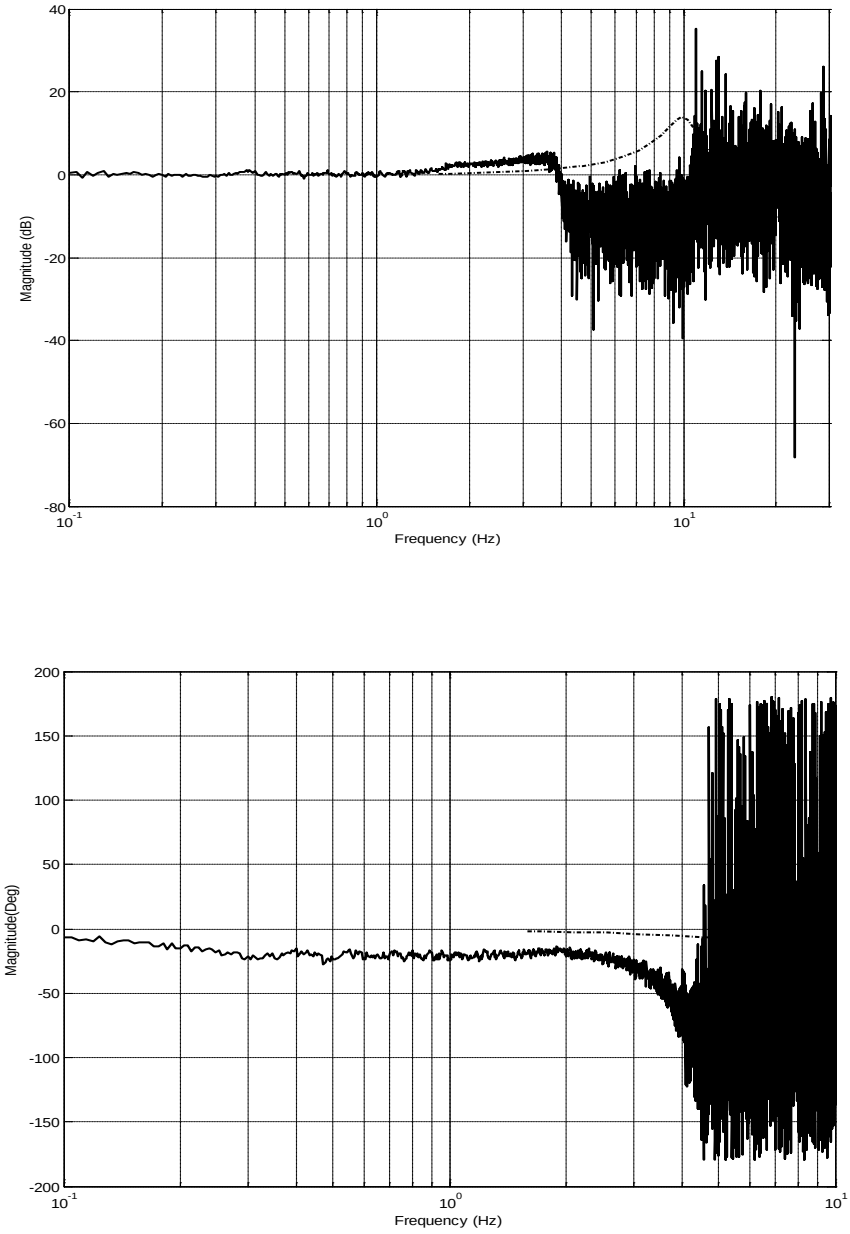

Figure A-50. Closed-loop frequency response $\Theta(i\omega)/T_L(i\omega)$ for reference model parameters $\omega_n = 20\pi$ rad/s and $\zeta = 0.1$.

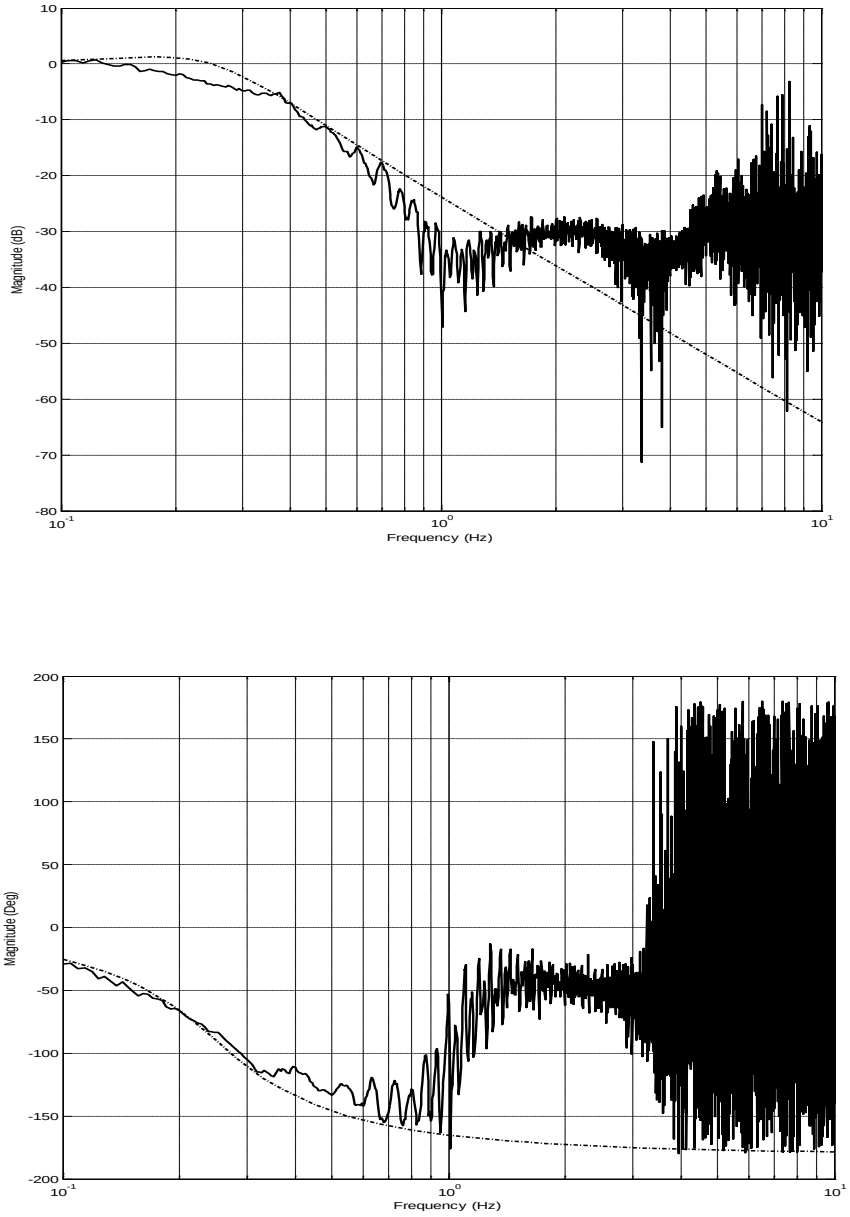

Figure A-51. Closed-loop frequency response $\Theta(i\omega)/T_L(i\omega)$ for reference model parameters $\omega_n = 0.5\pi$ rad/s and $\zeta = 0.5$.

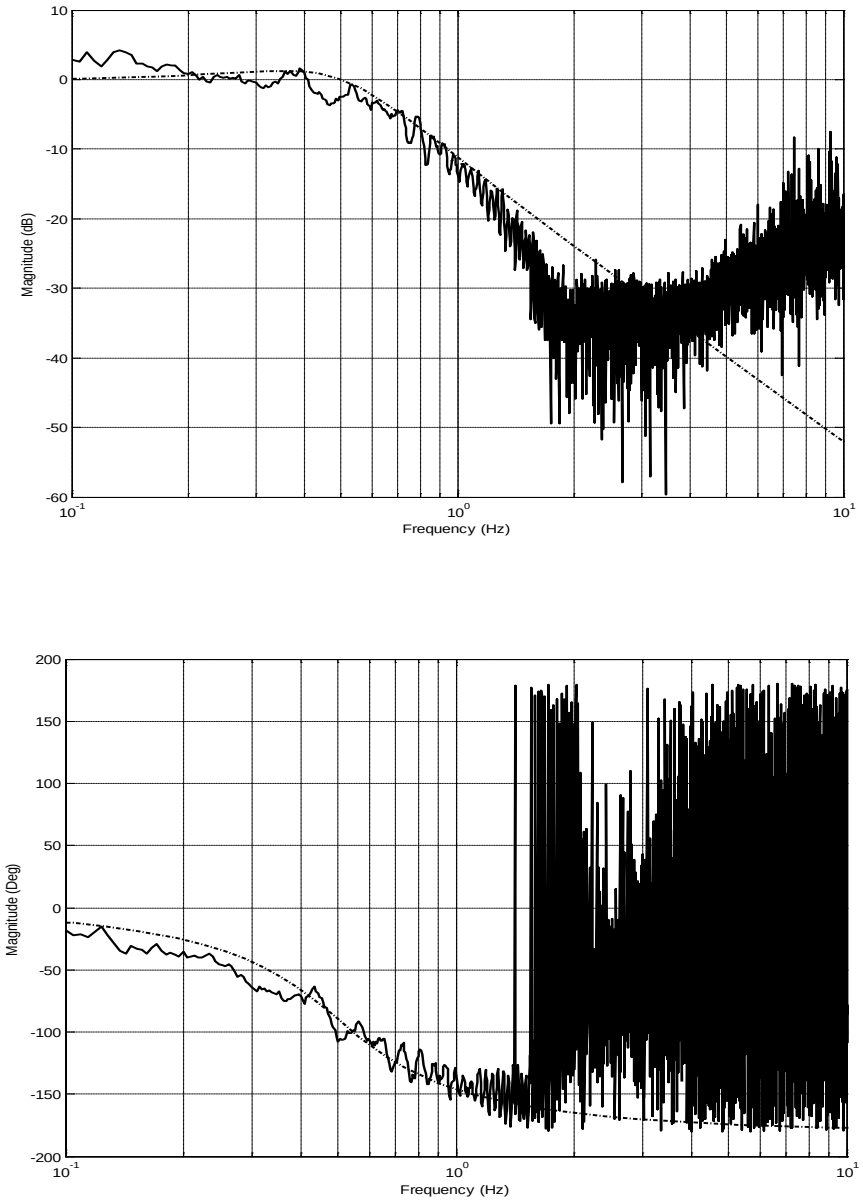

Figure A-52. Closed-loop frequency response $\Theta(i\omega)/T_L(i\omega)$ for reference model parameters $\omega_n \pi$ rad/s and $\zeta = 0.5$.

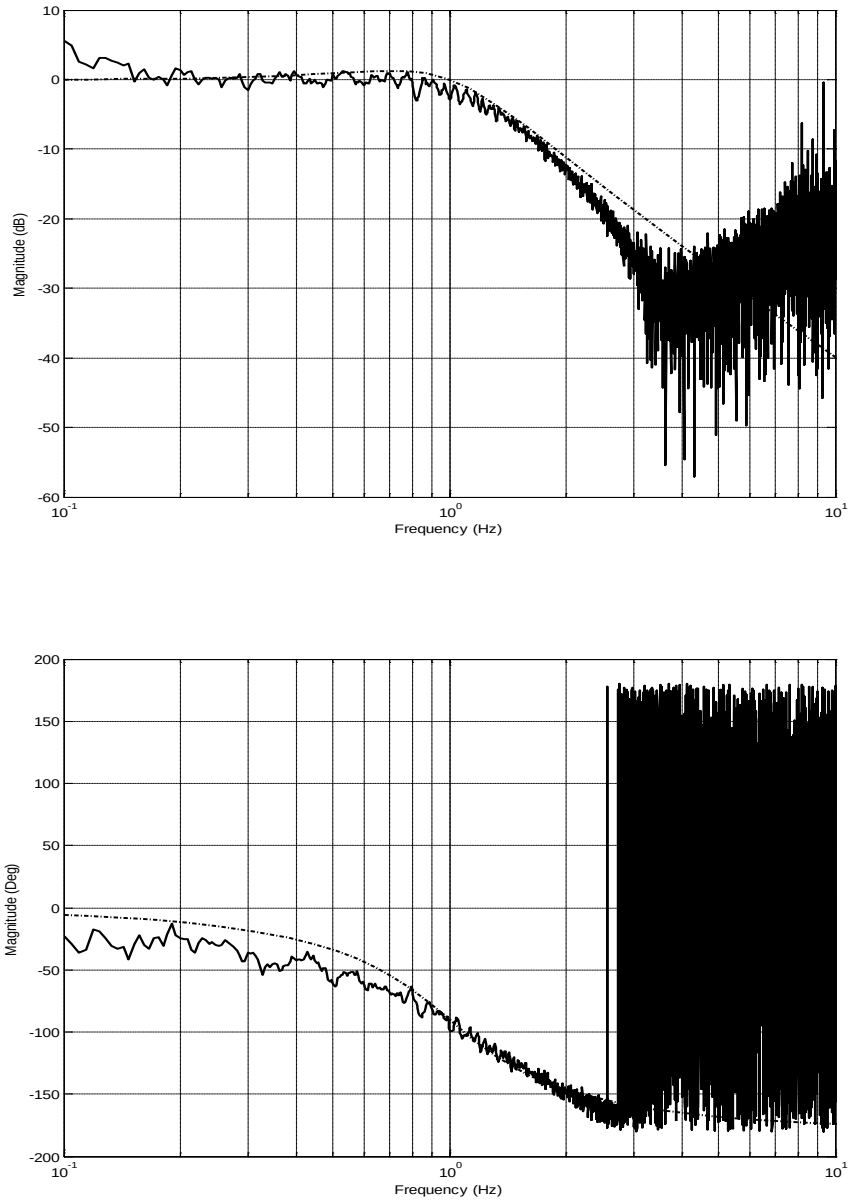

Figure A-53. Closed-loop frequency response $\Theta(i\omega)/T_L(i\omega)$ for reference model parameters $\omega_n = 2\pi$ rad/s and $\zeta = 0.5$.

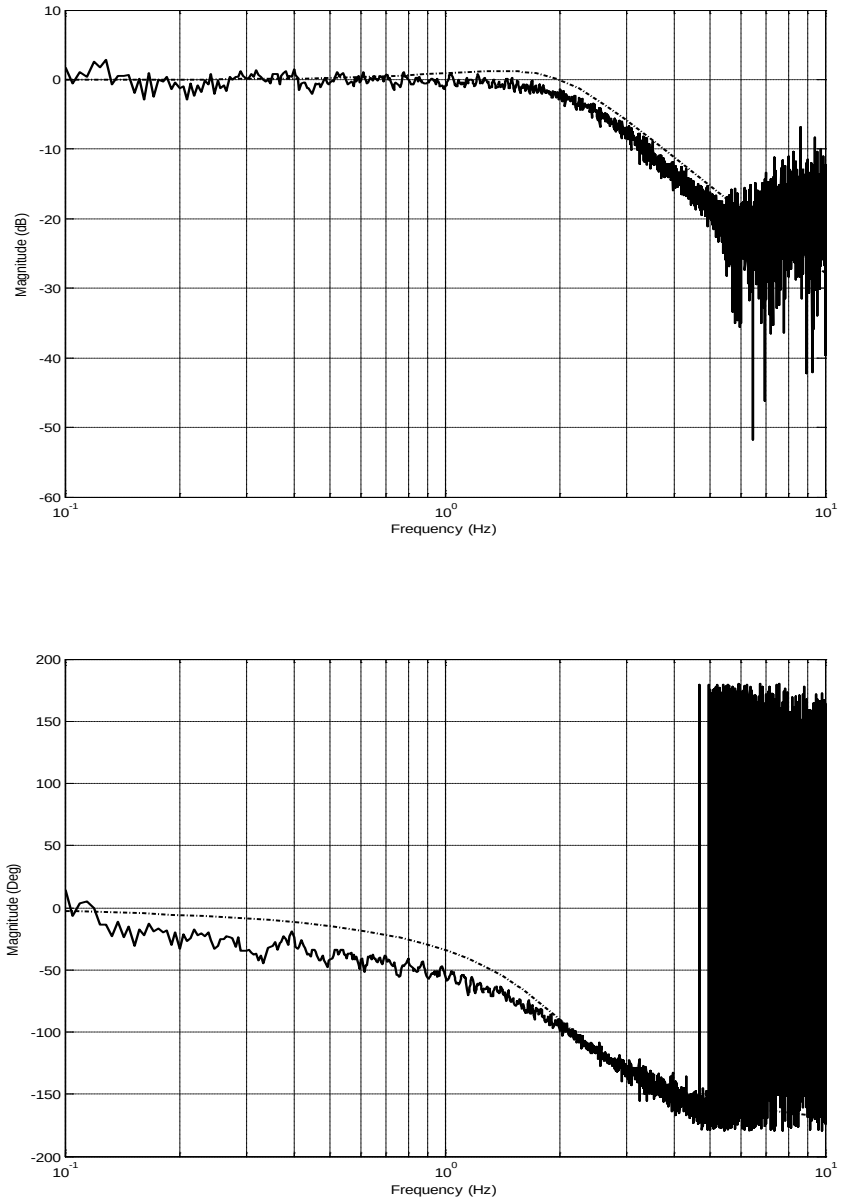

Figure A-54. Closed-loop frequency response $\Theta(i\omega)/T_L(i\omega)$ for reference model parameters $\omega_n = 4\pi$ rad/s and $\zeta = 0.5$.

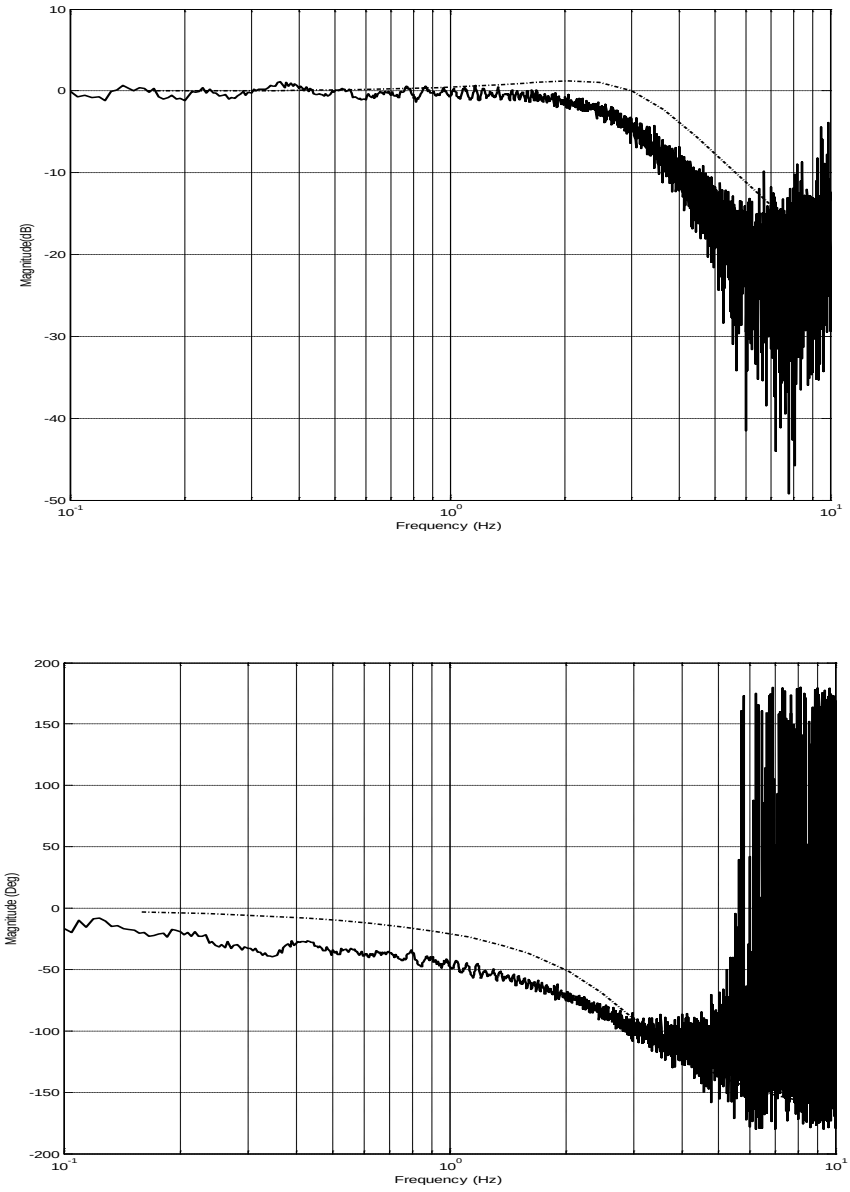

Figure A-55. Closed-loop frequency response $\Theta(i\omega)/T_L(i\omega)$ for reference model parameters $\omega_n = 6\pi$ rad/s and $\zeta = 0.5$.

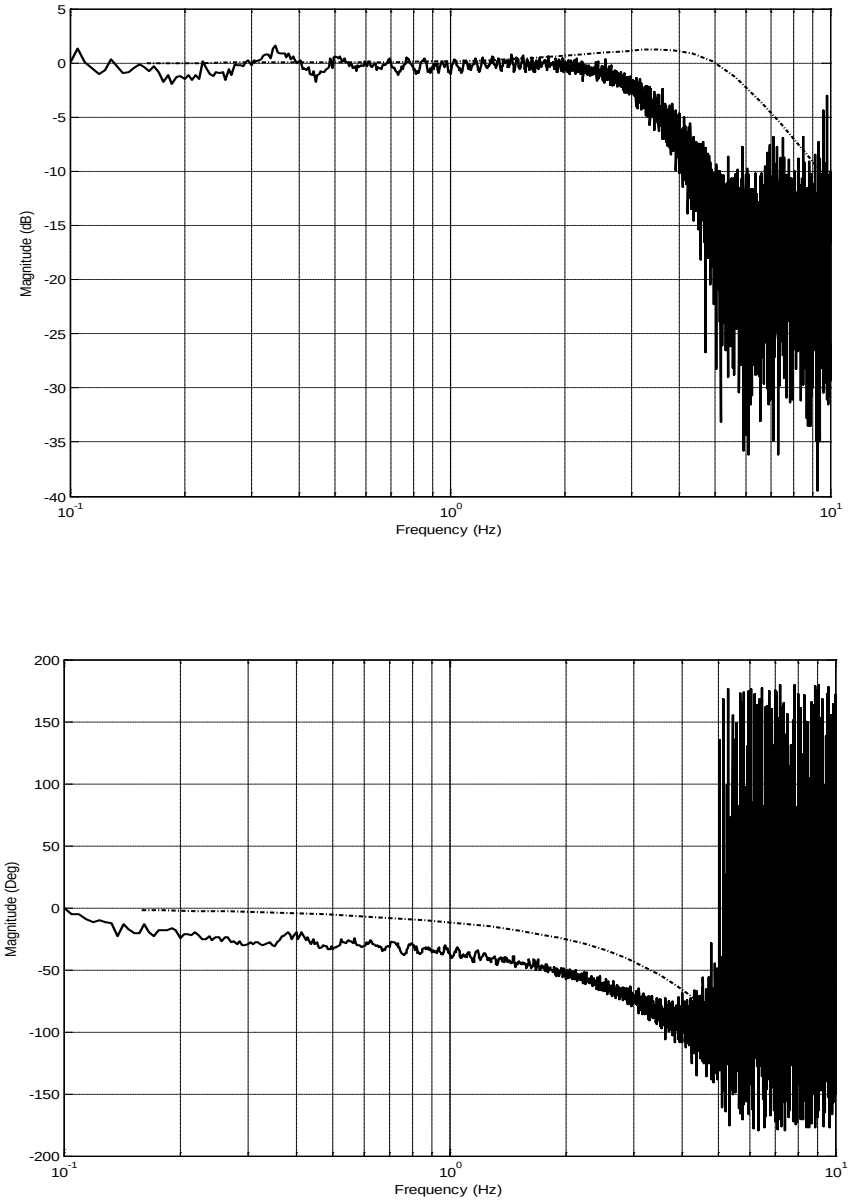

Figure A-56. Closed-loop frequency response $\Theta(i\omega)/T_L(i\omega)$ for reference model parameters $\omega_n = 10\pi$ rad/s and $\zeta = 0.5$.

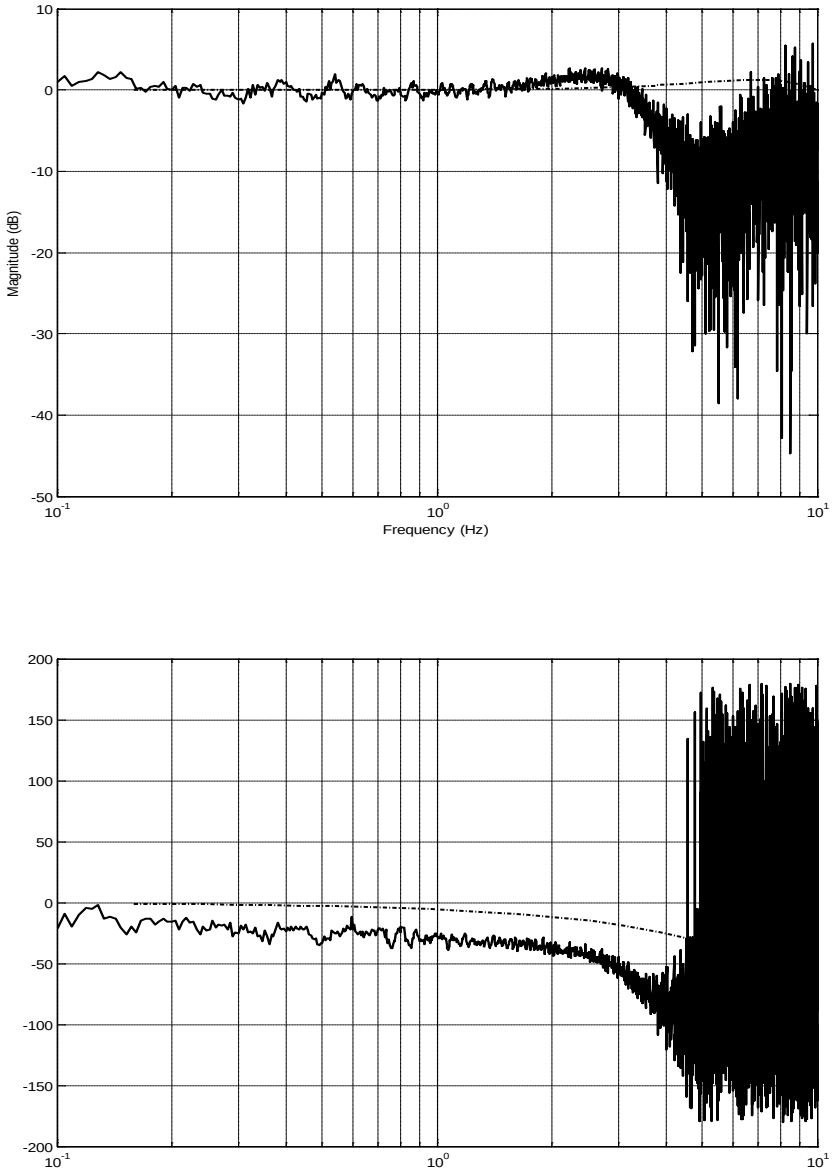

Figure A-57. Closed-loop frequency response $\Theta(i\omega)/T_L(i\omega)$ for reference model parameters $\omega_n = 20\pi$ rad/s and $\zeta = 0.5$.

APPENDIX B

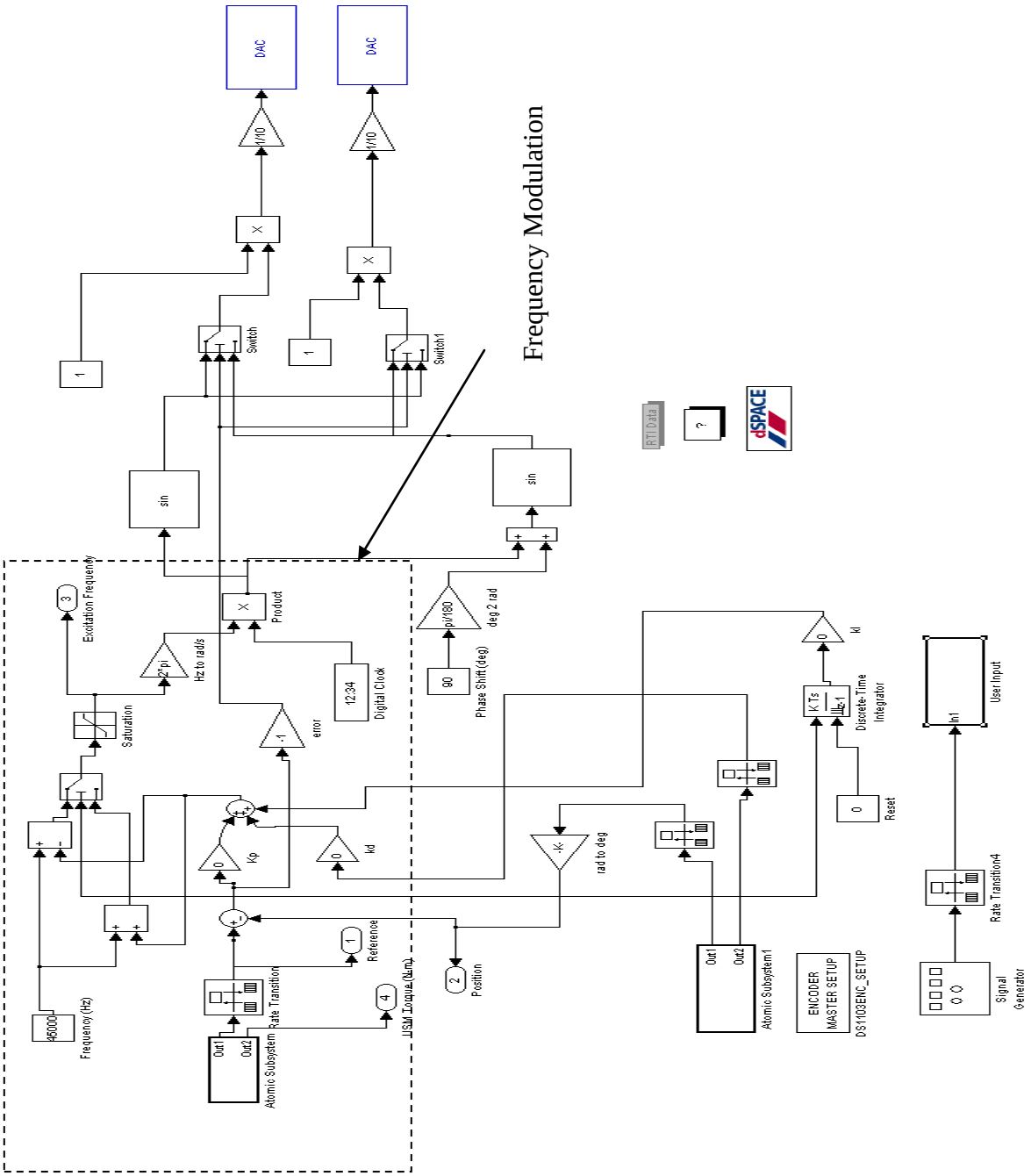

Figure B-1. Simulink Block Diagram for Frequency Control

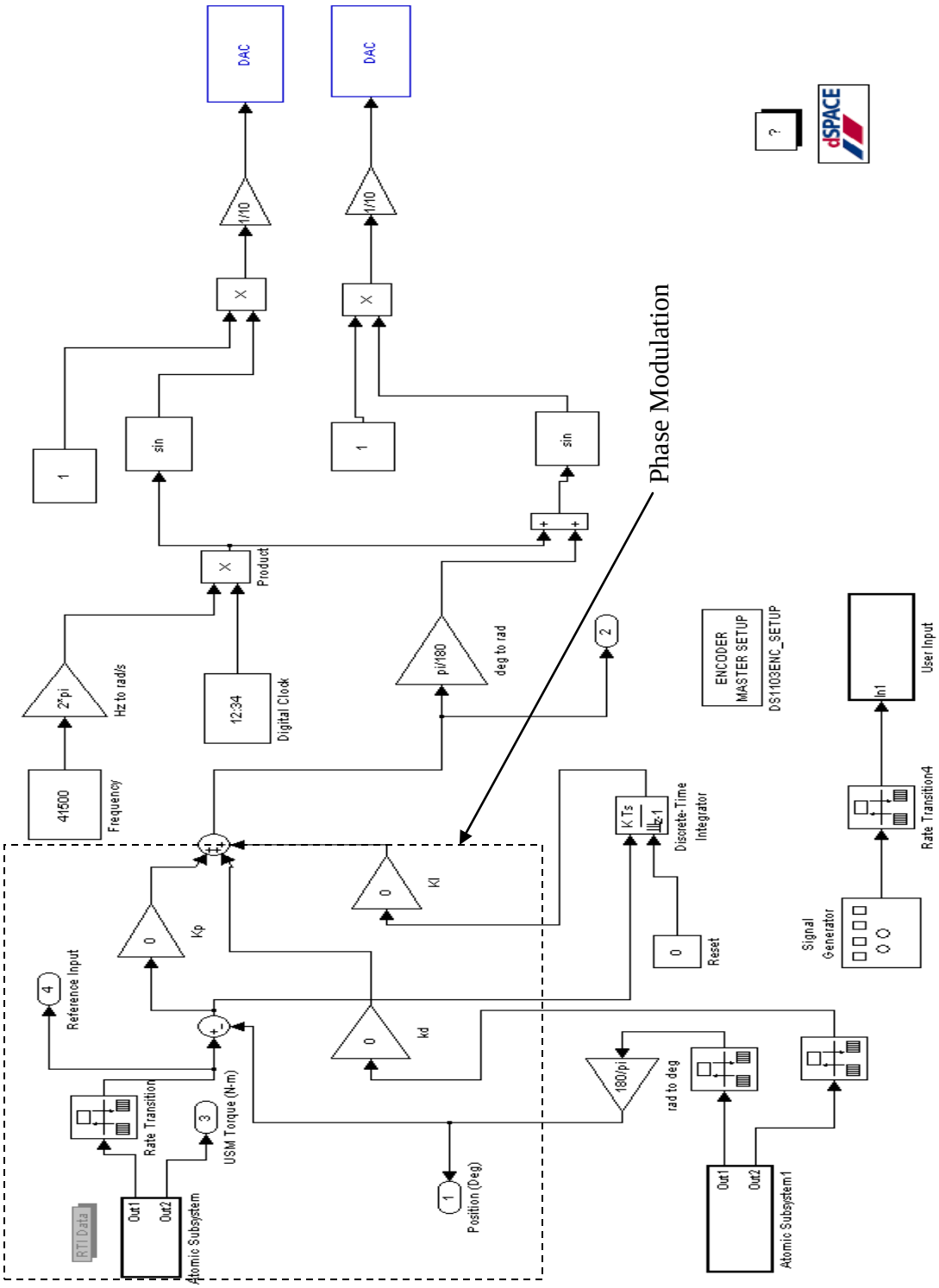

Figure B-2. Simulink Block Diagram for Phase Control

References

1. Kenji Uchino, “Piezoelectric ultrasonic motors: Overview” *Smart Materials and Structures Vol.7*(1998),273-285
2. k.Spanner, Karlsruhe, “ Various operating principles of ultrasonic piezomotors.” *White paper for actuator* 2006.
3. Nesbit W. Hagood IV and Andrew J. McFarland, “Modeling of Piezoelectric Rotary Ultrasonic Motor”, *IEEE Transactions on Ultrasonics, Ferroelectrics and Frequency Control, Vol. 42,* No.2, March 1995
4. Lim Chee Kian, “Systematic design of a disc type Traveling Wave Ultrasonic Motor” *Master’s Thesis of Science, Nanyang Technological University,*2001.
5. Jorg Wallaschek, “Piezoelectric Ultrasonic Motor” *Journal of Intelligent Material Systems and Structures, Vol. 6,* No. 1, 71-83 (1995)
6. Jianjun Qua, Tieying Zhoub “An electric contact method to measure contact state between stator and rotor in a traveling wave ultrasonic motor.” *Ultrasonics Vol.4*(2003), 561-567.
7. Yoseph Bar-Cohed, Xiaoqi Baoa, and Willem Grandiab, “Rotary motors actuated by Traveling Ultrasonic Flexural wave,”*International Symposium on Smart Structures San Diego, California, USA,*1998.
8. Xiaoqi Bao and Yoseph Bar Cohen,Jet Propulsion Laboratory, “Complete modeling of rotary Ultrasonic motors actuated by traveling flexural waves.” *7th annual symposium on Smart structures and materials,* paper no.3992-103.
9. Timothy Scott Glenn, “Mixed Domain performance model of the piezoelectric Traveling Wave motor and the development of a two sided device.” *Department of Aeronautics and Astronautics in partial fulfillment of Doctorate of philosophy,MIT,2002.*
10. Gungor Bal and Erdal Bekiroglu, “Charecteristic Estimation of Travelling Wave Ultrasonic motor using equivalent circuit model.” *IEEE Transactions on Ultrasonics,Ferroelectrics and frequency control,Vol 40 No.4*(1993).

11. Gungor Bal, “A Digitally controlled drive system for Traveling Wave Ultrasonic Motor.” *Journal of Electrical Engineering, Vol .11 No.3* (2003).

12. Matteo Bullo,Yves Perraird, “Influences of the Mechanical Performances of the Traveling wave Ultrasonic Motor by Varying the prestressing force between stator and rotor.” *Ultrasonics, Vol. 1* (2003), 593-596.

13. Xiaoqi Bao, Yoseph Bar-Cohen “Complete Modeling of Rotary Ultrasonic Motors Actuated By Traveling Flexural Waves.” *Procedings of SPIE,Vol.3992,Poster Session.*

14. F lu, H P Lee, S P Lim, “Contact Modeling of viscoelastic friction layer of traveling wave ultrasonic motors” *Smart materials and structures, Vol .10*(2001), 314-320.

15. Yoichi Ogahara, Takashi Maeno, “Torque charateristics Analysis of a Traveling Wave Type Ultrasonic Motor Impressed high Load Torque in Low Speed Range.” *Ultrasonics Symposium, 2004 IEEE Volume 3, Issue 23-27 Aug.* 2004 Page(s): 2271 - 2274 *Vol.3 Digital Object Identifier*

16. Jianjun Qu, Tieying Zhou, “ An electric contact method to measure contact state between stator and rotor in a traveling wave ultrasonic motor” *Ultrasonics Vol.41*(2003).

17. Gregor Kandare and Jorg Wallaschek, “Derivation and validation of a mathematical model for traveling wave ultrasonic motor.” *Smart Materials and Structures, Vol.11* (2002), 565-574.

18. Matteo Bullo, Yves Perriard, “Influences to the mechanical performances of the traveling wave ultrasonic motor by varying the pre stressing force between the stator and rotor.” *Ultrasonics, 2003 IEEE Symposium on Vol. 1*, 5-8 Oct. 2003 Page(s): 593 - 596 *Vol.1 Digital Object Identifier*.

19. Gungor Bal and Erdal Bekiroglu, “A PWM Technique for DSP controlled Ultrasonic Motor Drive system.” *Electric Power components and systems, Vol.33*(2005),21-38.

20. Anita M.Flynn, “Piezoelectric Ultrasonic Micromotors.” *Thesis,MIT Artificial Intelligence Laboratory,* December 1997.

21. Jorg Wallaschek, “Contact Mechanics Of Piezoelectric Ultrasonic Motor.” Smart materials and structures, *Vol 7* (1998), 369-381.

22. Gungor Bal, “A Digitally Controlled Drive System for Travelling Wave Ultrasonic Motor”*Turk JElec Engin, Vol.1,* No.3, 2003.

23. Gungor Bal, Erdal Bekiroglu, “Experimental Examination of Speed Control Methods for a Travelling Wave Ultrasonic Motor” *3. ULUSLARARASI İLERİ TEKNOLOJİLER SEMPOZYUMU, 18-20 AĞUSTOS 2003, ANKARA.*

24. D.Bai, T.Ishii, K.Nakamura, S.Ueha,T.I.Yonezawa, T.Takahashi, “An Ultrasonic Motor Driven by the Phase-Velocity Difference Between Two Traveling Waves” *IEEE Trans.Ultrason.Ferroelectr.Freq.Control,Vol.51*(6),680-685 (2004).

25. Tomonobu Senjyu,Hiroshi Miyazato and Katsumi Uezato, “Quick and Precise position control of an ultrasonic motor with dual mode control.” *International Journal of electronics, Vol. 80(1996), Issue 2,*191-200.

26. Tien-Chi Chen, Chih-Hsien Yu and Mi-Ching Tsai , “A new driver based on dual-mode frequency and phase control for traveling wave type ultrasonic motor.” *Energy Conversion and Management, 2008.*

27. T.Senjyu, S.Yokoda, H. Miyan=zato, K.Uezato, “Speed Control of Ultrasonic Motors by Adaptive Control With Simplified Mathematical model” *IEEE Proc.Elect.Power Appl,Vol 145*(3),180-184 (1998).

28. T.Senjyu, T.Kashiwagi, K.Uezato, “Position Control of Ultrasonic Motors using MRAC and Dead-Zone Compensation With Fuzzy Inference”*IEEE Trans. Power Electron,Vol 17*(2), 265-272 (2002).

29. G.Bal, E. Bekiroglu, S.Demibras, I.Colak, “Fuzzy Logic Based DSP Controlled Servo Position Control for Ultrasonic Motor”*Energy Convers.Manag,Vol 45,*3139-3153 (2004).

30. Li Huafeng , Zhao Chunsheng, Gu Chenglin, “Precise Position Control of Ultrasonic Motor Using Fuzzy Control With Dead–Zone Compensation” *Journal of Electrical Engineering,Vol.56*,No.1-2, 49-52(2005).

31. T.Senjyu, H.Miyazato,S.Yokoda, K.Uezato, “Speed Control of Ultrasonic Motors Using Neural Network”*IEEE Trans. Power Electron. Vol.13* (3),381-387 (1998).

32. F.J.Lin, R.J.Wai, C.M.Hong, “Identification and Control of Rotary Traveling-Wave Type Ultrasonic Motor Using Neural Networks”*IEEE Trans.Control Syst. Technol,Vol.9*(4),672-680 (2001).

33. Maas, J. T. Schulte, and N. Frohleke, “Model-based control for ultrasonic motors. Mechatronics” *IEEE/ASME Transactions on,Vol.5*(2), 165-180(2000).

34. Giraud, F., B. Semail, and J.T. Audren, “Analysis and phase control of a piezoelectric traveling-wave ultrasonic motor for haptic stick application” *Industry Applications, IEEE Transactions, Vol.40*(6),1541-1549 (2004).

35. J Maas, T Schulte, H Grotstollen, “ Controlled Ultrasonic motor for servo drive applications” *Reprint of a contributed paper published at the,,4th European Conf. on Smart Structures and Materials-2nd Int.Conf on Mucromechanics, Intelligent Materials and Robotics 1998(MIMR 98),Harrogate, (UK),701-708,July 6-7,1998.*

36. J.Maas, T.Schulte, H.Grotstollen,N.Frohleke, “Model based control of traveling wave type ultrasonic motors.” *IEEE/ASME Transaction on Mechatronics, Vol.5*(2), 165-180 (2000).

37. “Ultrasonic Motor-General Catalogue” *Shinsei Corporation*

38. “T&C Power Conversion AG 1006 Amplifier/Generator Data Sheet”

39. “Rotary Incremental Encoders-Data sheet”, *Gurley Precision Instruments*.

40. Burdea, G.C., “Haptic Feedback for Virtual Reality. 1999”*Rutgers - The State University of New Jersey: Piscataway*.

41. Chi-Yung Yen, Fu Liang Wen and Minsung Ouyang, “Non linear Positioning Compensator of a Novel Thin-Disc Ultrasonic Motor Using Fuzzy Sliding Mode Control” *International Journal of Applied Sciences and Engineering, Vol. 3*(2004), No.2 , 257-276.

42. M.T.El Hagry, A.A.Mahfouz, H.S. Ahmed, “Experimental evaluation of a mathematical model for traveling wave ultrasonic motor”

Vita

Nishant Venkatesan was born in Chennai, Tamil Nadu, India on June 30, 1985. He received his Bachelor's Degree in Mechanical Engineering in 2006 from Anna University, Chennai, India. He worked as a Research Assistant for Dr. Seigler at University of Kentucky, Lexington, Kentucky, USA.

_____

Nishant Venkatesan